UNIVERSIDADE DA BEIRA INTERIOR
Ciências da Saúde

Analysis of the expression of taste and olfactory receptors in choroid plexus and orbitofrontal cortex of Alzheimer's disease patients

Victória da Cunha Alves

Dissertação para obtenção do Grau de Mestre em
Ciências Biomédicas
(2º ciclo de estudos)

Orientadora: Prof. Dra Isabel Gonçalves

Coorientadoras: Dra. Joana Figueiró Silva e Dra. Eva Carro, Instituto de Investigación Hospital 12 de Octubre, Madrid

Covilhã, Junho de 2016

The content of this dissertation falls under the exclusive responsibility of the author.

(Victória da Cunha Alves)

Acknowledgments

Transformative achievements come from the concerted and at times unrecognized contributions of many. Any research is not an individual effort; it is a contributory effort of many hearts, hands and heads. I, therefore, attribute this successful endeavour to the vast array of significant players that I have had the grand fortune to have entered my life; this achievement is truly OURS. My deepest and sincere gratitude!

Specially note of thanks to Prof Dra Cecília Santos and to Prof Dra Isabel Gonçalves for placing this enormous opportunity in front of me and showing me the doors that might be useful to open.

I am as well forever grateful to Dra Eva Carro for welcoming me into her scientific group, for her endlessly guidance and encouragement, and for providing all necessary facilities for this research work.

Last but not least, I'd like to acknowledge and give my wholehearted gratitude to Joana Figueiró who has walked alongside me during this last months and whose guidance and continuous support could never be described in words. It has been a real pleasure and inspiration to work with such a brilliant mind. I thank you for challenging me intellectually, creatively and personally.

The bottom line is that without Joana's encouragement and faith in my abilities, I'd have never become any kind of researcher; and it is to her that I gratefully dedicate this dissertation.

Abstract

Alzheimer's disease (AD) is a chronic neurodegenerative disease characterized by progressive memory loss and cognitive deterioration, attributed to neuropathological lesions within specific regions in the brain. However, other areas of the brain such as the choroid plexus and the orbitofrontal cortex, have gained much attention since the choroid plexus is a multifunctional tissue responsible for a wide range of functions crucial to the central nervous system and the orbitofrontal cortex is considered among the most polymodal regions of the brain. Previous studies have shown the expression of taste and olfactory transduction pathways in rat choroid plexus as well as taste and olfactory regulation and activation of orbitofrontal cortex. Therefore the present work aimed to study the expression of taste and olfactory receptors in the choroid plexus and orbitofrontal cortex of AD patients. Towards this aim, transcriptomic analysis of these chemoreceptors were performed by means of Real-time quantitative Polymerase Chain Reaction (RT-qPCR), and compared between AD patients (at different Braak stages of the disease) and age-matched controls. Transcriptomic analysis indicated that orbitofrontal cortical olfactory receptors (*ORs*) and taste receptors (*TASRs*) are expressed and regulated at different stages of AD in female patients, whereas in male this regulation was not observed. Moreover, olfactory receptors *OR2K2*, *OR2H2*, and *OR1L8* and taste receptor *TAS2R14* were downregulated at Braak stages I, V, VI, compared to age-matched controls in the orbitofrontal cortex of female AD patients. The strongest differences were found at Braak stage I of AD, suggesting that dysregulation of *ORs* and *TASRs* is an early event in the pathogenesis of AD in female patients. Also, that *ORs* and *TASRs* in the orbitofrontal cortex might be differently affected in male and female AD patients. These receptors we also found to be expressed in choroid plexus, however, due to their low expression we were not able to quantify the relative mRNA levels by RT-qPCR. Nevertheless further studies are needed in order to strengthen these findings and to elucidate their potential physiologic functions in this brain area.

Keywords

Alzheimer's disease, olfactory receptors, taste receptors, choroid plexus, orbitofrontal cortex, Real Time quantitative PCR

Resumo alargado

A doença de Alzheimer é uma doença neurodegenerativa crónica caracterizada por uma perda progressiva da memória e défice das capacidades cognitivas. Estes défices cognitivos são atribuídos a lesões neuropatológicas intrínsecas a regiões específicas do cérebro. No entanto, outras áreas do cérebro, como o plexo coroide e o córtex orbito-frontal, têm sido objeto de grande atenção uma vez que o plexo coroide é um tecido multifuncional responsável por uma vasta gama de funções cruciais ao sistema nervoso central e o córtex orbito-frontal é considerado uma das regiões mais polimodais do cérebro. Estudos anteriores demonstraram a expressão das vias de transdução do gosto e do olfacto no plexo coroide de ratos, bem como a ativação e regulação olfativa e gustativa do córtex orbito-frontal. Inclusivamente, num estudo anterior foi demonstrado que no plexo coroide de ratos a expressão de genes relacionados com o sabor e o olfato se encontram sob o controlo de hormonas esteróides sexuais.

Por esse motivo, o presente trabalho teve como objetivo estudar a expressão dos recetores olfativos e gustativos no plexo coroide e no córtex orbito-frontal de pacientes com doença de Alzheimer de ambos os sexos. A fim de atingir esse objetivo, foi necessário desenhar primers específicos para esses recetores e optimizar as várias condições para obter curvas de calibração eficientes para a análise transcritómica quantitativa. A análise do transcriptoma destes quimiorrecetores foi então efectuada através de reação em cadeia da polimerase quantitativa em tempo real (em inglês, *Real-time quantitative Polymerase Chain Reaction*), e os níveis de expressão foram comparados entre pacientes com doença de Alzheimer (em diferentes estágios da doença) e controlos pareados.

A análise do transcriptoma revelou que os recetores olfativos (*ORs*) e gustativos (*TASRs*) orbito-frontal corticais se expressam e se encontram regulados em alguns estágios da doença em pacientes do sexo feminino, enquanto que em pacientes do sexo oposto essa mesma regulação nao foi observada. Nomeadamente, a expressão dos recetores olfativos *OR2K2*, *OR2H2* e *OR1L8* e o recetor gustativo *TAS2R14* encontra-se regulada negativamente nos estágios de Braak I, V e VI em comparação com os controlos pareados em córtex orbito-frontal de pacientes do sexo feminino com doença de Alzheimer. As diferenças mais evidentes foram encontradas no estágio de Braak I, sugerindo que a desregulação da expressão dos recetores olfactivos e gustativos é um evento que ocorre precocemente na patologia de Alzheimer em pacientes do sexo feminino. Apesar da sua tendência para aumentar em estágios mais avançados, possivelmente em resposta à progressão da doença (ao nível bioquímico e estrutural), o córtex orbito-frontal parece não ser capaz de restaurar os níveis observados em pacientes controlo. Além disso, estes resultados sugerem também que a expressão dos *ORs* e os *TASRs* no córtex orbito-frontal pode ser afetada de forma distinta entre pacientes de Alzheimer de um ou outro sexo.

Inclusivamente, verificou-se que estes recetores também se expressam em plexo coroide, no entanto, devido à sua baixa expressão não foi possível quantificar os seus níveis relativos de mRNA por PCR quantitativa em tempo real.

A utilização de tecidos *post-mortem* humanos para estudos de expressão génica é particularmente desafiador. Além do problema do RNA danificado, temos de enfrentar um elevadíssimo grau de variabilidade biológica dentro de um conjunto de amostras. As variações dos parâmetros individuais como a idade, a massa corporal, a saúde, mas também a causa e circunstâncias da morte e o intervalo *post-mortem* podem conduzir a um conjunto de amostras bastante inomogéneo.

Adicionalmente, mais estudos são necessários a fim de reforçar estas conclusões e elucidar as possíveis funções fisiológicas destes quimiorrecetores nestas áreas do cérebro.

Palavras-chave

Doença de Alzheimer, recetores olfativos, recetores gustativos, plexo coroide, córtex orbito-frontal, PCR quantitativa em tempo real

Index

Acronyms list

ABCA1	ATP binding cassette transporter 1
AC3	Adenylyl cyclase 3
AD	Alzheimer's disease
APOE	Apolipoprotein E
APP	Amyloid precursor protein
Aβ	Amyloid β
BDNF	Brain derived neurotrophic factor
cAMP	Cyclic adenosine monophosphate
cDNA	Complementary DNA
CNG	Cyclic nucleotide-gated
CP	Choroid plexus
CSF	Cerebrospinal fluid
Ct	Threshold cycle
dsDNA	double-stranded DNA
EOAD	Early-onset Alzheimer's disease
FFA	Free fatty acid
GAPDH	Glyceraldehyde3-phosphate desydrogenase
GI	Gastrointestinal
GPCR	G protein-coupled receptor
HRT	Hormone replacement therapy
IGF-1	Insulin-like growth factor-1
IP_3	Inositol-1,4,5-triophosphate
IP_3R3	IP_3 receptor type 3
LOAD	Late-onset Alzheimer's disease
MCI	Mild cognitive impairment
NO	Nitric oxide
NPH	Normal pressure hydrocephalus
OE	Olfactory epithelium
OFC	Orbitofrontal cortex
OR	Olfactory receptor
PCR	Polymerase chain reaction
PFC	Prefrontal cortex
PGK1	Phosphoglycerate kinase 1
PLCβ2	Phospholipase Cβ2

PSEN 1	Presenilin 1
PSEN 2	Presenilin 2
RT	Room temperature
RT-qPCR	Real Time quantitative polymerase chain reaction
SG	Salivary gland
ssDNA	single-stranded DNA
T1R	Taste receptor type 1
T2R	Taste receptor type 2
Ta	Annealing temperature
TAE	Tris-acetate-EDTA
TASR	Human taste receptor
Tasr	Rodent taste receptor
Tm	Melting temperature
TR	Taste receptor
TRPM5	Transient receptor potential ion channel, subfamily M, member 5
VGSC	Voltage-gated sodium channels
a-gustducin	G protein subunit α

I. Introduction

1. Overview of Alzheimer's Disease

Alzheimer's disease (AD) is a chronic neurodegenerative disease and the most common type of dementia (Wilson et al., 2012).

As a consequence of population aging worldwide, it has reached an incidence of a case every 7 seconds and a fourfold increase is expected to occur over the next decades (Cornutiu, 2015). Recent estimates foresee that more than 80 million individuals will be affected by the disease by 2040 (Wilson et al., 2012; Cornutiu, 2015).

Although AD was first identified more than 100 years ago, research into its symptoms, causes, risk factors, and treatment has gained momentum only in the past 30 years. Most experts agree that AD, like other common chronic diseases, develops as a result of multiple factors rather than a single cause. These factors include a variety of brain changes that begin as early as 20 years before symptoms appear, affecting one's memory, behaviour, and ability to think clearly (Scheltens et al., 2016).

1.1. Clinical phases and symptoms of AD

According to recent propositions, three clinical phases of AD may be defined:

(i) Asymptomatic (or pre-clinical) AD, which may last for several years or decades until the overproduction and accumulation of Amyloid *β* in the brain reaches a critical level that triggers the amyloid cascade;

(ii) Mild cognitive impairment (MCI) (pre-dementia phase of AD) compatible with the definition of progressive, amnestic MCI, in which early-stage pathology is present, ranging from mild neuronal dystrophy to early-stage Braak pathology, and may last for several years according to individual resilience and brain reserve;

(iii) Clinically defined dementia phase of AD, in which cognitive and functional impairment is severe enough to surmount the dementia threshold; at this stage there is significant accumulation of neuritic plaques and neurofibrillary tangles in affected brain areas, bearing relationship with the magnitude of global impairment (Figure 1).

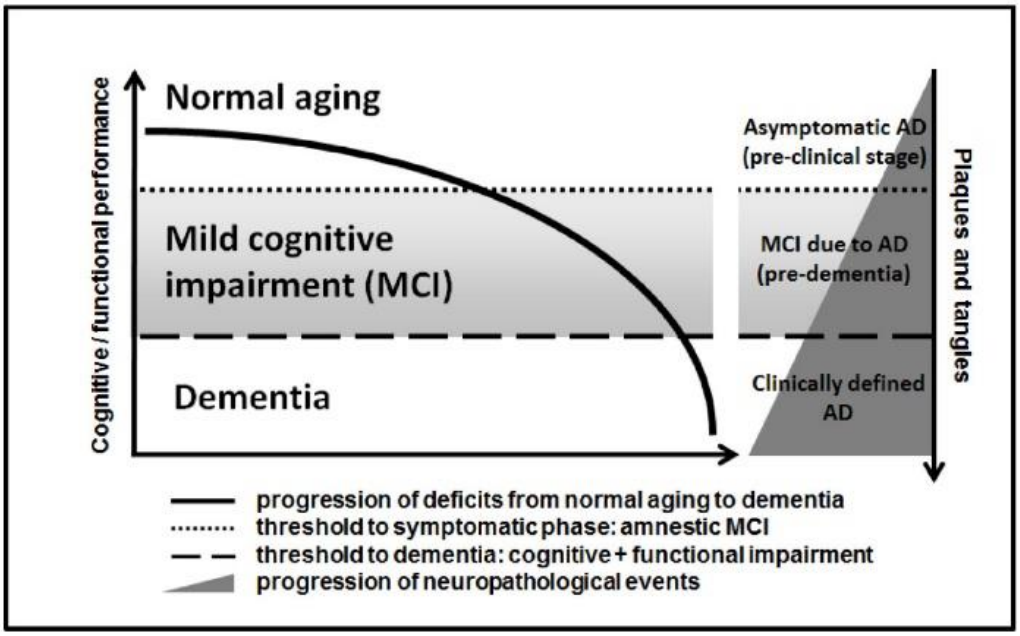

Figure 1 - Relationship between the progression of cognitive and functional symptoms and the neuropathological events in the transition from asymptomatic AD to mild cognitive impairment due to AD and clinically manifest dementia of the AD type. Adapted from Forlenza et al., 2010.

There is evidence of a long preclinical phase in AD, in which the aforementioned abnormalities gradually accumulate in affected brain areas prior to the presentation of significant cognitive decline and dementia (Tarawneh & Holtzman, 2012). Also, the neuropathological features of subjects with MCI are intermediate between those found in cognitively normal and demented individuals (Forlenza et al., 2010).

Recent models based on neuropathological, biochemical and neuroimaging methods have proposed that intracerebral amyloidosis precedes the onset of cognitive symptoms by several years, if not decades. Autopsy studies have shown that intracerebral amyloidosis may be observed in some subjects as early as in the third or fourth decades of life, with increasing magnitude in late middle age, and highest estimates in old age (Thal et al., 2000, Thal et al., 2002; Knopman et al., 2003). Therefore, the long pre-dementia phase in AD constitutes a unique time frame to search for clinical and neurobiological tools to reinforce the cross-sectional diagnosis and to predict the dementia outcome.

AD affects people in different ways, but the most common symptom pattern begins with gradually worsening ability to remember new information. This occurs because disruption of brain cell function usually begins in brain regions involved in forming new memories. As damage spreads, individuals experience other difficulties. The following are common symptoms of AD:

- Memory loss that disrupts daily life.
- Challenges in planning or solving problems.
- Difficulty completing familiar tasks at home, at work, or at leisure.
- Confusion with time or place.

- Trouble understanding visual images and spatial relationships.
- New problems with words in speaking or writing.
- Misplacing things and losing the ability to retrace steps.
- Decreased or poor judgment.
- Withdrawal from work or social activities.
- Changes in mood and personality.

Individuals progress from mild AD to moderate and to severe at different rates. As the disease progresses the individual's cognitive and functional abilities decline. Those in the final stages of the disease lose their ability to communicate, fail to recognize loved ones, and become bedbound and reliant on around-the-clock care. They even become more vulnerable to infections, including pneumonia. AD is ultimately fatal, and AD-related pneumonia is often a contributing factor (Castellani et al., 2010).

1.2. Sporadic and Familial AD

There are two types of AD: familial (also known as early onset) and sporadic (also known as late onset, LOAD). Although most cases of AD are sporadic, rare familial forms exists with an autosomal dominant pattern of inheritance. Familial AD accounts for less than 1% of all cases and is caused by any of three known genetic mutations (Bekris et al., 2010; Acosta-Baena et al., 2011). These mutations involve the gene for the amyloid precursor protein (*APP*) and the genes for the presenilin 1 (*PSEN1*) and presenilin 2 (*PSEN2*) proteins. Inheriting a mutation to the *APP* or *PSEN1* gene guarantees that an individual will develop AD. Those inheriting a mutation in the *PSEN2* gene have a 95% chance of developing the disease (Goldman et al., 2011). Individuals with mutations in any of these genes tend to develop AD before age 65 years, sometimes as young as 30 years (Acosta-Baena et al., 2011). In contrast to familial AD, LOAD is etiologically heterogeneous and results from a combination of many environmental conditions, lifestyle and genetic features of the individual (Huang et al., 2004; Liu et al., 2015). Although there is evidence of a strong genetic component to disease risk, until quite recently, the only established genetic factor for LOAD is apolipoprotein E (*APOE*). *APOE*-associated AD is due to *APOE ε4* allele, which is further explained in section 1.4.3.

1.3. Pathological changes in AD

AD is a disease with well-defined pathophysiological mechanisms, mostly affecting medial temporal lobe and associative neocortical structures (De-Paula et al., 2012). Neuritic plaques and neurofibrillary tangles represent the pathological hallmarks of AD, and are respectively related to the accumulation of the amyloid *β* peptide (*Aβ*) in brain tissues, and to cytoskeletal changes that arise from the hyperphosphorylation of microtubule-associated Tau protein in neurons (Takahashi et al., 2013). The accumulation of misfolded proteins in the aging brain

results in oxidative and inflammatory damage, which in turn leads to energy failure and synaptic dysfunction (Chen et al., 2012).

The accumulation of *Aβ* within structurally damaged mitochondria (Calkins et al., 2011) is consistent with other evidence of intraneuronal *Aβ* in AD (Gouras et al., 2012). *Aβ* is a potent mitochondrial toxic, especially affecting the synaptic pool (Querfurth & LaFerla, 2010). Dysfunctional mitochondria release oxidizing free radicals which cause considerable oxidative stress. Experimental models show that markers of oxidative damage precede pathological changes (Nunomura et al., 2001).

Vascular injury and parenchymal inflammation perpetuate the cycle of protein aggregation and oxidation in the brain in AD. Pervasive pathological changes include cerebral amyloid angiopathy (Greenberg et al., 2004), affecting more than 90% of AD patients, capillary abnormalities, disruption of the blood–brain barrier, and large-vessel atheroma (Roher et al., 2004).

1.3.1 Amyloid *β* plaques and Tau neurofibrillary tangles

According to the amyloid hypothesis of AD, the overproduction of *Aβ* is a consequence of the disruption of homeostatic processes that regulate the proteolytic cleavage of the amyloid precursor protein (*APP*). Genetic, age-related and environmental factors contribute to a metabolic shift favouring the amyloidogenic processing of *APP* in detriment of the physiological, secretory pathway. The neurotoxic potential of the *Aβ* peptide results from its biochemical properties that favour aggregation into insoluble oligomers and protofibrils. These further originate fibrillary *Aβ* species that accumulate into senile and neuritic plaques. These processes, along with a reduction of *Aβ* clearance from the brain, leads to the extracellular accumulation of *Aβ*, and the subsequent activation of neurotoxic cascades that ultimately lead to cytoskeletal changes, neuronal dysfunction and cellular death (De-Paula et al., 2012).

Neurofibrillary tangles, which are filamentous inclusions in pyramidal neurons, are also a pathologic marker of severity of AD. The major component of the tangles is an abnormally hyperphosphorylated and aggregated form of tau protein (Iqbal et al., 2010). Like *Aβ* oligomers, intermediate aggregates of abnormal tau molecules are cytotoxic (Khlistunova et al., 2006) and impair cognition (Querfurth & LaFerla, 2010). Neurofibrillary tangles appear first in allocortical structures, whereas amyloid plaques may first be found in the neocortex (Nelson et al., 2009; Forlenza et al., 2010). Interestingly, experimental evidence indicates that *Aβ* accumulation precedes and drives tau aggregation (Gotz et al., 2001; Lewis et al., 2001; Oddo et al., 2003). Increased oxidative stress, the impaired protein-folding function of the endoplasmic reticulum, and deficient proteasome-mediated and autophagic-mediated clearance of damaged proteins — all of which are also associated with aging — accelerate the accumulation of amyloid and tau proteins in AD (López et al., 2000; Hoozemans et al., 2005). In addition to amyloid accumulation

and neurofibrillary pathology, synaptic dysfunction leading to neuronal dystrophy are phenomena proxy to the structural changes of the brain, which ultimately triggers the clinical syndrome that characterizes incipient AD (Jack et al., 2010) – Figure 2. The cognitive manifestations associated with this process are compatible with subtle damage to hippocampal and related limbic and prefrontal structures, and may last for many years until the functional burden becomes severe enough to surmount the dementia threshold (Blass, 2002).

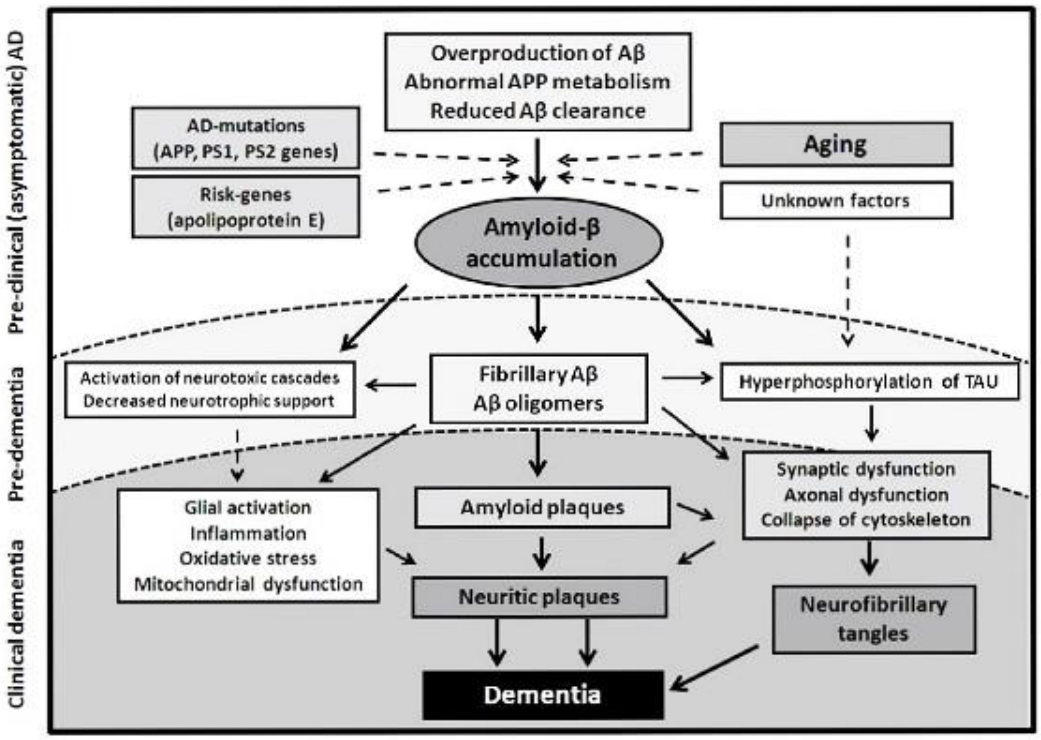

Figure 2 - Hypothetical model of the pathological processes in Alzheimer's disease (AD), focusing on the amyloid β peptide (Aβ) cascade. Adapted from Forlenza et al., 2010.

1.4. Risk factors for AD

With the exception of the rare cases of AD caused by genetic mutations, experts believe that AD develops as a result of multiple factors rather than a single cause. This section describes known risk factors for Alzheimer's.

1.4.1 Advancing age

The risk of developing AD increases exponentially with age (Plassman et al., 2007). Although the greatest risk factor is advancing age, AD is not a normal part of growing older. Most people with AD are diagnosed at age ≥65 years. These individuals are said to have LOAD. However, people aged <65 years can also develop the disease. When AD develops in a person aged <65 years, it is referred to as "early-onset" AD (EOAD) (Apter et al., 2015).

1.4.2 Family history

Individuals who have a parent, brother, or sister with AD are more likely to develop the disease than those who do not have a first-degree relative with AD (Green et al., 2002, Loy et al., 2014). Those who have more than one first-degree relative with AD are at even higher risk of developing the disease (Goldman et al., 2012). When diseases run in families, heredity (genetics), shared environmental/lifestyle factors or both may play a role.

1.4.3 Apolipoprotein E *ε4*

Individuals with the *ε4* allele of the gene apolipoprotein E (*APOE ε4*) are at increased risk of developing AD. *APOE ε4* is one of three common variants (*ε2*, *ε3*, and *ε4*) of the *APOE* gene, which provides the blueprint for a protein that carries cholesterol in the bloodstream. The *APOE* is an autosomal gene, and the presence of *APOE ε4* variant increases the risk of developing AD and of developing it at an earlier age (Spinney, 2014). Two *APOE ε4* genes grant an even higher risk (Loy et al., 2014, Holtzman et al., 2012). Researchers estimate that between 40-65% of people diagnosed with AD have one or two copies of this form of the *APOE* gene (Olgiati et al., 2011). However, unlike inheriting a genetic mutation that causes AD, inheriting the *ε4* form of the *APOE* gene does not guarantee that an individual will develop AD.

1.4.4 Mild cognitive impairment

MCI is a condition in which an individual has mild, but measurable, changes in thinking abilities that are noticeable to the person affected and to family members and friends, but do not affect the individual's ability to carry out everyday activities (Summers et al., 2012). People with MCI, especially MCI involving memory problems, are more likely to develop AD and other dementias compared to non-impaired age-matched adults. Between 10% and 20% of adults above the age of 65 are diagnosed with MCI (Kirova et al., 2015), and approximately 10% of MCI adults progress to AD (Forlenza et al., 2010). In some cases, such as when MCI is caused by certain medications, MCI can be reversed. In other cases, MCI reverts to normal cognition on its own or remains stable. Revised criteria and guidelines for diagnosis of AD suggest that in some cases, MCI is actually an early stage of AD or another dementia (Mckhann et al., 2011, Albert et al., 2011, Sperling et al., 2011).

1.4.5 Head injury and traumatic brain injury

Head injury, head trauma, and traumatic brain injury are associated with an increased risk of AD and other dementias. Moderate head injuries are associated with twice the risk of developing AD compared with no head injuries, and severe head injuries are associated with

4.5 times the risk (LoBue et al., 2016). Moderate head injury is defined as a head injury resulting in loss of consciousness or posttraumatic amnesia lasting more than 30 minutes; if either of these lasts more than 24 hours, the injury is considered severe. Groups that experience repeated head injuries, such as boxers, football players, and combat veterans, may be at increased risk of dementia, late-life cognitive impairment, and evidence of tau tangles (a hallmark of AD) at autopsy (Guskiewicz, 2005; Vincent et al., 2014).

1.4.6 Cardiovascular disease risk factors

Growing evidence suggests that the health of the brain is closely linked to the overall health of the heart and blood vessels. The brain is nourished by one of the body's richest networks of blood vessels. A healthy heart helps ensure that enough blood is pumped through these blood vessels to the brain, and healthy blood vessels help ensure that the brain is supplied with the oxygen- and nutrient-rich blood it needs to function normally.

Some data indicate that cardiovascular disease risk factors are associated with a higher risk of developing AD and other dementias. These factors include physical inactivity (Reitz et al., 2011; Willis et al., 2012), high cholesterol (especially in midlife) (Solomon et al., 2009; Meng et al., 2014), diabetes (Pendlebury et al., 2009; Reitz et al., 2011; Sekita et al., 2010), smoking (Anstey et al., 2007; Pendlebury et al., 2009; Rusanen et al., 2011), and obesity (Anstey et al., 2011; Rönnema et al., 2011; Loef et al., 2013). Other factors such as a higher level of education, as well as Mediterranean diet were shown to decrease the risk of developing AD (Gu et al., 2010; Reitz et al., 2011; Lourida et al., 2013). Table 1 shows some identified factors that modify the risk of AD. Unlike genetic risk factors, many of these cardiovascular disease risk factors are modifiable, that is, they can be changed to decrease the likelihood of developing cardiovascular disease and, possibly, the cognitive decline associated with AD and other forms of dementia.

Table 1 - Factors that modify the risk of Alzheimer disease. Adapted from Mayeux et al., 2012.

Antecedent	Direction	Possible mechanisms
Cardiovascular disease	Increased	Parenchymal destruction Strategical location ↑ *AB* deposition
Smoking	Increased	Cerebrovascular effects Oxidative stress
Hypertension	Increased and decreased	Microvascular disease
Type II diabetes	Increased	Cerebrovascular effect Insulin and *AB* compete for clearance
Obesity	Increased	Increased risk of type II diabetes inflammatory
Traumatic head injury	Increased	↑ *AB* and amyloid precursor protein deposition
Education	Decreased	Provides cognitive reserve
Leisure activity	Decreased	Improves lipid metabolism, mental stimulation
Mediterranean diet	Decreased	Antioxidant, anti-inflammatory
Physical activity	Decreased	Activates brain plasticity, promotes brain vascularisation

1.5. Gender differences in AD

The area of gender differences in AD and in neurodegenerative processes, although still largely unexplored, appears to offer great promise for the future development of better intervention strategies for patients. Prevalence studies on dementia generally show a higher risk in women than in men (Mielke et al., 2014). A possible gender difference in the risk of AD is further supported by recent evidence suggesting that the brain's so called cognitive reserve is reduced in women. Also, in patients with MCI and AD, brain volumes have been found to decline faster in women than men, supporting the evidence of faster progression of women from MCI to AD (Skup et al., 2011). In addition, the majority of studies have reported that the effects of the *ε4* genotype - the strongest known genetic risk factor for LOAD (Liu et al., 2013) - are more pronounced in women than in men (Ungar et al., 2013). It was also reported that women with one *ε4* allele had about a four-fold risk of AD, whereas men showed little increased risk (Mielke et al., 2014; Ungar et al., 2013). The *APOE* ε4 allele also has a greater deleterious effect on hippocampal pathology, functional connectivity changes in the default mode network, cortical thickness, and memory performance in women compared with men at different stages of AD (Liu et al., 2010; Damoiseaux et al., 2012). Furthermore, a large autopsy study found that

amyloid plaque and neurofibrillary tangle pathology was greater among women who were ε4 carriers (Holland et al., 2013).

Other genes and polymorphisms have also been shown to increase risk and progression of AD in one sex, but not the other. A study reported that the *Met66* allele of Brain derived neurotrophic factor (*BDNF*) gene, which reduces the transport of *BDNF*, is associated with an increased risk of AD in women, but not in men (Fukumoto et al., 2010). This finding is biologically plausible since oestrogen plays an important role in the expression of *BDNF*. Postmenopausal women with the *Met66* allele would therefore have both reduced transport and expression of *BDNF*, thus causing an increased risk of AD. Also the *219K* allele of the ATP Binding Cassette Transporter 1 (*ABCA1*) gene had a 1.75-fold increased risk of developing AD in women, but was found to be protective in men (Mielke et al., 2014). *ABCA1*-mediated pathways have been linked to some of the physiological benefits of oestrogen (Mielke et al., 2014).

In fact, most studies finding sex differences link the association to sex hormone levels. Oestrogens and other gonadal steroids act on target sites and groups of neurons in the brain that possess intranuclear oestrogens receptors (Jung et al., 2008). Most of these actions have the potential to contrast the neurodegenerative process that characterizes AD.

The beneficial effects of oestrogens on the brain might explain why AD in women is rarely seen before the menopause and why, in observational studies, hormone replacement therapy (HRT) is associated with a reduced incidence of AD (Maki & Henderson, 2012).

1.6. Post-mortem diagnosis of AD

The development of intraneuronal lesions at selectively vulnerable brain sites is central to the pathological process in AD. The lesions consist mostly of hyperphosphorylated tau protein and include pretangle material, neurofibrillary tangles in cell bodies, neuropil threads in neuronal processes, and material in dystrophic nerve cell processes of neuritic plaques (Braak et al., 2006).

AD-related neurofibrillary changes occur at predisposed cortical and subcortical sites. The distribution pattern and developmental sequence of the lesions are predictable and permit identification of six Braak stages, which can be subsumed under three more general units: I–II, III–IV, V–VI (Braak et al., 2006; Mufson et al., 2016).

In more detail, in stage I the involvement is slight and confined to the transentorhinal region, located on the medial surface of the rhinal sulcus (Figure 3a). In stage II, the lesions encroach upon the layer pre-α or layer II of the entorhinal region. The layer gradually sinks into a deeper position in the transentorhinal region. The lesions also make headway into the hippocampus (Figure 3b). In stage III, the lesions in the hippocampal formation worsen. Entorhinal layers pre-α and, additionally, pri-α of the deep layers become strongly involved. Lesions extend through the transentorhinal region into the adjoining high order sensory association areas of the

temporal neocortex (Figure 3c). Additionally, it is revealed the severe involvement of the entorhinal cortex (anterior portions of the parahippocampal gyrus) at stage III and the tendency of the pathology to extend from there into the adjacent neocortex, i.e., occipito-temporal gyrus laterally and lingual gyrus posteriorly (Figure 3d). In stage IV, the third and fourth sectors of the Ammon's horn and a large portion of the insular cortex become affected. The involvement of the neocortical high order sensory association cortex of the temporal lobe now extends up to the medial temporal gyrus and stops short of the superior temporal gyrus. The primary fields of the neocortex and, to a large extent, also the premotor and first order sensory association areas of the neocortex remain intact (Figure 3e). In stage V, in addition to the presence of AD-related lesions in all of the regions involved in stage IV, pathological changes appear in the superior temporal gyrus and even encroach to a mild degree upon the premotor and first order sensory association areas of the neocortex (Figure 3f). Also, in the occipital lobe, the peristriate region shows varying degrees of affection, and lesions occasionally can even be seen in the parastriate area (Figure 3g). Ultimately, in stage VI, the pathology reaches even the first order sensory association areas (e.g., the parastriate area) and the primary areas of the neocortex (e.g., the striate area) of the occipital neocortex (Figure 3h,i).

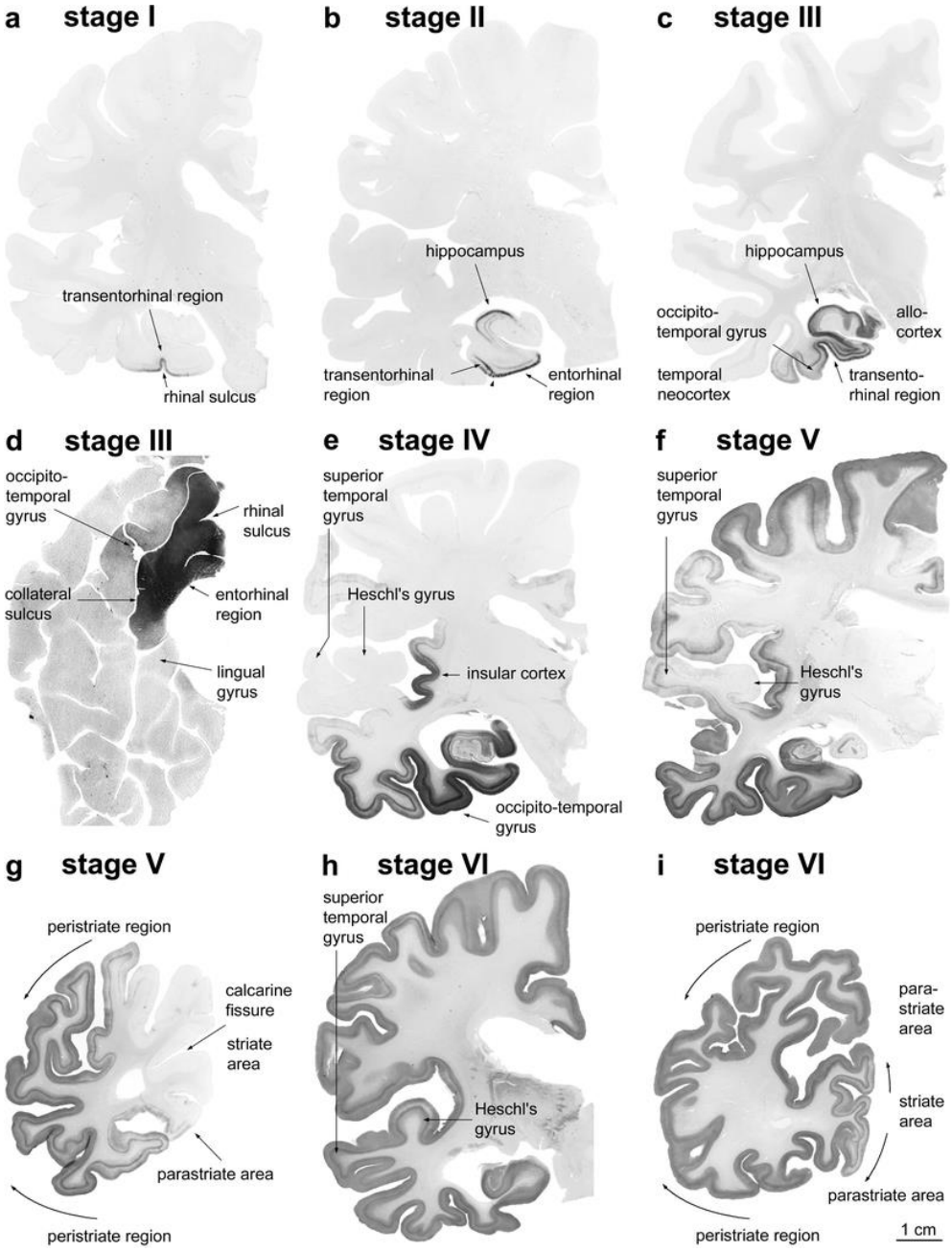

Figure 3 - Stages I-VI of cortical neurofibrillary pathology in 100 µm polyethylene glycol-embedded hemisphere sections immunostained for hyperphosphorylated tau (AT8, Innogenetics). ***a*** *Stage I: Lesions develop in the transentorhinal region.* ***b*** *Stage II: Lesions extend into the entorhinal region.* ***c,d*** *Stage III: Lesions extend into the neocortex of the fusiform and lingual gyri.* ***e*** *Stage IV: The disease process progresses more widely into neocortical association areas.* ***f,g*** *Stage V: The neocortical pathology extends fanlike in frontal, superolateral, and occipital directions, and reaches the peristriate region.* ***h,i*** *Stage VI: The pathology reaches the secondary and primary neocortical areas and, in the occipital lobe, extends into the striate area. Adapted from Braak et al., 2006.*

2. Choroid plexus

For decades, the choroid plexuses have attracted much attention because of their contribution to cerebrospinal fluid (CSF) formation and because they are strikingly dissimilar to most other transporting epithelia. The choroid plexus (CP) epithelium is a secretory epithelium par

excellence with unique cellular transport mechanisms being the most efficient tissue in terms of secretory rate (Damkier et al., 2013).

2.1 Location and structure

The CP is a highly vascularised tissue that is located within each ventricle of the brain: one in each of the two lateral ventricles, one in the third, and one in the fourth ventricle (Figure 4).

CSF flows from the lateral to the third ventricle via the interventricular foramina (also known as the foramen of Monro), and then through the cerebral aqueduct to the fourth ventricle (Figure 4). Subsequently, the CSF flows down the central canal of the spinal cord or circulates in the subarachnoid space, where it is reabsorbed by arachnoid villi and granulations (Lehtinen & Zappaterra, 2011; Damkier et al., 2013), either by classical lymphatics in sinonasal tissues that underlie the cribriform plate (Johnston et al., 2005; Koh et al., 2006) or by the recently described meningeal–dural sinus lymphatics (Louveau et al., 2015) back into the systemic circulation or to regional and cervical lymph nodes. Blood flow and CSF secretion are thought to be regulated in part by sympathetic and parasympathetic innervations (ter Laan et al., 2013; Damkier et al., 2013).

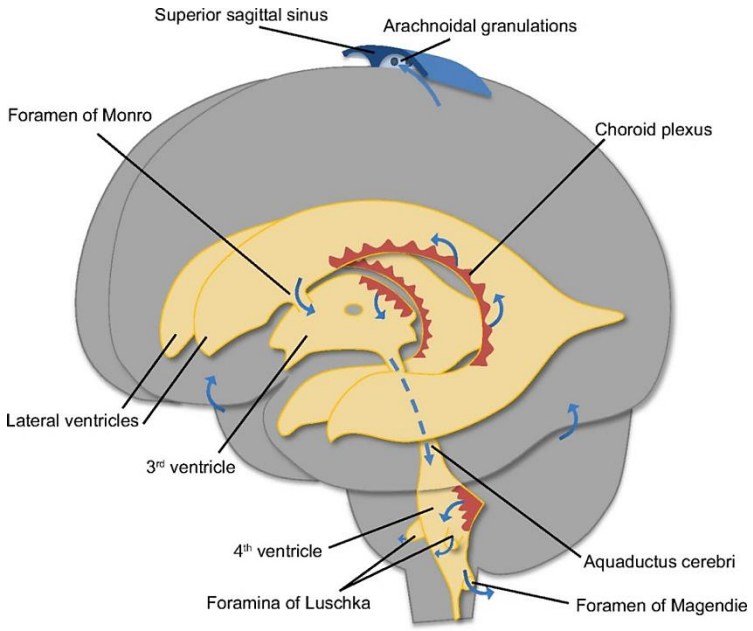

Figure 4 - Organization of the ventricular system of the brain. *The brain parenchyma is shown in gray, the ventricles and aquaducts are in yellow, and the choroid plexuses are marked in red. Cerebrospinal fluid is formed by the choroid plexus of the two lateral ventricles, the 3rd and 4th ventricles. Lateral ventricle fluid converges in the 3rd ventricle via the foramen of Monro and reaches the 4th ventricle via the aquaductus cerebri. The cerebrospinal fluid exits from the 4th ventricle through the foramina of Magendie and Luschka to the outer surface of the central nervous system. The majority of the fluid is reabsorbed in the arachnoidal granulations draining to the superior sagittal sinus. Adapted from Damkier et al., 2013.*

The CP has a relatively simple structure, similar in the lateral, third and fourth ventricles. It consists of a single layer of cuboidal to low cylindrical epithelial cells that reside on a basement membrane and surround a core of capillaries and connective tissue (Figure 5) (Damkier et al., 2013; Mortazavi et al., 2014). The epithelial cells are joined by tight junctions, which form the blood–CSF barrier (Lun et al., 2015). Unlike the endothelium in the brain's parenchyma, capillaries of the CP are fenestrated (Wolburg & Paulus, 2010). These endothelial fenestrae are connected by thin membranous diaphragms that are permeable to small molecules and water, thus enabling the rapid delivery of water via the blood to epithelial cells for CSF production. Solutes may cross from the blood into the stromal space by diffusion across endothelial fenestrae or by vesicular transport (Lun et al., 2015). As with capillaries in other tissues, pericytes are found in the CP and wrap around the endothelial cells. Finally, the CP harbours various immune cells and is considered to be a gateway for immune cell entry into the CNS (Ransohoff & Engelhardt, 2012; Lun et al., 2015).

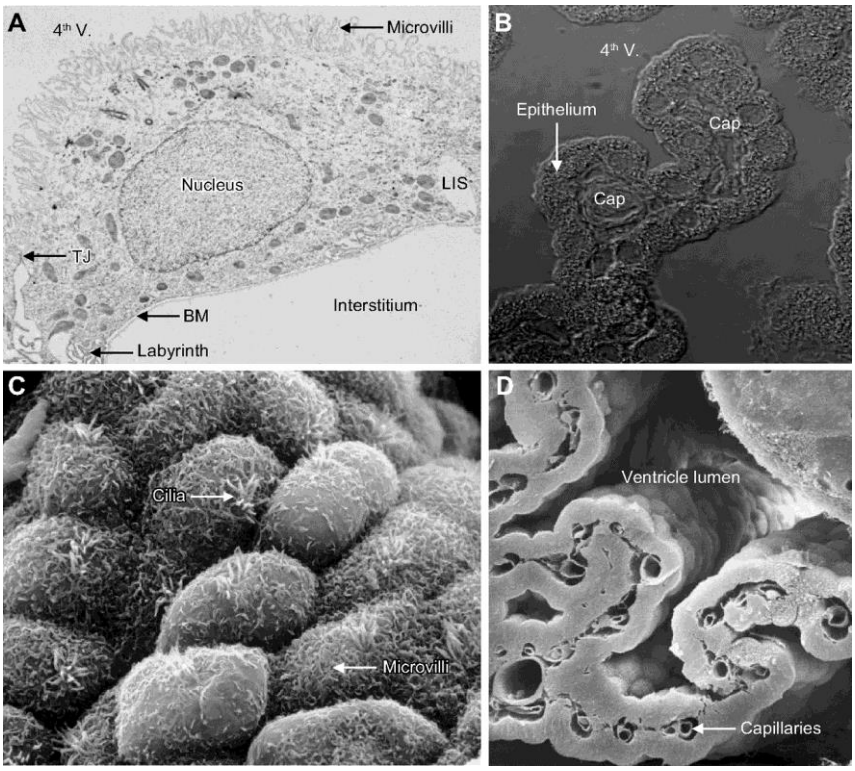

Figure 5 - Choroid plexus ultrastructure. *A: transmission electron micrograph of a rat CP epithelial cell. The luminal surface contains numerous microvilli and is separated from the lateral intercellular space (LIS) by tight junctions (TJ). A labyrinth of plasma membrane infoldings is seen at the border between the relatively smooth lateral and basal membranes. The basement membrane (BM) separates the epithelium from the interstitium, which in this image lacks its connective tissue because of the preparation technique. B: differential interference contrast micrograph of the tip of a 4th ventricle (4th V) - CP villus with its capillaries (Cap) in the sparse interstitial connective tissue and the single layer of cuboidal epithelium. C: scanning electron micrograph of the ventricular surface of human CP. Examples of microvilli and motile cilia are indicated. D: cryo-fractured preparation of mouse CP. The capillaries of the sheetlike CP and the lateral ventricle lumen are indicated. Adapted from Damkier et al., 2013.*

2.2 The choroid plexus as a 'bioreactor' to brain diseases - impact on AD

Choroidal epithelial cells can be regarded as 'bioreactors' that respond to chemical changes in extracellular fluid. Their response includes the synthesis of peptides, growth factors and sundry molecules for homeostatically repairing injured neurons. CP epithelium together with other interfaces handle catabolites and peptide fragments (Johanson et al., 2004) by reabsorbing them into the systemic circulation for clearance or by sequestering toxic substances in lysosomes for metabolic conversion. Signalling molecules are also carried from diseased regions of the brain to the CP where they bind to specific receptors and consequently elicit a variety of bioreactive responses (Chodobski et al., 2001).

Accumulating evidence supports the idea that continuous decrease of CP function in advanced ageing exacerbates AD. Structural alterations and functional failures in CP as well as brain capillary transport systems adversely affect fluid dynamics and composition. Efficient CSF turnover is essential for a healthy brain; it depends upon an exquisite balance between CSF formation and reabsorption (Johanson et al., 2004). Compromised secretory phenomena at the CP predispose the brain to AD-type problems. On the other hand, defective clearance of CSF at the arachnoid membrane leads to normal pressure hydrocephalus (NPH) (Silverberg et al., 2003). The pivotal role of the CP in CSF homeostasis and brain viability becomes more evident when the system fails.

Involvement of the CP in AD is reflected by increased amyloid burden (Fig. 6a), impaired mitochondrial function and oxidative stress damage in CP tissue (Perez-Gracia et al., 2009; Krzyzanowska & Carro, 2012). These pathogenic processes along with morphological structural changes contribute to decreased efficacy of CP in clearing *Aβ*, thus resulting in increased *Aβ* accumulation in the brain. This in turn induces further pathological cascades of toxicity, inflammation and neurodegeneration, which may enhance the disease process.

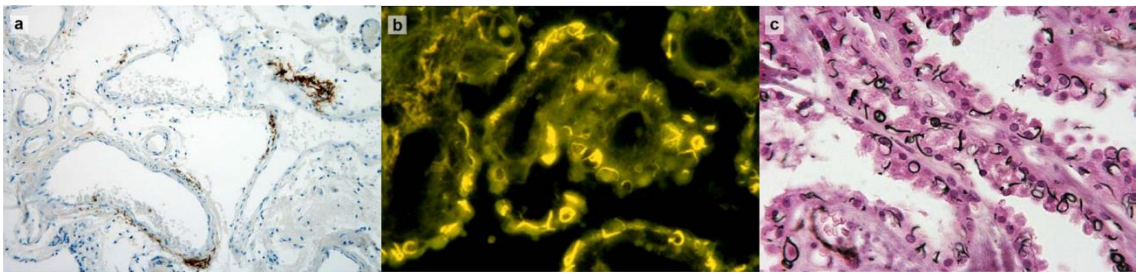

***Figure 6 - Involvement of the choroid plexus in Alzheimer's disease**. a: Deposition of Aβ in blood vessel walls of choroid plexus stroma (immunohistochemistry for Aβ). b,c: Biondi ring tangles are annular, serpentine or curled inclusion in the cytoplasm of choroid plexus epithelial cells, as visualized using thioflavin S (b) and Jones' methenamine silver stain (c). Modified from Wolburg et al., 2010.*

2.2.1 Morphological alterations

The CP is subject to morphological and physiological changes that produce a wide range of effects. In AD the CP develops abnormalities similar to those observed with aging, although greatly enhanced. In LOAD, there are CP significant changes: epithelial atrophy, thickening of the basement membrane, and stroma fibrosis. Epithelial atrophy is significantly accentuated: a decrease in cell height is observed compared to age-matched controls (Krzyzanowska & Carro, 2012). Epithelial cells acquire Biondi bodies (ring-like structures) and numerous lipofuscin deposits (Alvira-Botero & Carro, 2010). Nuclei become irregular and flattened, and the basement membrane is thickened. The stroma thickens and contains collagen fibres, hyaline bodies, calcifications and psammomas (Serot et al., 2000). These modifications explain the decrease of functional capacities of CP, including synthesis, secretion, and transport of proteins and other molecules.

2.2.2 *Aβ* deposits

Besides accumulating in brain parenchyma, *Aβ* also accumulates in CP and in cerebrovascular walls, where it induces blood-brain barrier disruption (Spuch et al., 2012; Dietrich et al., 2008). Recent studies suggested the existence of a direct relationship between *Aβ* deposits at CP epithelium and the development of a functional and structural disruption of the organ (Dietrich et al., 2008; Vargas et al., 2010).

CP has been reported to produce several key enzymes involved in *Aβ* production, metabolism, and alternate processing (Crossgrove et al., 2007). Soluble *Aβ*, a product of the secretory pathway in amyloid precursor protein (*APP*) processing, is produced by the CP as observed in both rat and human post-mortem tissue (Krzyzanowska & Carro, 2012).

The source of *Aβ* deposited in the CP is unclear, but A*β* is probably taken up by CP epithelial cells from the CSF (Crossgrove et al., 2005). Deposition of A*β* in the CP may be mediated by interactions of *Aβ* and *aquaporin-1*, the latter being restricted to the CP in the normal brain but expressed by reactive astrocytes under pathological conditions (Misawa et al., 2008). Furthermore, there is evidence that circulating insulin-like growth factor-1 (*IGF-1*) participates in brain *Aβ* clearance by modulating CP function, because blockade of the *IGF-1* receptor on CP exacerbates AD-like pathology in old transgenic mice (Carro et al., 2006). Substances produced by the CP and secreted into the CSF may bind *Aβ* and subsequently affect Alzheimer pathology. Furthermore, Biondi ring tangles are markedly increased in CP epithelial cells and ependymal cells during aging (with a sharp rise at about 45 years) and in AD. These annular, serpentine, or curled inclusions (Fig. 6b, c) with histochemical properties of amyloid are biochemically and ultrastructurally different from neurofibrillary tangles and from *β* amyloid, suggesting that they represent a distinct type of filaments accumulating in the aged and diseased CP. It has been suggested that Biondi ring tangles may be among the earliest manifestations of AD. The exact

molecular nature of these enigmatic structures and their functional consequences remain to be determined (Wolburg et al., 2010).

2.2.3 Impaired mitochondrial function

Mitochondrial dysfunction is one of the earliest deficits identified in AD brains (Wang et al., 2014; García-Escudero et al., 2013). It has been described that mitochondrial enzyme activity defects occur in hippocampal neurons and choroidal epithelial cells more frequently in AD patients (Cottrell et al., 2001). An increase in the number of *COX*-deficient choroidal epithelial cells provides strong evidence that a substantial decline of mitochondrial enzyme activity occurs more frequently in AD than in normal aging. This deficiency in mitochondrial enzyme activity is likely to result in decreased transport across the epithelial cells and thus have implications in choroidal *Aβ* clearance (Krzyzanowska & Carro, 2012). *Aβ* itself can also impair mitochondrial function (Readnower et al., 2011) and since *Aβ* deposits accumulate in the CP of AD patients (Dietrich et al., 2008), it is likely that *Aβ* interferes with their function. A recent study showed that mitochondrial dysfunction in CP from AD subjects occurs through a down-regulation of mitochondrial proteins and activity (Vargas et al., 2010).

2.2.4 Oxidative stress and cell death

Oxidative damage to proteins is a relative early phenomenon in the pathogenesis of AD. It has been reported in hippocampus and inferior parietal lobules of MCI and AD cases (Butterfield et al., 2006; Reed et al., 2008). In the CP it occurs at later stages of AD compared with other brain areas (Perez-Gracia et al., 2009). Such oxidation may result in impaired protein interaction, protein folding and protein kinase activity; abnormal function of endothelial and vascular smooth muscle cells, and impaired *HDL*-cholesterol metabolism, thus having important implications in the deterioration of CP functions (Perez-Gracia et al., 2009; Krzyzanowska & Carro, 2012).

Abnormal patterns of stress protein expression were found in cerebral cortex and hippocampus of AD subjects (Anthony et al., 2003). Moreover, heat shock proteins such as *HSP90* and *GRP94*, presumably reflecting stress response, are upregulated in CP of AD patients (Johanson et al., 2004).

An increase in nitric oxide (NO) production by CP of AD patients was also reported and associated with *Aβ* deposits (Vargas et al., 2010). Excessive generation of NO has been implicated in the pathogenesis of AD (Aliyev et al., 2004), and plays an important role in *Aβ*-induced mitochondrial dysfunction (Keil et al., 2004). *Aβ* could interfere with oxidative phosphorylation, which results in oxidative stress.

Aβ is also involved in cell death pathway in CP, since increased expression of caspases 3 and 9 in *Aβ*-treated CP epithelial cells and *APP* transfected cells was reported by several studies

(Vargas et al., 2010; Krzyzanowska & Carro, 2012). Furthermore, inhibition of *Aβ* levels through viral-directed overexpression of gelsolin reduced cell death in CP of *APP*/*PSEN1* transgenic mice (Antequera et al., 2009), suggesting that deposition of *Aβ* is neurotoxic for CP epithelial cells.

3. Cerebral cortex

The cerebral cortex plays a key role in the most complex neural functions, such as sensory perception, voluntary control of movement, language, personality traits, and other sophisticated mental events, such as thinking, memory, decision making, creativity, and self-consciousness. It is the highest, most complex, integrating area of the brain (Sherwood, 2013).

The human cerebral cortex undergoes numerous structural changes over the lifespan. In AD, the loss of neurons and subsequent axonal degeneration leads to cerebral atrophy; the structural effects on the cerebral cortex include widening of sulci and thinning of the cortical ribbon (McGinnis et al., 2011).

3.1 The structure and functional localization of the cerebral cortex

The cerebral cortex is a complex, highly organized, six-layered structure that contains hundreds of different neuronal cell types and a diverse range of glia (Gaspar & Vanderhaeghen, 2011).

The six layers are numbered I-VI from superficial to deep (Figure 7). Layer I is the molecular layer, which contains very few neurons; layer II the external granular layer; layer III the external pyramidal layer; layer IV the internal granular layer; layer V the internal pyramidal layer; and layer VI the multiform, or fusiform layer. Each cortical layer contains different neuronal shapes, sizes and density as well as different organizations of nerve fibers (Barret & Simmons, 2015).

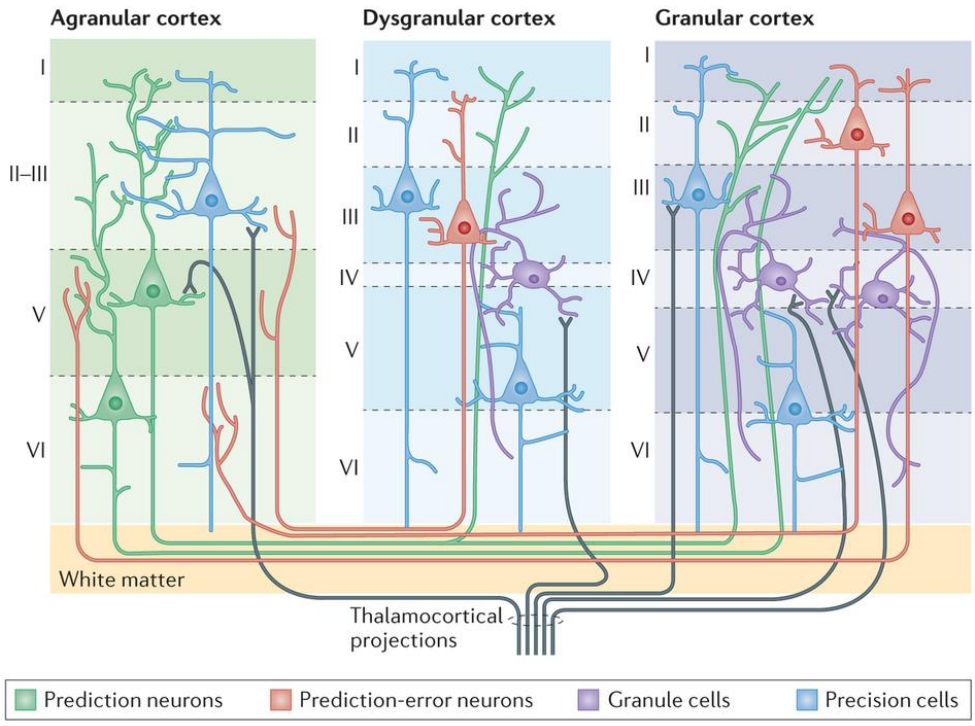

***Figure 7 - Illustration of intracortical architecture and intercortical connectivity**. Cortical columns are defined by different numbers of layers, with each layer having characteristic cell types and patterns of intracortical and intercortical connectivity. Cortical areas that lack a layer IV are called agranular. Cortical areas that have only a rudimentary layer IV are called dysgranular. Adapted from Barret & Simmons, 2015.*

3.2 Orbitofrontal cortex

The orbitofrontal cortex (OFC) is a region in the prefrontal cortex of the brain that is involved in the cognitive processing of decision-making. The OFC is so named because of its position on top of the eye orbits (Figure 8). In humans it consists of Brodmann area 10, 11 and 47 (Kringelbach, 2005). The prefrontal cortex (PFC), latest evolutionary addition to the mammalian brain, has long been known to endow qualities that differentiate human beings from all other animals. Yet the clinicians considered it "a silent" area in the absence of clinically discernible neurological deficits following its damage (Tandon, 2013).

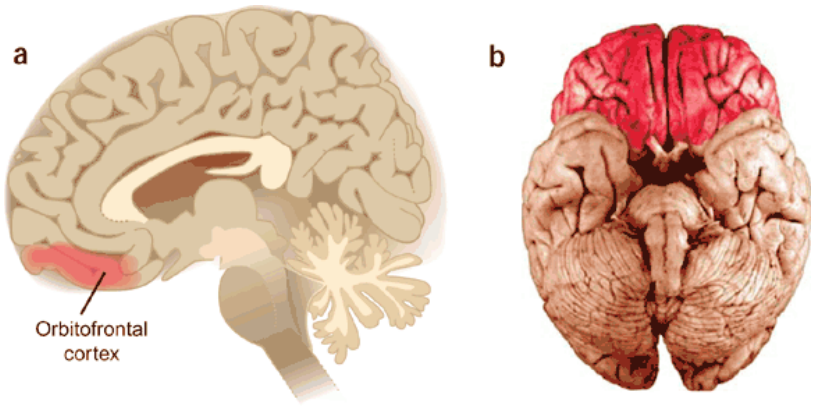

Figure 8 - (a) A schematic of a mid-sagittal section through the head, depicting the OFC (red shaded region). (b) A post-mortem photograph of the ventral surface of the brain. The OFC is so named because of its position on top of the eye orbits. Adapted from Wallis, 2006.

The human OFC is among the least-understood regions of the human brain; but it is considered among the most polymodal regions of the brain. OFC receives multi-sensory inputs of taste, smell, auditory, visual and somatosensory as well as visceral signals, due to its wide and deep connections to functionally diverse cortical and subcortical regions, including the amygdala, cingulate cortex, insula, hypothalamus, hippocampus, striatum, as well as its neighbouring dorsolateral prefrontal cortex (Kringelbach, 2005; Nestor et al., 2013).

The OFC is located between the frontopolar gyri rostrally, the anterior perforated substance caudally, the inferior frontal gyrus laterally and the ventromedial margin of the cerebral hemisphere medially (Chiavaras & Petrides, 2000). Its anatomically heterogeneous sulcogyral morphology (Chiavaras & Petrides, 2000; Nakamura et al., 2007) is thought to be reflective of the rich molecular processes underlying neuronal migration, local neuronal connection, synaptic development, as well as lamination and formation of cytoarchitecture (Nestor et al., 2013).

Medial and lateral OFC regions can be dissociated, both functionally and anatomically. The medial OFC has its strongest connections to the hippocampus and associated areas of the cingulate, retrosplenial and entorhinal cortices and anterior thalamus, which would also be consistent with its involvement in higher order cognition, especially declarative episodic memory. On the other hand, while the lateral OFC also has strong connections to brain regions critical for higher order cognition, its links to the inferior parietal lobule and dorsolateral prefrontal cortex may suggest a special role in traits related to detecting and evaluating social threats to self-interest (Spitzer et al., 2007, Nestor et al., 2013).

When OFC connections are disrupted, a number of cognitive, behavioural, and emotional consequences may arise. In humans, damage to the orbitofrontal cortex causes major changes in emotion, personality, behaviour and social conduct. Patients often show lack of affect, social inappropriateness and irresponsibility (Hornak et al., 2003; Kringelbach et al., 2005).

Some dementias have been associated with OFC connectivity disruptions (Seeley et al., 2008). Some research suggested that later stages of AD are impacted by altered connectivity of OFC systems (Tekin & Cummings, 2002). Moreover, neurofibrillary tangles involving the OFC bilaterally have been associated with agitation and aggression in patients with MCI and AD (Trzepacz et al., 2013).

4. Olfactory and Taste Receptors

Olfactory receptors (*ORs*) and taste receptors (*TRs*) account for over half of the G protein-coupled receptors (*GPCRs*) repertoire (Kanageswaran et al., 2015). *GPCRs* are seven transmembrane-spanning proteins that represent the largest receptor superfamily in the human genome (Katritch et al., 2013). *GPCRs* recognize and bind an array of sensory inputs and ligands, including photons, ions, bioamines, lipids, carbohydrates, peptides and proteins, as well as a diverse range of volatile compounds. Ligand-induced activation of *GPCRs* converts extracellular stimuli into intracellular signals, mediating diverse cellular and physiological responses, including the senses of smell, taste, and vision. Not surprisingly, mutations and modifications of *GPCRs*, G proteins and their regulatory partners are linked to dysfunction and disease (Overington et al., 2006; Foster et al., 2013b), and the importance of these receptors is reflected in the fact that 40% of drugs on the market target *GPCRs*.

4.1 Olfactory Receptors

4.1.1 Olfactory receptor genes

With the sequencing of mammalian genomes, it is now clear that there are around 900 olfactory receptors (*ORs*) in humans (including pseudogenes) and ~1500 in rodents (representing 3–5% of all encoded genes) (Gaillard et al., 2004, Aloni et al., 2006, Henion et al., 2007, Niimura et al., 2007). In humans, there are 390 putatively functional (protein-coding) *OR* genes (Adipietro et al., 2012).

ORs are genes of around 1 kb in length and characteristically possess a hypervariable sequence region in the transmembrane segments, which constitutes the putative odorant binding pocket (Lagerstrom & Schioth, 2008). They are distributed throughout the genome, residing in clusters of various sizes on nearly all chromosomes (except chromosomes 20 and Y) (Figure 9).

ORs are highly variable at a sequence level, and are further grouped into 18 families and hundreds of subfamilies defined by their aminoacid identity (Olender et al., 2008). While forming the largest group of *GPCRs*, the *OR* repertoire is still small in comparison to the number of potential odorants. To some extent, this is explained by the capacity of *ORs* to detect odorants in a 'combinatorial' manner, whereby one *OR* recognizes multiple odorants and one odorant is detected by multiple *ORs* (Niimura, 2012).

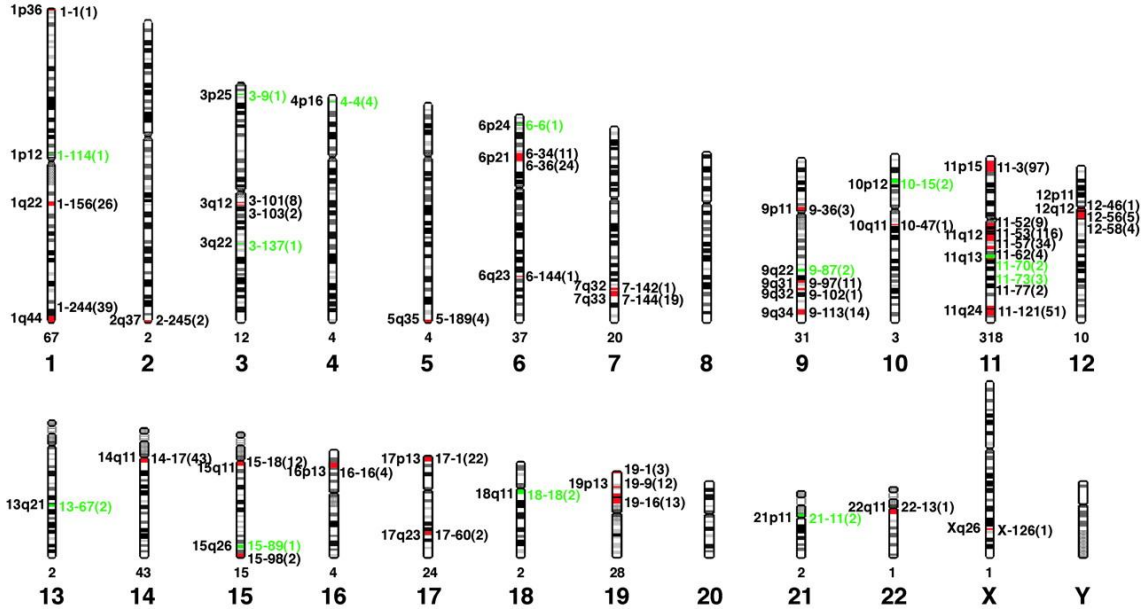

Figure 9 - Chromosome locations of human OR genes. *Six hundred thirty OR genes were localized to 51 different chromosomal loci distributed over 21 human chromosomes. OR loci containing one or more intact OR genes are indicated in red; loci containing only pseudogenes are indicated in green. The cytogenetic position of each locus is shown on the left, and its distance in megabases from the tip of the small arm of the chromosome is shown on the right (chromosome-Mb). The number of OR genes at each locus is indicated in parentheses, and the number of OR genes on each chromosome is indicated below. Adapted from Malnic et al., 2004.*

4.1.2 *ORs* expression

The *ORs* were first identified in the olfactory system, being expressed in the cilia of olfactory sensory neurons in the olfactory epithelium (OE). However, soon after their initial discovery, reports surfaced of so-called 'ectopic' expression of "olfactory-like" receptors outside of the OE (Kang & Koo, 2012). Moreover, despite the label "olfactory receptor" only a subset (~75%) of the OR repertoire is actually expressed in the OE (Zhang et al., 2007).

While it is true that the expression level of *ORs* is highest within the OE, it is now clear that at least some *ORs* are expressed in a variety of additional tissues. With new techniques such as whole transcriptome sequencing, the list of "ectopic *ORs*" has greatly expanded in the last few years, and these sites now include, for example, the gastrointestinal (GI) tract, muscle, heart, pancreas, liver, lung, and skin (Spehr et al., 2003; Feldmesser et al., 2006; Griffin et al., 2009; Kang & Koo, 2012; Pluznick & Caplan, 2012; Kim et al., 2015; Wu et al., 2015; Shepard & Pluznick, 2016). An overview of identified human *ORs* expressed in non-chemosensory tissues is shown in more detail in *Supplementary Table 1*.

While the physiological functions that each of these *ORs* plays in non-chemosensory tissues remain an ongoing area of research, it is evident that *ORs* serve important roles in physiology. Notably, murine and human *ORs* have been found in sperm and play a key role in sperm chemotaxis (Spehr et al., 2003; Fukuda et al., 2004).

ORs have been also identified in several areas of the brain such as the cerebral cortex in mice (Kang & Koo, 2012) and the murine choroid plexus (Gonçalves et al., 2016). The presence of *ORs* and some obligate downstream components of *OR* signalling was also demonstrated in neurons of the cerebral cortex and other regions in the human brain (Garcia-Esparcia et al., 2013). These studies speculated on the possibility that some predicted *OR* genes may not be olfactory receptors *per se*, but may subsume other functions.

4.1.3 Olfactory signal transduction in olfactory neurons

ORs display a highly specialized signal transduction pathway (Figure 10). This canonical pathway involves the coupling of odorant-bound receptor to a G protein called Ga_{olf} and activation of an olfactory isoform of adenylyl cyclase (*AC3*) to generate the second messenger cyclic adenosine monophosphate (*cAMP*) (Wong et al., 2000). Elevated levels of cellular *cAMP* in turn activate cation-selective cyclic nucleotide-gated (CNG) channels that lead to increased permeability to Ca^{2+} ions (Zheng & Zagotta, 2004), membrane depolarization and the generation of action potentials in olfactory neurons.

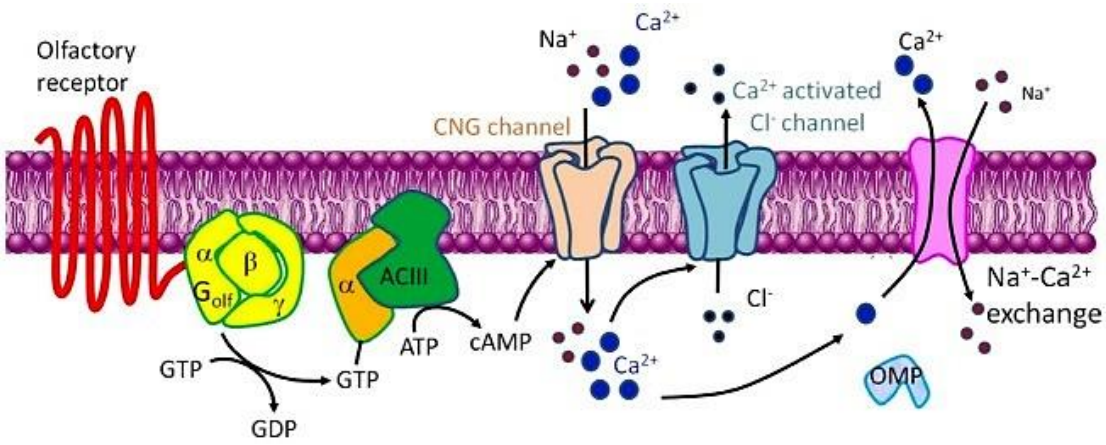

***Figure 10 - A schematic diagram of olfactory signal transduction**. The olfactory signaling pathway involves the coupling of ligand bound receptors to the olfactory isoform of the heterotrimeric G protein Gaolf and the activation of adenylyl cyclase (ACIII) to generate cAMP as a second messenger. This leads to influx of Ca2+ via cyclic-nucleotide gated channels (CNG), membrane depolarization and the generation of action potentials in neurons. Adapted from Kang & Koo, 2012.*

4.2 Taste Receptors

The mammalian gustatory system recognizes five basic taste qualities: sweet, umami, bitter, salty and sour, which together enable the assessment of nutritional value of food constituents, while avoiding potentially harmful substances. In the past two decades, the molecular mediators of sweet, umami and bitter tastes have been identified as families of *GPCRs*, referred to collectively as taste receptor type 1 (*T1R*) and taste receptor type 2 (*T2R*). The *T1R* family has 3 members that form sweet and umami receptors, whereas the *T2R* family consists of 25 highly divergent *GPCRs* that mediate bitter taste. In addition, there is evidence that another

taste quality related to lipid sensing is mediated via the free fatty acid (*FFA*) *GPCR* family (Foster et al., 2014).

The five taste qualities are detected by specialized taste receptor cells located in the oral cavity. Here, taste receptor cells occur in morphological structures of 50–100 cells, called taste buds (Figure 11). The majority of taste buds are found on the tongue surface embedded in gustatory papillae, on the soft palate and on the throat (Chaudhari & Roper, 2010; Roper, 2013). Within each taste bud a variety of specialized cells are found, which can be classified by functional and morphological characteristics. The type II cells express taste receptors of the *GPCR* type, type III cells form synapses with afferent nerve fibers, type I cells are believed to have supporting functions and type IV cells, located at the basal parts of taste buds, are a pool of undifferentiated precursor cells devoted to replace the other cell types throughout life (Chaudhari & Roper, 2010).

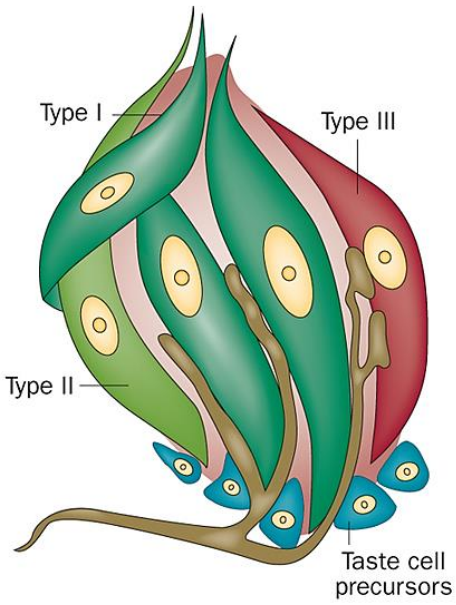

Figure 11 - Schematic representation of a taste bud. The diagram shows an onion-like taste bud structure and the four subtypes of taste bud cells. Of the four subtypes, only type III taste bud cells form recognizable synapses with the afferent nerve fibres. Adapted from Calvo & Egan, 2015.

4.2.1 Taste receptor genes

Taste receptors are divided into two groups: *GPCRs* and channel type receptors (Chaudhari & Roper, 2010, Niki et al., 2010).

Sweet and umami taste are recognized by the taste receptor type 1 (*T1R*; genes are designated *TAS1* in humans and *Tas1* in rodents) family - *T1R1, T1R2* and *T1R3* - that belongs to family C of *GPCRs* (Vegezzi et al., 2014, Niki et al., 2010). *T1Rs* assemble into heterodimeric receptor complexes to function as sweet (*T1R2*+*T1R3*) or umami (*T1R1*+*T1R3*) taste receptors (Nelson et al., 2001, 2002; Niki et al., 2010). Thus the *T1R2*+*T1R3* heterodimer is activated by various sweeteners (i.e., sugars, artificial sweeteners, sweet amino acids, and sweet proteins),

whereas the *T1R1+T1R3* heterodimer is activated primarily by monosodium L-glutamate in humans and by amino acids in animals (i.e., mouse) (Nelson et al., 2002; Li et al., 2002; Niki et al., 2010).

Bitter taste is recognized by the taste receptor type 2 (*T2R*) family that belongs to family A of *GPCRs* (Niki et al., 2010, Meyerhof et al., 2010). A list of human and mouse *T1R* e *T2R* genes, including their names, synonyms, and orthologues, can be found in *Supplementary Table 2*, and can also be found in human and mouse genome databases. In humans, ~25 members of the *T2R* family may function as bitter taste receptors detecting and responding to an incredibly broad range of structurally diverse aversive and toxic compounds (Niki et al., 2010, Meyerhof et al., 2010; Clark et al., 2012; Vegezzi et al., 2014). These receptors are single exon genes that characteristically possess very short N-terminal extracellular domains. Although bitter taste is evoked by perhaps tens of thousands of synthetic and natural compounds (Clark et al., 2012), bitter ligands for some of the *T2Rs* (i.e., *T2R41, T2R42, T2R45, T2R48, T2R60*) are still unknown (Niki et al., 2010, Meyerhof et al., 2010). The number of compounds perceived by humans as bitter is much larger than the number of human *TAS2R* genes, implying that each human *T2R* responds to more than one bitter ligand (Behrens & Meyerhof, 2006). The same is likely to be true for other species. Some *T2Rs* interact with a wide range of bitter tasting ligands (e.g., *TAS2R14* and *TAS2R16*; see *Supplementary Table 3*). However, some other *T2Rs* appear to have narrow ligand specificities (e.g., *TAS2R5*).

4.2.2 Taste receptors expression

Taste *GPCRs* are often low abundance genes and appear below the limits of detection of arrays, compounded by the fact that arrays often are not optimized to detect taste *GPCRs* (Insel et al., 2012). In any case, small scale RT-PCR screens have provided ample transcript data to lay the foundations for investigation of taste receptors beyond the mouth. In addition to the oral cavity, *TASRs* expression has been detected in a variety of tissues including the respiratory and cardiovascular system, digestive tract, pancreas, liver, kidney, heart, testis, several mouse forebrain regions and choroid plexus (Ren et al., 2009; Behrens & Meyerhof, 2010; Meyer et al., 2012; Yamamoto & Ishimaru, 2013; Xu et al., 2013; Foster et al., 2013b; Tomás et al., 2016). Bitter *TASRs* together with downstream functional mediators were also found to be expressed in the brain of rats and in frontal cortex in humans (Singh et al., 2011; Dehkordi et al., 2012; Garcia-Esparcia et al., 2013) and in the choroid plexus of rats (Tomás et al., 2016). An overview of identified human *TASRs* expressed in non-chemosensory tissues is shown in more detail in *Supplementary Table 4*.

4.2.3 Taste signal transduction

Despite the structural and functional differences between the *T1R* and *T2R GPCRs*, the canonical taste transduction cascade downstream of receptor activation shares common elements (Figure 12). These include: the heterotrimeric G protein subunits - Ga_{t3} (also known as *α-gustducin* or *GNAT3*), *Gβ3* and *Gγ13* - a phospholipase C, *PLCβ2*, and a transient receptor potential ion channel, TRPM5 (Niki et al., 2010).

Tastants binding to sweet, umami, and bitter receptors activate the α-gustducin, and subsequent stimulation of phospholipase Cβ2 (*PLCβ2*) (Zhang et al., 2003). Activation of *PLCβ2* produces inositol-1,4,5-triophosphate (IP_3), a ligand for IP_3 receptor type 3 (*IP_3R3*) in the Ca^{2+} stores (Yasuo et al., 2008; Huang & Roper, 2010; Vegezzi et al., 2014). Then Ca^{2+} is released from intracellular calcium stores and stimulates TRPM5 which depolarizes the taste cell leading to the generation of action potentials by means of the voltage-gated sodium channels (VGSC) of cells (Yasuo et al., 2008; Niki et al., 2010; Vegezzi et al., 2014). The generation of action potential leads to the release of ATP through membrane depolarization-dependent channels. Then ATP is detected by receptors of the taste axons which convey information from the taste cells towards the brain (Figure 12) (Yasuo et al., 2008; Chaudhari et al., 2010; Chaudhari, 2014).

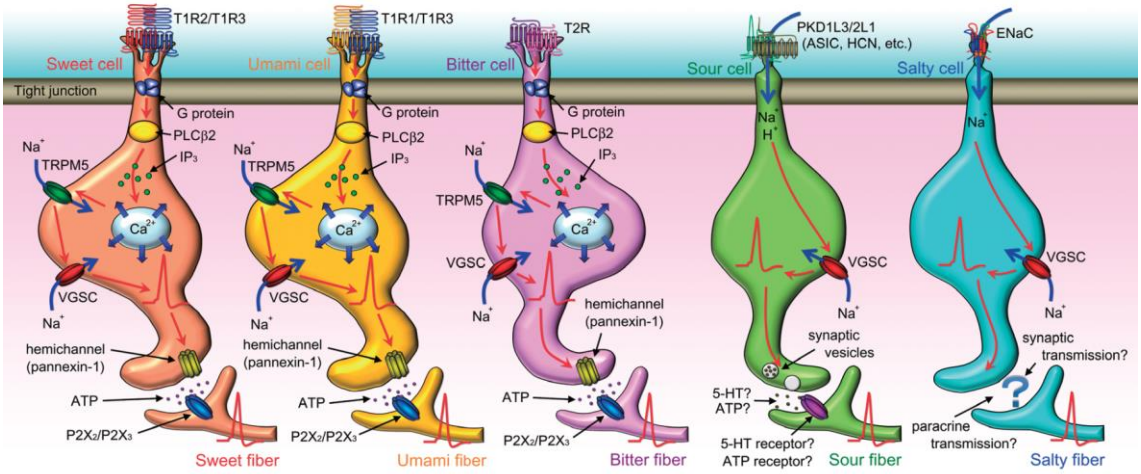

Figure 12 - Receptors and transduction mechanisms for each basic taste. *(VGSC: voltage gated sodium channel. 5-HT: serotonin).*

II. Aim

Aim

The main goal of the present work is to study the expression of the taste and olfactory receptors in the choroid plexus and the orbitofrontal cortex of AD patients. Towards this aim, transcriptomic analysis of taste and olfactory receptors will be performed by means of RT-qPCR and compared between AD patients (at different stages of the disease) and age-matched controls. Therefore, the specific objectives for this work are the following:

1. Design primers specific for taste and olfactory receptors.
2. Test primers and optimize RT-qPCR conditions.
3. Extract RNA from human post-mortem brain samples.
4. Perform RT-qPCR and analysis of data, comparing the mRNA expression levels of taste and olfactory receptors in human brain samples (choroid plexus and cortex) of AD patients and age-matched controls.

III. Materials and Methods

1. Samples

CP tissue was obtained from the Department of Pathology and Neuropathology (Xerencia de Xestión Integrada de Vigo – SERGAS, Spain) and the Neuropathology Brain Bank (HUB-ICO-IDIBELL Biobank) (Table 2). Orbitofrontal cortex tissue was obtained from the Neuropathology Brain Bank (HUB-ICO-IDIBELL Biobank) (Table 3). All samples were obtained following the guidelines both of Spanish legislation on this matter and of the local ethics committee. The postmortem interval between death and tissue processing was between 3 and 14 hours in all cases. The neuropathologic diagnosis of AD was based on the classification of Braak.

Table 2 - Pathological characteristics of patients - male choroid plexus samples.

Sample	Gender	Age	Diagnostic
1	M	44	C
2	M	40	C
3	M	52	C
4	M	52	C
5	M	80	C
6	M	63	C
7	M	28	C
8	M	73	AD I
9	M	64	AD I
10	M	68	AD I
11	M	64	AD I
12	M	67	AD I
13	M	58	AD I
14	M	63	AD I
15	M	63	AD I
16	M	70	AD I
17	M	55	AD II
18	M	65	AD II
19	M	60	AD II
20	M	70	AD II
21	M	73	AD III
22	M	81	AD III
23	M	77	AD III
24	M	82	AD III
25	M	76	AD III
26	M	79	AD IV
27	M	75	AD V
28	M	82	AD V

Table 3 - Pathological characteristics of patients - orbitofrontal cortex samples.

Sample	Gender	Age	Diagnostic
1	M	47	C
2	M	46	C
3	M	64	C
4	M	76	C
5	M	61	C
6	M	77	C
7	M	63	C
8	M	84	AD IV
9	M	74	AD IV
10	M	79	AD V
11	M	73	AD V
12	M	93	AD V
13	M	75	AD V
14	M	82	AD V
15	M	77	AD V
16	F	81	C
17	F	64	C
18	F	75	C
19	F	55	C
20	F	57	AD I
21	F	59	AD I
22	F	79	AD I
23	F	67	AD I
24	F	79	AD I
25	F	73	AD I
26	F	74	AD V
27	F	74	AD V
28	F	81	AD V
29	F	63	AD VI
30	F	86	AD VI
31	F	56	AD VI

2. Total RNA

2.1 Total RNA extraction

CP and OFC tissue samples were homogenized in 1mL TRIzol reagent (Life Technologies, CA, USA) using a PYREX potter tissue grinder. Homogenization occurs as the pestle is forced lower

into the tube and the sample is forced between the straight outside wall of the pestle and the inside wall of the tube, compressing the tissue cells until they rupture. TRIzol reagent maintains the integrity of the RNA due to highly effective inhibition of RNase activity while disrupting cells and dissolving cell components during sample homogenization. The homogenization process was followed by an incubation of 5 minutes at room temperature (RT) to permit complete dissociation of the nucleoprotein complex. Then 200 µl of chloroform (200 µl of chloroform per 1 mL of TRIzol reagent) were added and the samples were homogenized by shaking the tubes vigorously by hand for 15 seconds. Samples were incubated at RT for 2-3 minutes and then centrifuged at 12000 *g* for 15 minutes at 4°C. The mixture separates into a clear upper aqueous layer (containing RNA), an interphase, and a red lower organic (phenol-chloroform) layer (containing the DNA and proteins). RNA remains exclusively in the aqueous phase which represents ~50% of the total volume. The aqueous phase of the samples was removed by angling the tube at 45° and pipetting the solution out and avoiding drawing any of the interphase or organic layer into the pipette. The aqueous phase was then placed into a new tube to proceed to the RNA isolation procedure. To precipitate RNA from the aqueous layer 500 µl of 100 % isopropanol (500 µl of 100 % isopropanol per 1 mL of TRIzol reagent) were added, followed by incubation at RT for 10 minutes and centrifugation at 12000 *g* for 10 minutes at 4°C. The RNA is often invisible prior to centrifugation, and forms a gel-like pellet on the side and bottom of the tube. After removal of the supernatant from the tubes (leaving only the RNA pellet), the precipitated RNA was washed with 1 mL of 75% ethanol (1 mL of 75% ethanol per 1 mL of TRIzol reagent) to remove impurities. The samples were briefly vortexed and then centrifuged at 7500 *g* for 5 minutes at 4°C. Then the wash was discarded and the RNA pellets were air dried for 5-10 minutes, watching so they wouldn't dry completely and loose its solubility. Finally, the RNA pellets were resuspended in 20 µl of RNase-free water by passing the solution up and down several times through a pipette tip and incubated in a heat block set at 60 °C for 10-15 minutes. After quantification, samples were stored at -80°C.

2.2 Quality assessment and quantification of total RNA

2.2.1 Agarose Gel Electrophoresis

To assess the integrity of rRNA an aliquot of the RNA sample was run on a denaturing agarose gel stained with GelRed (Biotium, USA). GelRed is an ultra-sensitive, extremely stable and environmentally safe fluorescent nucleic acid dye designed to replace the highly toxic ethidium bromide for staining dsDNA, ssDNA or RNA in agarose gels or polyacrylamide gels. Intact rRNA run on a denaturing gel have sharp, clear 28S and 18S rRNA bands. The 28S rRNA band is approximately twice as intense as the 18S rRNA band. This 2:1 ratio (28S:18S) is a good indication that the RNA is completely intact. Partially degraded RNA has a smeared appearance, lack the sharp rRNA bands, or don't exhibit the 2:1 ratio of high quality RNA. Completely degraded RNA appears as a very low molecular weight smear. Inclusion of RNA size markers on

the gel allow the size of any bands or smears to be determined and also serve as a good control to ensure the gel was run properly.

2.2.2 Quantification

RNA quality and quantity control was also assessed using the NanoDrop ND-1000 UV-Vis Spectrophotometer (NanoDrop Technologies, USA) by UV measurement from the *A*260/*A*280 and *A*260/A230 ratios. The absorbance reading was directly converted into concentration (ng/ul) and both *A*260/280 and *A*260/230 absorbance ratios were given. The *A*260/280 ratio was used to assess the quality of DNA and RNA and only samples with ratios >1.7 were accepted. Any ratios appreciably lower than this could indicate protein contamination, which can lower reaction efficiency. The *A*260/A230 ratio was helpful in evaluating the carryover of components containing phenol rings such as the chaotropic salt guanidine isothiocyanate and phenol itself, which are inhibitory to enzymatic reactions. These ratios were often higher than the 260/280 and the values were commonly in the range of 2.0-2.2.

The measurement was made by pipeting 1 µl of the sample directly onto one measurement pedestal and then the spectrum and its analysis were shown on the screen of the attached computer.

2.3 Removal of genomic DNA contamination

No RNA isolation method can extract RNA that is completely free from DNA contamination. Genomic DNA contamination can shift Ct values dramatically in qPCR reactions, especially for genes with low expression levels. Further Dnase treatment is necessary for cases where the mRNA expression is low and there is potential genomic interference due to the use of intra-exon primers. Under some circumstances it is just not possible to design intron-spanning primers, which was the case of the genes in study.

Genomic DNA contamination was removed from RNA preparations, without incurring RNA loss or risk of degradation, using the TURBO DNA-free DNase Treatment & Removal Reagents (Ambion, USA). DNase Digestion Reagents (10X Turbo DNase Buffer and TURBO DNase) were added to the RNA samples according to the amount of contaminating DNA and the nucleic acid concentration of the sample for a rigorous DNase treatment, usually in a 20µL or 30µL reaction. After gently mixing, the samples were incubated at 37°C for 20 minutes. Then resuspended DNase Inactivation Reagent (typically 0.1 volume) was added and the samples mixed well, followed by an incubation of 5 minutes at room temperature. During the incubation period the tubes were flicked 2-3 times to redisperse the DNase Inactivation Reagent. The samples were then centrifuged at 10 000 *g* for 1.5 minutes and the supernatant, which contained the RNA, was carefully transferred into a fresh tube.

3. Reverse-Transcription

The synthesis of DNA from an RNA template, via reverse transcription, produces complementary DNA (cDNA) in a reaction catalysed by the enzyme reverse transcriptase.

cDNA synthesis was performed using the iScript™ cDNA synthesis kit (Bio-Rad, USA) according to its instructions manual. iScript cDNA synthesis kit provides a sensitive and easy-to-use solution for two-step RT-PCR. This kit includes just three tubes – iScript reaction mix (5x), nuclease-free water and iScript reverse transcriptase – a comprehensive of reagents required for successful reverse transcription. The iScript reverse transcriptase is RNase H+, which provides greater sensitivity than RNase H- enzymes in quantitative PCR. Also the enzyme is provided preblended with RNase inhibitor. The unique blend of oligo(dT) and random hexamer primers in the iScript reaction mix works exceptionally well with a wide variety of targets and this blend is optimized for the production of targets <1kb in length.

Usually for a 20 µL reaction, 4 µL of iScript reaction mix (5x) and 1 µL of iScript reverse transcriptase were added to a 0.2 ml PCR tube. Also up to 1µg total RNA were added to the tube and the final volume was made up with water. When using amounts of input RNA > 1µg, the reaction was scaled up, for example 40 µL for 2 µg, to ensure optimum synthesis efficiency. Then the complete reaction mix was incubated for 5 minutes at 25°C, 30 minutes at 42°C and 5 minutes at 85°C in a thermocycler (Thermal cycler 2400, Perkin).

4. Polymerase chain reaction (PCR)

cDNA generated by reverse transcription can be amplified using polymerase chain reaction (PCR). PCR involves the following three steps: Denaturation, Annealing and Extension. In the first step of the PCR process, the cDNA is denatured by heating to 95°C, which disrupts the hydrogen bonds between complementary strands, yielding single-stranded molecules. The temperature is then lowered in order to allow primers complementary to the sequence(s) of interest to anneal. The DNA polymerase included in the reaction will then begin DNA synthesis. At this point, the temperature is raised to the optimal activity temperature of the DNA polymerase (usually 72°C) to synthesize a new strand complementary to the template. The process of denaturing, annealing, and extension can be repeated multiple times, with a two-fold increase in the amount of DNA molecules with each cycle. Because PCR can selectively amplify a template, it is an important method for detecting specific nucleic acid molecules.

In traditional (endpoint) PCR, detection and quantification of the amplified sequence are performed at the end of the reaction after the last PCR cycle, and involve post-PCR analysis such as gel electrophoresis and image analysis. In real-time quantitative PCR, explained further below, PCR product is measured at each cycle. By monitoring reactions during the exponential

amplification phase of the reaction, users can determine the initial quantity of target with great precision.

4.1 Primer design

Primer design is the most important factor affecting the quality of SYBR® Green real-time PCR analyses. Although they seem to generate acceptable results at first, many homemade or "do-it-yourself" primers often come up short in their specificity, PCR amplification efficiency, reproducibility, and sensitivity. This is why many researchers choose to purchase TaqMan® Assay products - primers and probes for real-time PCR designed using a proven algorithm and trusted by scientists around the world. We chose to design our own real-time PCR primers using the NCBI tool Primer BLAST. Here is how we designed the best PCR/qPCR assays for our experiments:

STEP 1: Enter the target sequence in FASTA format or an accession number of an NCBI nucleotide sequence in the PCR Template section of the Primer BLAST submission form.

STEP 2: In the Primer Parameters section of the form specify a minimum 70bp and a maximum 200bp for PCR product size.

STEP 3: In the Primer Pair Specificity Checking Parameters section, select the appropriate source Organism - Homo sapiens - and the smallest Database - Refseq RNA (refseq_rna) - that is likely to contain the target sequence. These settings give the most precise results. Also, check the box in the Splice variant handling parameter to allow primers to amplify mRNA splice variants.

STEP 4: In the Advanced parameters section, specify Max Self Complementarity and Max Pair Complementarity values to 4 (Any) and 1 (3□).

STEP 5: Click the "Get Primers" button to submit the search and retrieve specific primer pairs.

In general, primers should be 18–24 nucleotides in length; however, the most important considerations for primer design should be their Tm value and specificity. Primers should also be free of strong secondary structures and self-complementarity. Our PCR primers were selected according to the following standard guidelines:

Melting temperature (Tm): The optimal melting temperature of the primers is 60–64°C, with an ideal temperature of 62°C, which is based on typical cycling and reaction conditions and the optimum temperature for PCR enzyme function. Ideally, the melting temperatures of the 2 primers should not differ by more than 2°C in order for both primers to bind simultaneously and efficiently amplify the product.

Annealing temperature (Ta): The annealing temperature chosen for PCR relies directly on length and composition of the primers. This temperature should be no more than 5°C below

the Tm of your primers. One consequence of having Ta too low is that one or both primers will anneal to sequences other than the intended target because internal single-base mismatches or partial annealing may be tolerated. This can lead to nonspecific PCR amplification and will consequently reduce the yield of the desired product. Conversely, if Ta is too high, reaction efficiency may be reduced because the likelihood of primer annealing is reduced significantly. Optimal annealing temperatures will result in the highest product yield with the correct amplicon.

GC content: Primer pairs should have GC content between 35–65%, with an ideal content of 50%, which allows complexity while still maintaining a unique sequence. Primers with high GC content can form stable imperfect hybrids. Conversely, high AT content depresses the Tm of perfectly matched hybrids. If possible, the 3' end of the primer should be GC rich (GC clamp) to enhance annealing of the end that will be extended. Analyze primer pair sequences to avoid complementarity and hybridization between primers (primer-dimers).

Intron-spanning primers: For RT-qPCR, primers should be designed in order to anneal to exons on both sides of an intron (or span an exon/exon boundary of the mRNA) to allow differentiation between amplification of cDNA and potential contaminating genomic DNA by melting curve analysis.

In our case, we were unable to design primers according to this last parameter as there were no suitable primers with thermodynamically favourable conditions that span or flank introns, or simply because the gene of interest does not contain introns. For this reason, our primers would also amplify genomic DNA which is not desired. In order to prevent that, gDNA contamination was removed from the RNA samples prior to cDNA synthesis by TURBO DNA-free DNase Treatment, which was further explained previously in section 2.3.

Table 4 - Primer sequences.

Gene	Accession number	Primer sequences	Product size	Tm (°C)
Taste receptors, type 1				
TAS1R1	NM_138697.3	Fw ATTTAAGCAACTGGCCTCCTTAGA	211	60,02
		Rv CCAGAATGGAGAGGGAACAGG		59,79
TAS1R2	NM_152232.2	Fw CCTGGCACACCATCAACAAC	189	59,69
		Rv AGGACCACTCGTTATTCGGG		59,18
TAS1R3	NM_152228.1	Fw GCAGGGCTAAATCACCACCA	94	60,32
		Rv CTGAGGCGTTGCACTGAAGA		60,60
Taste receptors, type 2				
TAS2R14	NM_023922.1	Fw GGTGCTGCTTCTTGTGACTT	246	58,69
		Rv TGCATCTTCTTGCGATGTTTCC		59,84
TAS2R5	NM_018980.2	Fw CGGCCTACTTGTGGCTGAA	142	60,00
		Rv TACCGAATGCTGCTGTTTCCT		60,00
Olfactory receptors				
OR13A1	NM_001004297.2	Fw TGCTGAAGAAATGACTGGCTG	88	58,84
		Rv TGAGATCAAAGAATCGGGGCT		59,16
OR1L8	NM_001004454.1	Fw CCATTCGCTTCAACCCCCA	148	60,30
		Rv CACCCAGCATAGGAGATGGTC		59,93
OR2H2	NM_007160.3	Fw GGGCAAGTTCTTTGGTCTCTTC	131	59,45
		Rv TTTGTGTGAGCCCCATTTCCTT		60,69
OR2K2	NM_205859.1	Fw TGCCCATTTGACTGTGGTGA	117	59,82
		Rv AGCACTCCGTAAAGCAACGA		59,97
OR7A17	NM_030901.1	Fw CAGCTTACTCCTGGCTGTGA	132	59,39
		Rv TTCAGGGCAGCAATCATCCA		59,67
Housekeeping genes				
GAPDH	NM_002046.5	Fw TCACCAGGGCTGCTTTTAACT	218	59,86
		Rv AGCATCGCCCCACTTGATTT		60,32
Β-actin	NM_001101.3	Fw CGCCGCCAGCTCACC	232	60,56
		Rv GCTCGATGGGGTACTTCAGG		59,89
PGK1	NM_000291.3	Fw GAATCACCGACCTCTCTCCC	216	59,25
		Rv AAGGACTACCGACTTGGCTC		59,10

4.2 Primer testing

Conventional PCR was performed to validate the specificity of each primer set. PCR was performed in 0.2 ml thin-walled PCR tubes in a 25 µl final volume containing 0.75 µl of forward and reverse primers, 0.75 µl $MgCl_2$, 0.5 µl dNTPs, 0.625 µl iTaq DNA Polymerase, 2.5 µl Buffer, up to 1 µg cDNA template (pool CDNA from plexus or cortex samples) and sterile water to make final volume (Roche, IN, USA).

Conventional PCR was performed in a DNA Engine PTC-200 Thermal Cycler (MJ Research, Inc., MA, USA) with the following temperature program: (i) 5 min at 94°C; (ii) 35 cycles, with 1 cycle consisting of 45 s at 94°C, 30 s at the optimum annealing temperature, and 30 s at 72°C, and (iii) a final extension step of 10 min at 72°C. All experiments included negative control reaction mixtures without added DNA and a positive control with cDNA template from a known expressed tissue (salivary gland).

Presence of single bands was analysed using gel electrophoresis. 10 µl of PCR mixture were run on 1% - 2% agarose gels (depending on the length of PCR products) in 1× Tris-acetate-EDTA (TAE) buffer stained with Gel Red (Biotium, USA).

4.3 Real Time quantitative PCR (RT-qPCR)

RT-qPCR is a variation of the standard PCR technique that is commonly used to quantify DNA or RNA in a sample. In RT-qPCR, the amount of DNA is measured after each cycle via fluorescent dyes that yield increasing fluorescent signal in direct proportion to the number of PCR product molecules (amplicons) generated. Data collected in the exponential phase of the reaction yield quantitative information on the starting quantity of the amplification target. The change in fluorescence over the course of the reaction is measured by an instrument that combines thermal cycling with fluorescent dye scanning capability. By plotting fluorescence against the cycle number, the RT-qPCR instrument generates an amplification plot that represents the accumulation of product over the duration of the entire PCR reaction. If a particular sequence (DNA or RNA) is abundant in the sample, amplification is observed in earlier cycles; if the sequence is scarce, amplification is observed in later cycles.

RT-qPCR was performed on LightCycler 480 II Instrument (Roche, IN, USA) in 96-well plates. Amplification mixture, in a total 15 µL reaction volume, consisted of SYBR Green master mix (Bio-Rad, CA, USA), 100 nM or 200 nM forward and reverse primers (Eurofins Genomics, Ebersberg, Germany), depending on the condition optimization of each assay, and a maximum 5 µg of cDNA template. Amplification was carried out with an initial denaturation step at 95℃ for 30 s followed by 45 cycles of 95℃ for 15 s and 60℃ to 64℃ for 30 s or 60 s (depending on the condition optimization for each assay). This was followed by 95℃ for 5 s, 55℃ for 30 s and 95℃ in continuous acquisition mode for melting curves, and a final cooling step of 40℃ for 10 s. All reactions were run in duplicate or triplicate and the mean was used for further calculations. Melt curve analysis was carried out after each run to confirm the lack of primer-dimers.

4.3.1 Conditions optimization

There are a number of factors that can be altered to obtain optimum assay performance and thereby lead to higher molecular sensitivity, specificity and precision. An assay that has been

designed such that all desirable design criteria were met is likely to perform well under a wide range of conditions. However, all assays have a set of optimal conditions. Most optimization procedures are focused on modification of primer binding kinetics using primer concentration or annealing temperature (Ta)/melting temperature (Tm).

Prior to the quantitative analysis, optimization procedures were performed by running RT-qPCRs to verify the reaction condition, including the annealing temperatures of the primers and specific products.

Annealing temperature/ Extension time

The Ta and the extension time were optimized in order to improve assay performance using the following protocol:

STEP 1: Start at the low end of the Ta range to be tested, which is determined by the Ta of the primers, and increase the temperature stepwise in gradual increments of 2°C (usually tested between 60°C and 64°C). Extension time could also be adjusted between 30 s and 1 min.

STEP 2: Test each reaction product for specificity, either by post-PCR melt curve analysis or agarose gel electrophoresis.

The optimal Ta is the one that results in the lowest Ct, a negative NTC, a melt curve analysis revealing detection of a specific product and high reproducibility between replicate reactions. If the Ta is too low, the reaction will be nonspecific. However, if the Ta is too high, the stringency may affect reaction efficiency, resulting in a lack of amplification or very high Ct values, very poor yields and low reproducibility.

Primers concentration

Primer concentrations should be high enough to allow sufficient sensitivity, specificity and fidelity within the assay. However, high primer concentrations increase the risk of primer-dimers formation. Therefore, each primer concentration was adjusted to optimal 100 nM or 200 nM. The combination of concentrations yielding the lowest Ct, lowest variation in replicates and a negative NTC was chosen.

Number of cycles

Reactions were generally run for 45 cycles.

Melting curve analysis

A melting curve charts the change in fluorescence observed when double-stranded DNA (dsDNA) with incorporated dye molecules dissociates, or "melts" into single-stranded DNA (ssDNA) as the temperature of the reaction is raised. For example, when double-stranded DNA bound with SYBR® Green I dye is heated, a sudden decrease in fluorescence is detected when the melting point (Tm) is reached, due to dissociation of the DNA strands and subsequent release of the dye. The fluorescence is plotted against temperature (Figure 13A), and then the -ΔF/ΔT (change in fluorescence/ change in temperature) is plotted against temperature to obtain a clear view of the melting dynamics (Figure 13B).

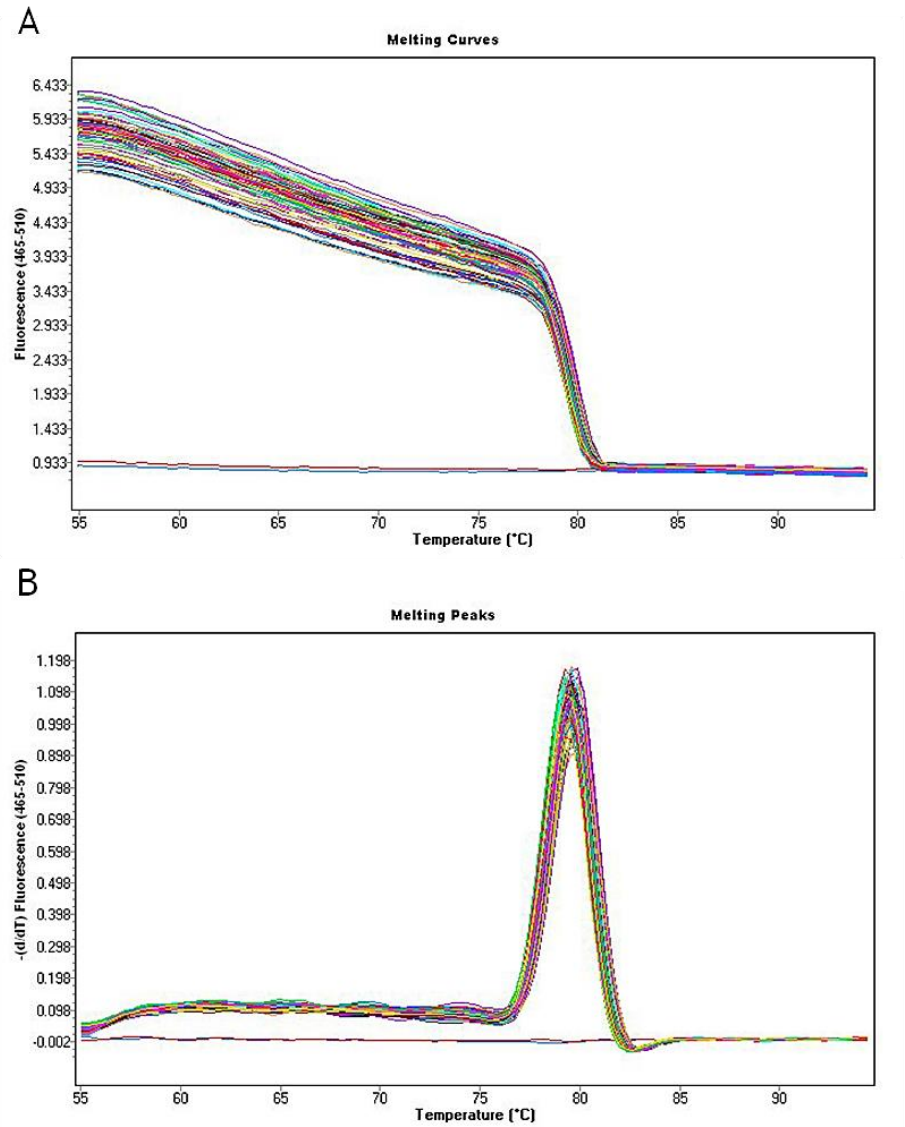

Figure 13 – Example of melting curves (A) and melting peaks (B) of a real-time PCR data. *Data corresponds to TAS2R14 real time PCR performed with human frontal orbital cerebral cortex cDNA.*

Post-amplification melting-curve analysis is a simple, straightforward way to check real-time PCR reactions for primer-dimers artefacts and to ensure reaction specificity. Because the melting temperature of nucleic acids is affected by length, GC content, and the presence of base mismatches, among other factors, different PCR products can often be distinguished by their melting characteristics. The characterization of reaction products (e.g., primer-dimers vs. amplicons) via melting curve analysis reduces the need for time-consuming gel electrophoresis.

4.3.2 Standard curve

A dilution series of cDNA concentrations can be used to establish a standard curve for determining the initial starting amount of the target template in experimental samples or for assessing the reaction efficiency (Figure 14). The log of each known concentration in the dilution series (x-axis) is plotted against the Ct value for that concentration (y-axis). From this standard curve, information about the performance of the reaction as well as various reaction parameters (including slope, y-intercept, and efficiency) can be derived. The concentrations chosen for the standard curve encompass the expected concentration range of the target in the experimental samples.

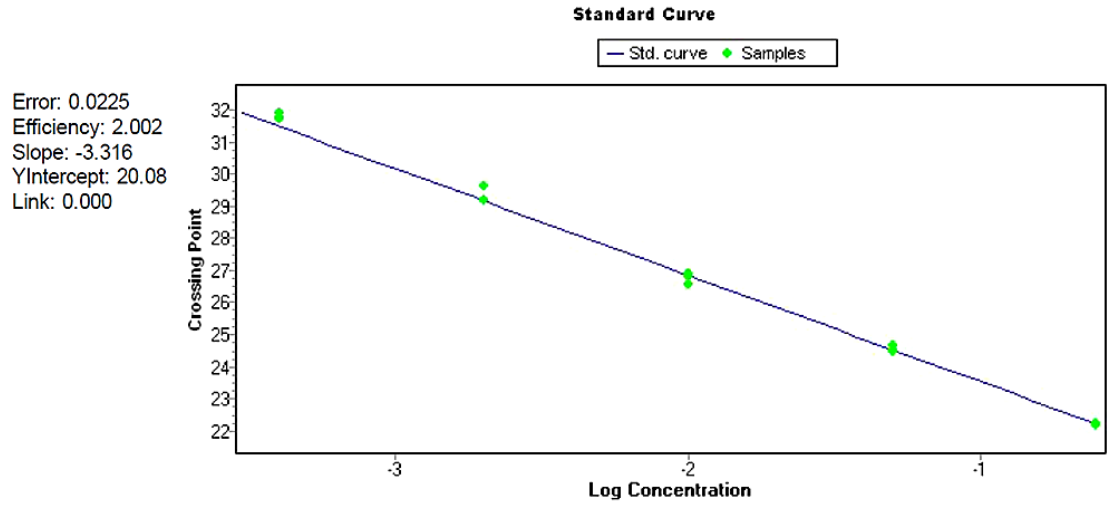

Figure 14 - Example of a standard curve of real-time PCR data. *GAPDH standard curve performed through 5-fold serial dilutions of human salivary gland cDNA (0.25 - 0.0004 ug). Standard curve is graphically represented as a semi-log regression line plot of threshold cycle (Ct) value vs. log concentration of cDNA. Slope, y-intercept, and efficiency values are used to provide information about the performance of the reaction. A standard curve slope of -3.32 indicates a PCR reaction with 100% efficiency.*

Slope

The slope of the log-linear phase of the amplification reaction is a measure of reaction efficiency. To obtain accurate and reproducible results, reactions should have an efficiency as close to 100% as possible, equivalent to a slope of -3.32 (see Efficiency, below, for more detail).

Efficiency

A PCR efficiency of 100% corresponds to a slope of -3.32, as determined by the following equation:

$$Efficiency = 10^{(-1/slope)} - 1$$

Ideally, the efficiency of a PCR reaction should be 100% (~2), meaning the template doubles after each thermal cycle during exponential amplification. The actual efficiency can give valuable information about the reaction. Experimental factors such as the length, secondary structure, and GC content of the amplicon can influence efficiency. Other conditions that may influence efficiency are the dynamics of the reaction itself, the use of non-optimal reagent concentrations, and enzyme quality, which can result in efficiencies below 90%. The presence of PCR inhibitors in one or more of the reagents can produce efficiencies of greater than 110%. A good reaction should have efficiency between 90% (~1.9) and 110% (~2.1), which corresponds to a slope of between -3.58 and -3.10.

Table 5 sums up the optimization procedures performed by RT-qPCR prior to the quantitative analysis to verify the reaction conditions, including primers concentration, annealing temperatures and extension times of the primer sets. We were able to optimize these conditions in different tissues except for the *TAS1R2* primer set, which inexplicably never worked under any circumstance. This fact was also confirmed by agarose gel electrophoresis as it will be showed in the next chapter.

Table 5 - Primers concentration, annealing temperature and extension time optimization with the different tissue samples.

Gene	[primers] (nM)	T Annealing (°C)	Extension time (sec)	cDNA sample(s)
Gapdh	100	60	60	SG, CP, OFC
β-Actin	100	62	30	OFC
PGK1	200	60	60	OFC
OR2H2	200	64	30	SG, OFC
OR2K2	200	62	60	SG, CP, OFC
OR1L8	100	64	30	SG, OFC
TAS2R14	100	60	60	SG, CP
	100	62	60	SG, OFC
TAS2R5	100	62	60	SG, OFC
OR7A17	100	64	30	SG, OFC
OR13A1	200	60	30	SG, OFC
TAS1R1	100	64	60	SG, OFC
TAS1R2	-	-	-	SG, CP, OFC
TAS1R3	100	64	60	SG, OFC

SG, Salivary gland; OFC, orbitofrontal cortex; CP, Choroid plexus.

4.3.3 Data analysis

RT-qPCR data was analysed by the $2^{-\Delta\Delta Ct}$ method where the mean Ct values of the genes of interest were directly normalized to each of the housekeeping genes and then compared. First, the difference between the Ct values (ΔCt) of the gene of interest and the housekeeping gene was calculated for each sample. Then, the difference in the ΔCt values between the AD Braak stage samples and control samples ($\Delta\Delta Ct$) was calculated. The fold difference in expression of the gene of interest between samples was then equal to $2^{-\Delta\Delta Ct}$ (Livak and Schmittgen, 2001).

5. Statistical analysis

Statistical significance was determined by calculating probability values using the *GraphPad Prism* software (Version 6.01). Data was expressed as means ± SEM and multiple comparisons were assessed by *one-way ANOVA* analysis followed by *Bonferroni's* post-hoc test. Differences were considered statistically significant when $p<0.05$.

IV. Results

1. Primer testing

Polymerase Chain Reaction (PCR) was performed with salivary gland cDNA to validate the specificity of each primer set, and the presence of single bands were analysed using gel electrophoresis as described previously. The results from agarose gel electrophoresis of PCR amplified products using the housekeeping genes primer pairs – Glyceraldehyde 3-phosphate dehydrogenase (*GAPDH*), Phosphoglycerate kinase 1 (*PGK1*) and *β-Actin* – are shown in Figure 15. From left to right, MW denotes the molecular weight marker, lane 1 displays the positive sample and lane 2 the negative sample. A single band appeared in the expected 218bp, 216bp and 232bp in comparison to the molecular weight marker, corresponding respectively to *GAPDH* (Figure 15A), *PGK1* (Figure 15B), and *β-Actin* (Figure 15C) products size.

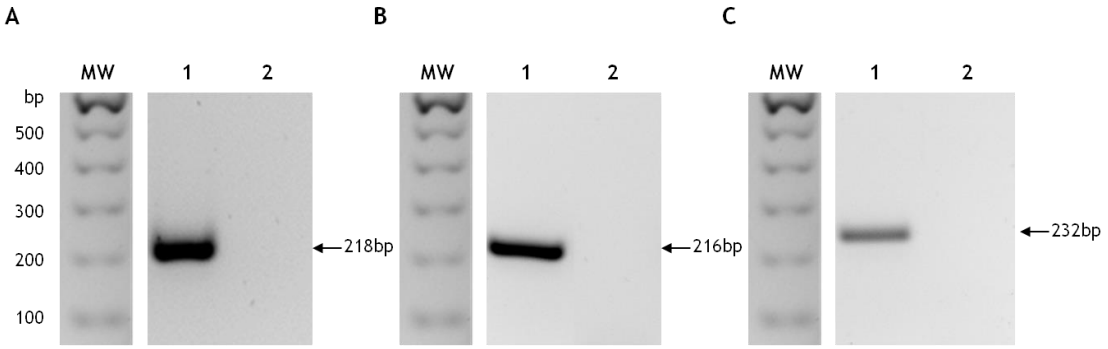

Figure 15 – Agarose gel electrophoresis of PCR amplified products using housekeeping genes primer pairs: GAPDH with 218bp (A), PGK1 with 216bp (B) and β-Actin with 232bp (C). MW, denotes the molecular weight (Ladder), lane 1 displays the human salivary gland cDNA and lane 2 the negative sample.

The results from agarose gel electrophoresis of PCR amplified products using the olfactory receptor genes primer pairs are shown in Figure 16. A single band appeared in the expected 148bp, 131bp, 117bp, 88bp, and 132bp in comparison to the molecular weight marker, corresponding respectively to *OR1L8* (Figure 16A), *OR2H2* (Figure 16B), *OR2K2* (Figure 16C), *OR13A1* (Figure 16D), and *OR7A17* (Figure 16E) products size. The faint bands observed below 100bp represent primer-dimers as these PCRs were performed previous to primers concentrations optimization.

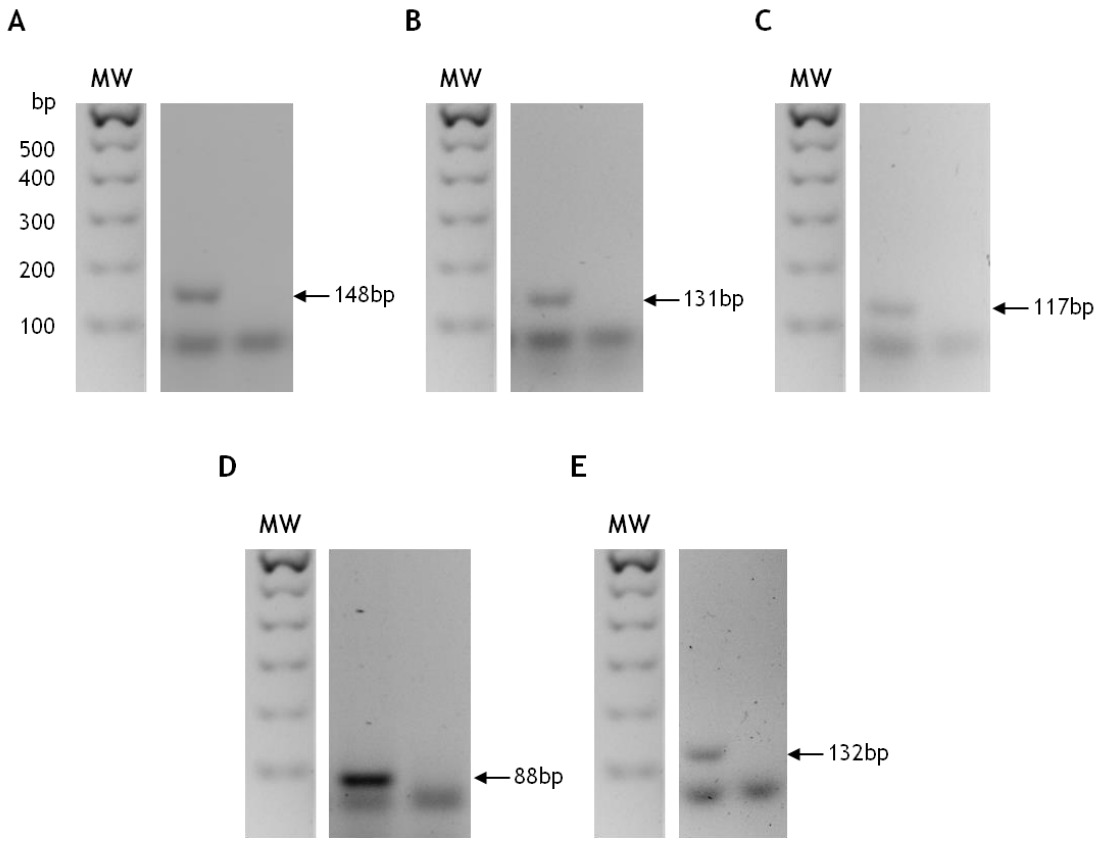

Figure 16 – Agarose gel electrophoresis of PCR amplified products using olfactory receptor genes primer pairs: OR1L8 with 148bp (A), OR2H2 with 131bp (B), OR2K2 with 117bp (C), OR13A1 with 88bp (D), and OR7A17 with 132bp (E). MW, denotes the molecular weight (Ladder), lane 1 displays the human salivary gland cDNA and lane 2 the negative sample.

The results from agarose gel electrophoresis of PCR amplified products using the taste receptor genes primer pairs are shown in Figure 17. A single band appeared in the expected 211bp, 94bp, 246bp, and 142bp in comparison to the molecular weight marker, corresponding respectively to *TAS1R1* (Figure 17A), *TAS1R3* (Figure 17C), *TAS2R14* (Figure 17D), and *TAS2R5* (Figure 17E) products size. Except for the *TAS1R2* primer sets that inexplicably never worked under any circumstance and therefore no amplified product appeared in the expected 189bp. The faint bands observed below 100bp in almost every case represent primer-dimers as these PCRs were performed previous to primers concentrations optimization.

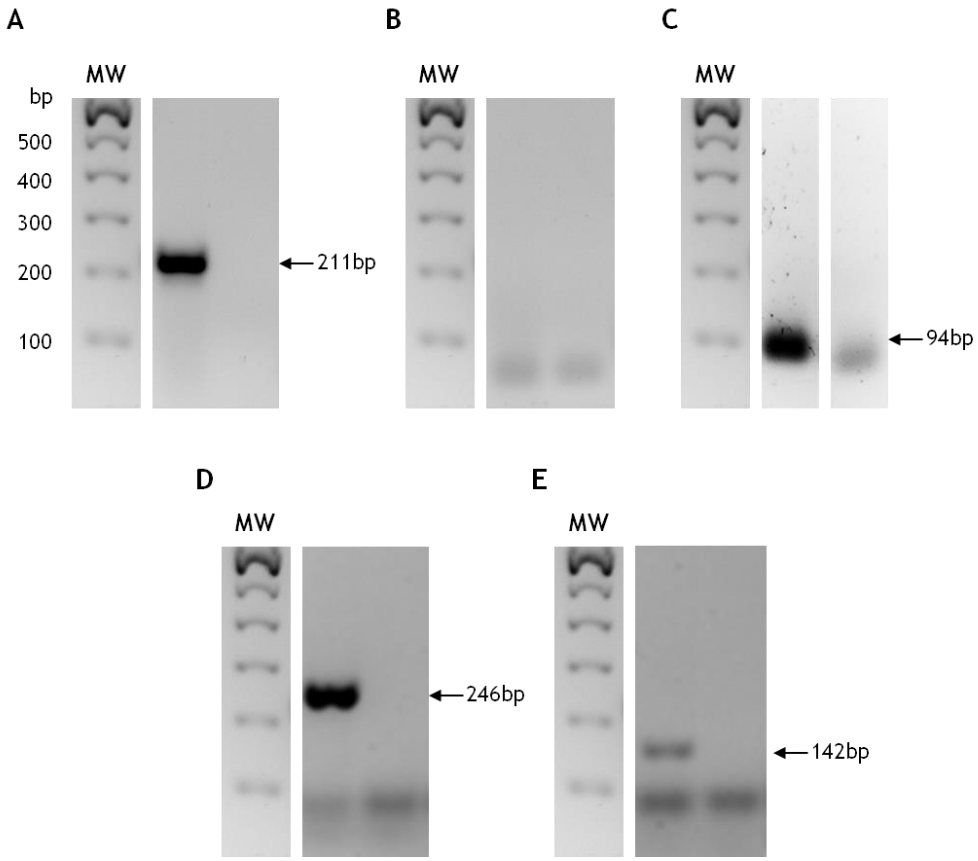

Figure 17 - Agarose gel electrophoresis of PCR amplified products using taste receptor genes primer pairs: TAS1R1 with 211bp (A), TAS1R2 with no amplified product (B), TAS1R3 with 94bp (C), TAS2R14 with 246bp (D), and TAS2R5 with 142bp (E). MW, denotes the molecular weight (Ladder), lane 1 displays the human salivary gland cDNA and lane 2 the negative sample.

2. RT-qPCR optimization

Prior to the quantitative analysis, optimization procedures were performed by RT-qPCR to obtain an efficient standard curve for each primer set (Table 6). In most cases, there was the need to use salivary gland cDNA samples to obtain a larger efficient range in the standard curve. The salivary gland, as a positive tissue control used in this study, was characterized by a stronger expression profile.

We were able to acquire an efficient standard curve except for the taste receptors type I genes (*TAS1R1, TAS1R2*, and *TAS1R3*). In these 3 type I taste receptors, no amplification was detected by RT-qPCR when orbitofrontal cortex samples were used. In the case of *TAS1R2* no amplification was detected by this technique in any of the tissue samples used, i.e. nor in choroid plexus nor in orbitofrontal cortex, or even in salivary gland. On the other hand, when using salivary gland cDNA samples it was possible to detect an amplification product in the case of *TAS1R1* and *TAS1R3*. However, *TAS1R1* amplified beyond the reliable detection limit of the RT-qPCR technique making it impossible to get an efficient standard curve, and *TAS1R3* even though amplifying earlier was unable to ensure an efficient standard curve.

Table 6 – Standard curves optimization with the different tissue samples and the corresponding melting temperature of the amplified products.

Gene	T Melting (°C)	cDNA sample	Standard curve (ug/ul)	Ct Standard Curve	Efficiency
Gapdh	81,6	SG	0,05 - 0,00008	22,2 - 31,8	2,002
		OFC	0,1 - 0,00039	24 - 32,1	2,007
Β-Actin	91,0	OFC	0,1 - 0,003125	24,2 - 29,1	1,970
PGK1	82,7	OFC	0,02 - 0.000078	26,9 - 35,6	2,036
OR2H2	82,1	SG	0,5 - 0,0078	27,9 - 33,8	2,015
OR2K2	79,4	SG	0,25 - 0,0039	28,6-35,8	2,001
OR1L8	80,4	SG	0,125 - 0,0078	30,1 - 34,4	1,957
TAS2R14	79,6	SG	0,125 - 0,00098	28,0 - 36,5	2,002
TAS2R5	80,9	SG	0,5 - 0,0078	26,9 - 32,6	2,090
OR7A17	84,0	SG	0,5 - 0,0156	28,0 - 32,9	1,987
OR13A1	79,2	SG	0,5 - 0,0156	27,3 - 32,2	2,004
TAS1R1	88,6	SG	0,5	Ct >>> 35	
	-	OFC	1	No amplification	
TAS1R2	-	SG, CP, OFC	1	No amplification	
TAS1R3	84	SG	1 - 0,0625	Standard curve not efficient	
	-	OFC	1	No amplification	

SG, Salivary gland; OFC, orbitofrontal cortex; CP, Choroid plexus.

3. Housekeeping genes validation in orbitofrontal cortex

Real-time quantitative PCR has been widely used as a powerful technique to determine gene expression levels, due to its high sensitivity, specificity and reproducibility. It must be noted that the accuracy of RT-qPCR results strongly depends on the stability of reference gene(s) used for data normalization. A good reference gene, which can be used as an internal control, is characterized by expression stability in all samples and under different conditions. The stability of expression is ideally not affected by tissue types, developmental stages, physiological situations, and experimental conditions.

Since we were operating with human post-mortem samples, it was essential to use a combination of at least two validated reference genes for accurate quantitative evaluation. For that matter, the following genes were selected: *GAPDH* (Figure 18), *Β-Actin* (Figure 19) and *PGK1* (Figure 20). *GAPDH* and *Β-Actin* are highly expressed genes and therefore were amplified at Ct values around 27, whereas *PGK1* is a lower expression gene and consequently, amplified at Ct values around 30. Overall, we found that all candidate genes were suitable since no

differences were observed under the different Braak stages of AD and age-matched controls (Braak stage 0), both in male and female samples.

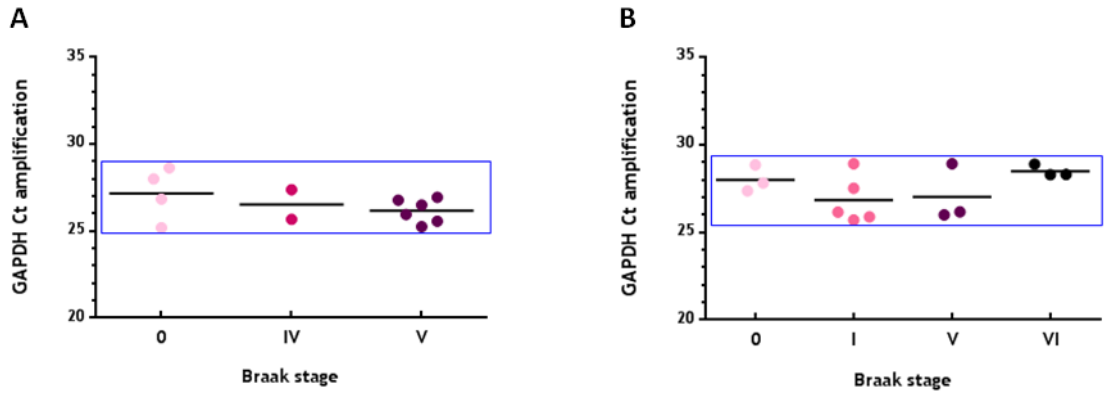

Figure 18 - GAPDH Ct values of amplification of male (A) and female (B) vs. male orbitofrontal cortex samples by Braak stage of AD groups. Braak stage 0 corresponds to age-matched controls.

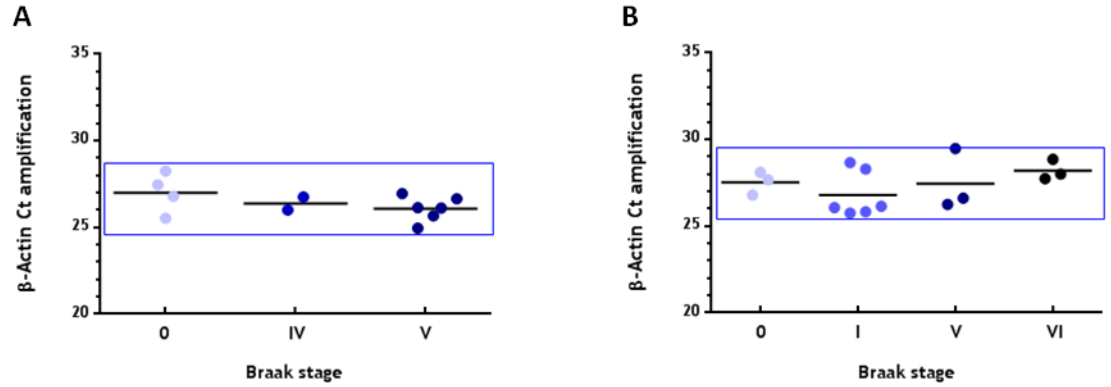

Figure 19 - B-Actin Ct values of amplification of male (A) and female (B) orbitofrontal cortex samples by Braak stage of AD. Braak stage 0 corresponds to age-matched controls.

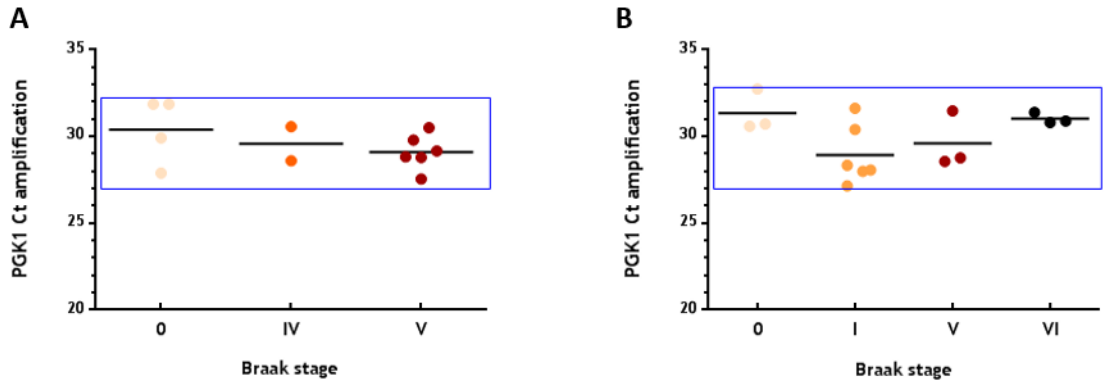

Figure 20 - PGK1 Ct values of amplification of male (A) and female (B) orbitofrontal cortex samples by Braak stage of AD. Braak stage 0 corresponds to age-matched controls.

4. Olfactory and taste receptors expression in orbitofrontal cortex

4.1 Olfactory receptors

4.1.1 *OR2K2* mRNA expression

In male, the olfactory receptor *OR2K2* mRNA levels displayed a general tendency to increase from stages 0, to IV and V (Figure 21), but it did not reach statistical significance. In AD Braak stage V, this effect seemed more pronounced and consistent with the three housekeeping genes, but it did not reach statistical significance. This lack of statistical significance is probably due to the low number of subjects and the variability between subjects of the same group.

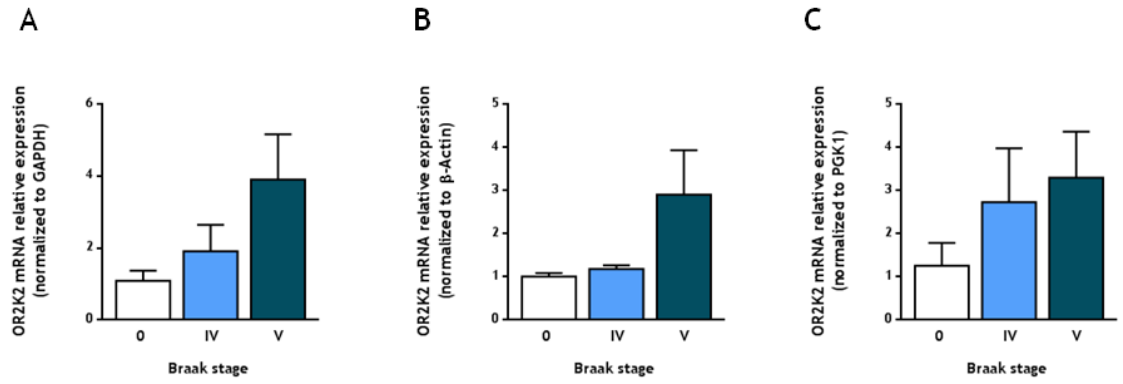

Figure 21 - OR2K2 mRNA relative expression in male samples of orbitofrontal cortex. Values are mean ± SEM, relative to age-matched controls (Braak stage 0) and normalized to GAPDH (A), Β-Actin (B) and PGK1 (C).

In female samples, an interesting feature came to our attention. *OR2K2* mRNA levels at AD Braak stage I were significantly decreased compared to age-matched controls when normalizing to the three different housekeeping genes – *GAPDH* ($p<0.01$) (Figure 22A), *Β-Actin* ($p<0.01$) (Figure 22B) and, *PGK1* ($p<0.0001$) (Figure 22C). *OR2K2* mRNA levels at the later stages V and VI were also significantly decreased compared to controls when normalizing to *GAPDH* ($p<0.05$) and *PGK1* ($p<0.0001$). When normalized to *Β-Actin*, even though behaving similarly, it didn't reach statistical significance most likely due to the slight variation noticed inside these groups.

Furthermore, *OR2K2* mRNA levels at AD Braak stage VI were significantly increased compared to stage I when normalized to *GAPDH* ($p<0.05$). When normalized to the others housekeeping genes it didn't reach statistical significance, yet it is noticeable its tendency to be increased compared to stage I.

Remarkably, it was noticed a difference in the expression levels between the normalization to the different housekeeping genes, namely the similarity between levels of expression when

normalized to *GAPDH* and *β-Actin*, and the more remarkable shift when normalized to PGK1. This difference is supported by the fact that *GAPDH* and *β-Actin* are highly expressed genes whereas the PGK1 is a lower expressed gene, as mentioned before.

It was also perceived quite some variability between subjects of the control group (Braak stage 0) which is most likely due to the small number of subjects that comprises it.

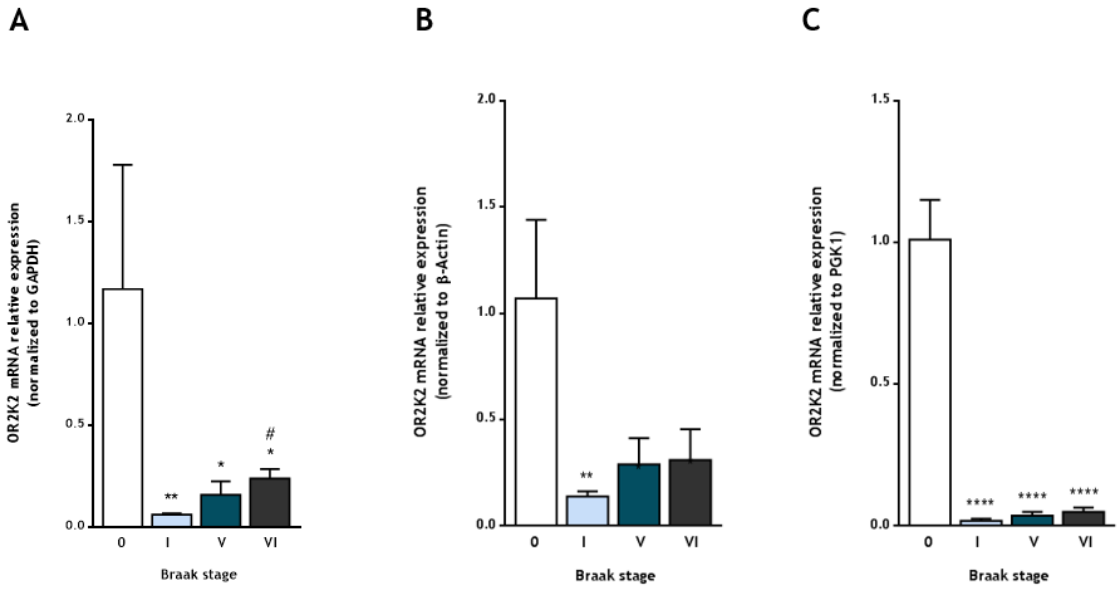

*Figure 22 - OR2K2 mRNA relative expression in female samples of orbitofrontal cortex. Values are mean ± SEM, relative to age-matched controls (Braak stage 0) and normalized to GAPDH (A), β-Actin (B) and PGK1 (C). * p< 0.05, ** p< 0.01, **** p< 0.0001, significantly different from Braak stage 0. # p< 0.05, significantly different from Braak stage I.*

4.1.2 *OR2H2* mRNA expression

In male, the *OR2H2* mRNA levels were not significantly altered in the AD Braak stages studied when compared to age-matched controls (Figure 23), except when normalized to *β-Actin* (Figure 23B). In this case, *OR2H2* mRNA levels were significantly decreased in AD Braak stage IV ($p<0.05$) and more remarkably in stage V ($p<0.01$). On the other hand, when normalized to *GAPDH* (Figure 23A) and *PGK1* (Figure 23C), despite not reaching statistical significance, *OR2H2* mRNA expression appeared to be increased in stage IV in both cases. This tendency is most likely due to the variation noticed in mRNA levels between subjects in this group. Despite the differences, in all cases *OR2H2* mRNA levels in stage IV and V seemed to share this sort of descendant ladder pattern, i.e. mRNA levels in stage V appeared decreased in all cases comparing to stage IV. This ladder pattern was dissimilar in the other *ORs* studied, given that instead of descendant they showed an ascendant ladder pattern as it could be remarked in section 4.1.1 and section 4.1.3.

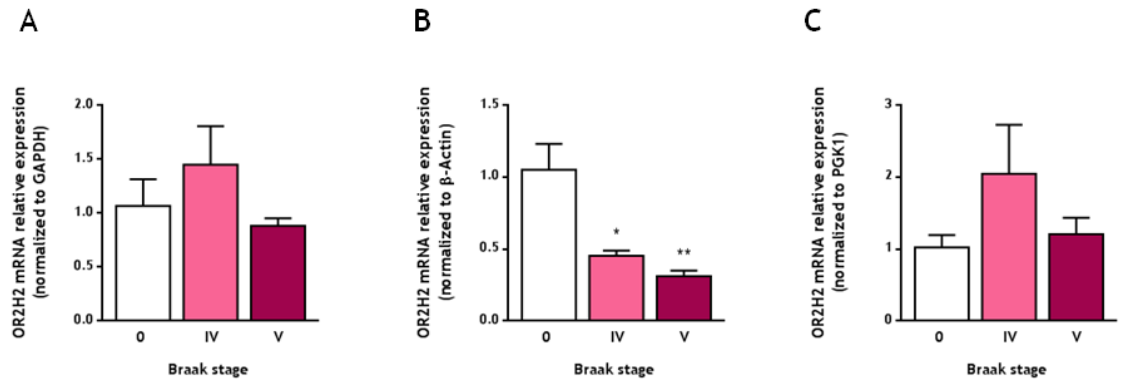

*Figure 23 - OR2H2 mRNA relative expression in male samples of orbitofrontal cortex. Values are mean ± SEM, relative to age-matched controls (Braak stage 0) and normalized to GAPDH (A), β-Actin (B) and PGK1 (C). * p< 0.05, ** p<0.01, significantly different from Braak stage 0.*

When analysing female samples, the *OR2H2* mRNA expression showed a different pattern comparing to males (Figure 24). As noticed previously in *OR2K2* (Figure 22), OR2H2 mRNA levels at AD Braak stage I were significantly decreased compared to age-matched controls when normalizing to different housekeeping genes - *GAPDH* ($p<0.05$) (Figure 24A) and *PGK1* ($p<0.01$) (Figure 24C). Exception noticed when normalized to *β-Actin* where it did not reach statistical significance despite the similar but yet more subtle pattern (Figure 24B). The *OR2H2* mRNA levels in later Braak stages V and VI didn't reach statistical significance when normalized to any of the different housekeeping genes. Yet *OR2H2* mRNA levels in stage IV appeared to be decreased when normalized to *GAPDH* and *PGK1*, and in stage VI they seemed to be decreased only when normalized to *PGK1*. Despite these differences, in the overall the *OR2H2* mRNA levels showed the previously mentioned ascendant ladder pattern in all cases, i.e. mRNA levels in stage V seemed increased comparing to stage I and in stage VI they seemed increased comparing to stage V. Nevertheless, statistical significance was only reached in *OR2H2* mRNA levels in stage VI compared to stage I when normalized to *GAPDH* ($p<0.05$) and *PGK1* ($p<0.05$).

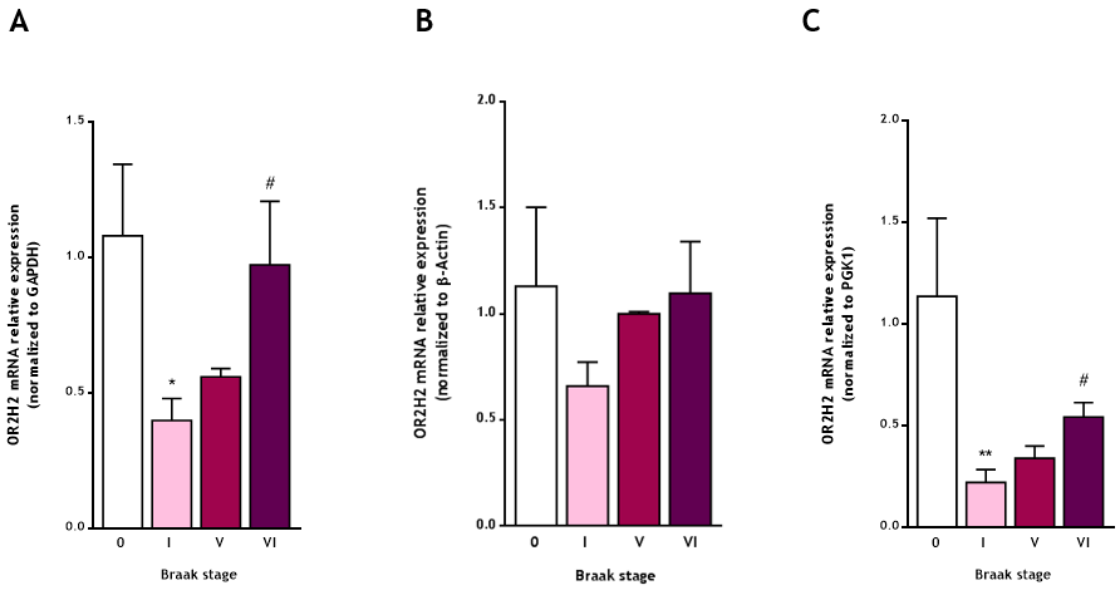

*Figure 24 - OR2H2 mRNA relative expression in female samples of orbitofrontal cortex. Values are mean ± SEM, relative to age-matched controls (Braak stage 0) and normalized to GAPDH (A), Β-Actin (B) and PGK1 (C). * p< 0.05, ** p< 0.01, significantly different from Braak stage 0. # p< 0.05, significantly different from Braak stage I.*

4.1.3 *OR1L8* mRNA expression

In male, the *OR1L8* mRNA levels were not significantly altered in the AD Braak stages studied when comparing to age-matched controls (Figure 25). Despite the observed tendency to decrease in stage IV and to increase in stage V compared to controls, it did not reach statistically significance. This behaviour was notably maintained among the three housekeeping-genes applied.

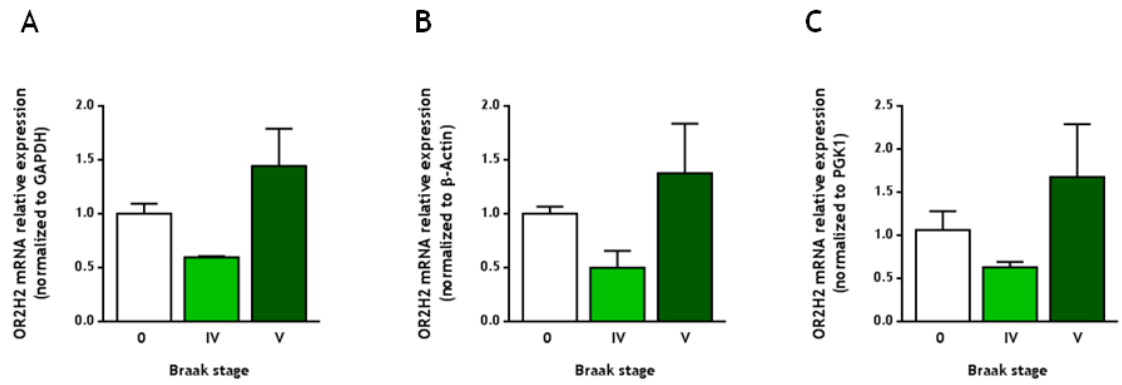

Figure 25 - OR1L8 mRNA relative expression in male samples of orbitofrontal cortex. Values are mean ± SEM, relative to age-matched controls (Braak stage 0) and normalized to GAPDH (A), Β-Actin (B) and PGK1 (C).

When exploring female samples, some differences were observed when normalizing to the three different housekeeping genes (Figure 26). *OR1L8* mRNA levels at AD Braak stage I were significantly decreased compared to controls when normalized to *GAPDH* ($p<0.05$) (Figure 26A)

and to *PGK1* ($p<0.01$) (Figure 26C). The same tendency was seen when normalized to *β-Actin* even though it did not reach statistical significance (Figure 26B). *OR1L8* mRNA levels in stages V appeared to be decreased when normalized to *GAPDH* and *PGK1*, although it only reached statistical significance in the last case ($p<0.05$) (Figure 26C). Similarly, *OR1L8* mRNA levels in stage VI appeared to be decreased when normalized to *GAPDH* and *PGK1*, although not reaching statistical significance. Instead, when normalized to *β-Actin*, *OR1L8* mRNA levels in both stage V and VI seemed to be slightly increased compared to controls.

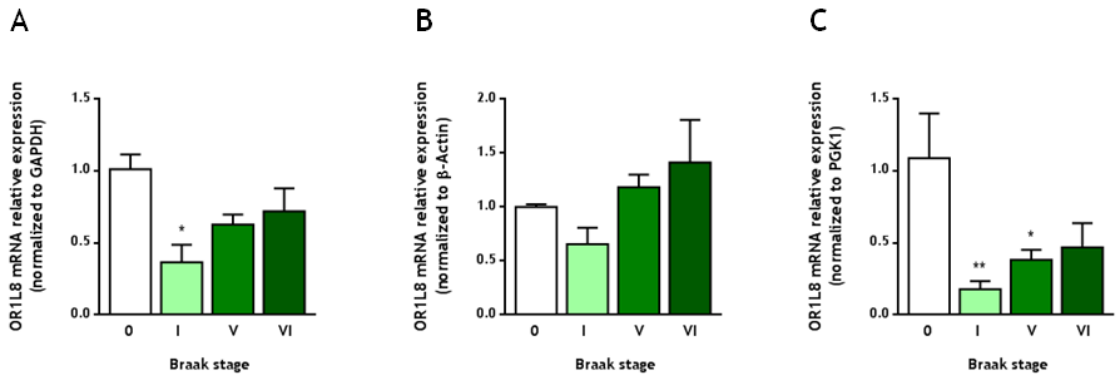

*Figure 26 - OR1L8 mRNA relative expression in female samples of orbitofrontal cortex. Values are mean ± SEM, relative to age-matched controls (Braak stage 0) and normalized to GAPDH (A), β-Actin (B) and PGK1 (C). * p< 0.05, * p< 0.01, significantly different from Braak stage 0.*

4.1.4 *OR13A1* mRNA expression

In male, even though the maximum amount of cDNA per reaction was employed, *OR13A1* amplified at Ct values around 35. Likewise, in female, *OR13A1* amplified at Ct values around 34 using equally the maximum amount of cDNA per reaction. Therefore, we were unable to quantify the *OR13A1* mRNA expression both in male and female orbitofrontal cortex samples as its amplification resided excessively close to the reliable detection limit for RT-qPCR technique. Furthermore, downregulation in the expression correspond to amplifications further below the detection limit.

4.1.5 *OR7A17* mRNA expression

Both in male and female orbitofrontal cortex samples, it was not detected any amplification of *OR7A17* mRNA by RT-qPCR technique. In both cases, the maximum amount of cDNA was applied.

4.2 Taste receptors

4.2.1 *TAS2R5* mRNA expression

The bitter taste receptor *TAS2R5* mRNA levels were not significantly changed in the AD Braak stages studied when compared to age-matched controls in male (Figure 27). Despite the observed tendency to decrease in stage IV, it did not reach statistical significance. This behaviour was observed and maintained among the three housekeeping-genes used.

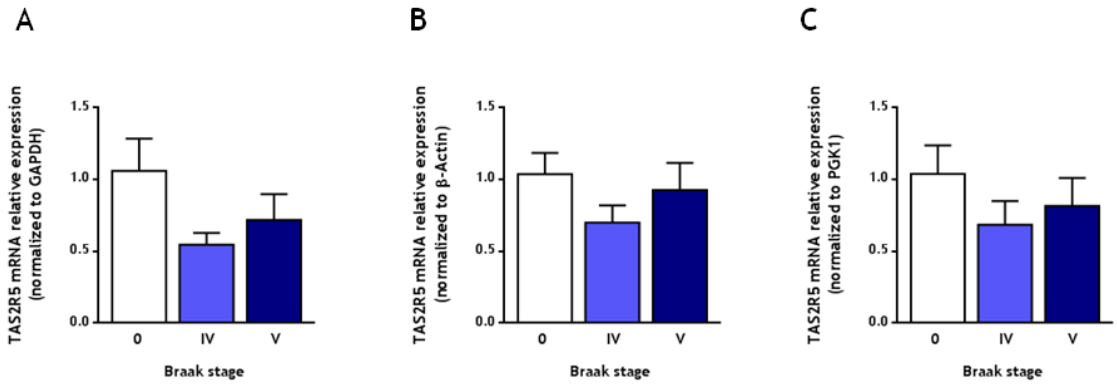

Figure 27 - TAS2R5 mRNA relative expression in male samples of orbitofrontal cortex. Values are mean ± SEM, relative to age-matched controls (Braak stage 0) and normalized to GAPDH (A), B-Actin (B) and PGK1 (C).

When analysing female samples (Figure 28), we noticed quite some variability when normalizing to the three different housekeeping genes. When *GAPDH* was used, no significant differences were found (Figure 28A). Similarly, when *B-Actin* was employed no significant differences were found, although the *TAS2R5* mRNA levels in AD Braak stages I, V and VI showed a subtle tendency to be increased compared to age-matched controls (Figure 28B). Yet, when normalized to *PGK1*, the *TAS2R5* mRNA levels in AD Braak stage I were significantly decreased ($p<0.05$) (Figure 28C), a tendency also observed in stages V and VI although not reaching statistical significance.

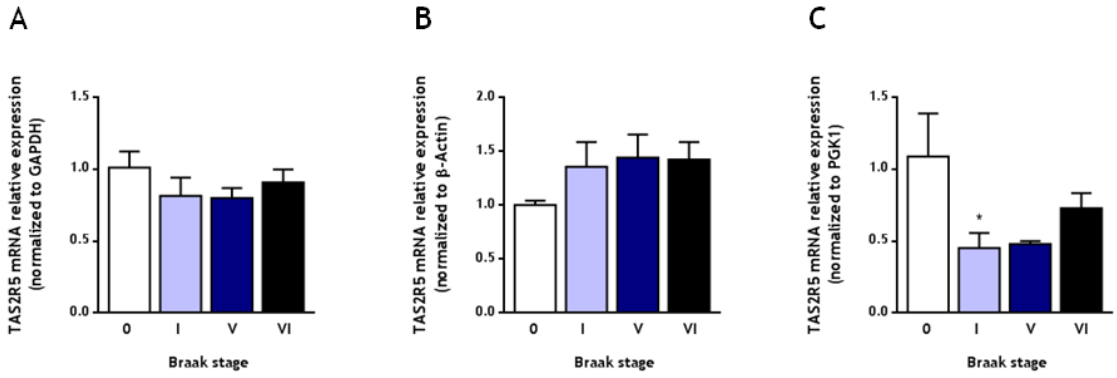

*Figure 28 - TAS2R5 mRNA relative expression in female samples of orbitofrontal cortex. Values are mean ± SEM, relative to age-matched controls (Braak stage 0) and normalized to GAPDH (A), B-Actin (B) and PGK1 (C). * p< 0.05, significantly different from Braak stage 0.*

4.2.2 *TAS2R14* mRNA expression

In male, the *TAS2R14* mRNA levels were not significantly changed in AD Braak stages under study when comparing to age-matched controls (Figure 29), In fact, they seemed to remain constant. This behaviour was noticed and maintained among the three housekeeping-genes employed.

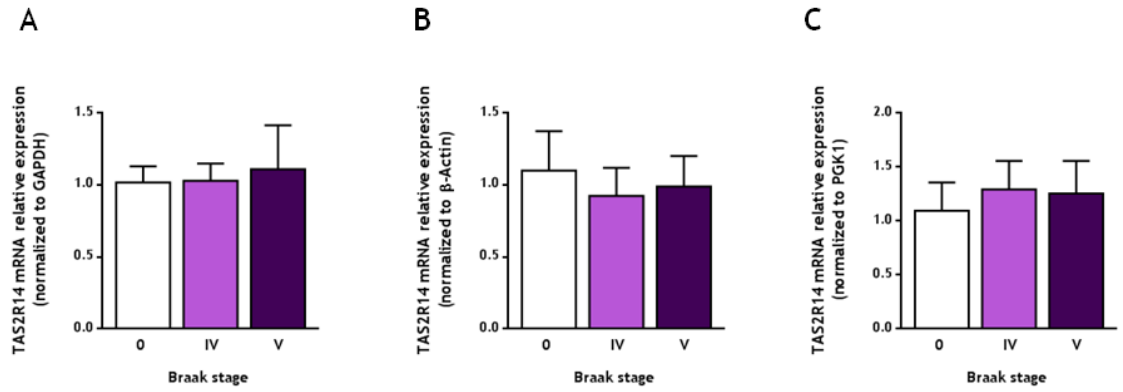

Figure 29 - TAS2R14 mRNA relative expression in male samples of orbitofrontal cortex. Values are mean ± SEM, relative to age-matched controls (Braak stage 0) and normalized to GAPDH (A), Β-Actin (B) and PGK1 (C).

In female samples, the *TAS2R14* mRNA expression showed some variability when normalized to the different housekeeping genes (Figure 30). When *GAPDH* and *PGK1* were applied, *TAS2R14* mRNA levels at AD Braak stage I were significantly decreased when compared to age-matched controls ($p<0.05$) (Figure 30, A and C). However, when *Β-Actin* was used, no significant differences were found between *TAS2R14* mRNA levels at Braak stage I and age-matched controls (Figure 30B). Regarding the *TAS2R14* mRNA levels in the later stages V and VI, no significant differences were found compared to controls when normalizing to the three different housekeeping genes. Nevertheless, they appeared to be decreased when normalized to *GAPDH* and more evidently when normalized to *PGK1*, even though not reaching statistical significance. Yet, when normalized to *Β-Actin*, *TAS2R14* mRNA levels in stage V seemed to be slightly increased compared to controls whereas in stage VI no differences were observed.

Nevertheless, statistical differences were reached in *TAS2R14* mRNA levels in stage VI compared to stage I when normalized to *GAPDH* ($p<0.01$) and *PGK1* ($p<0.05$). Yet, then again when normalized to *Β-Actin*, no differences were observed in *TAS2R14* mRNA levels in stage VI compared to stage I.

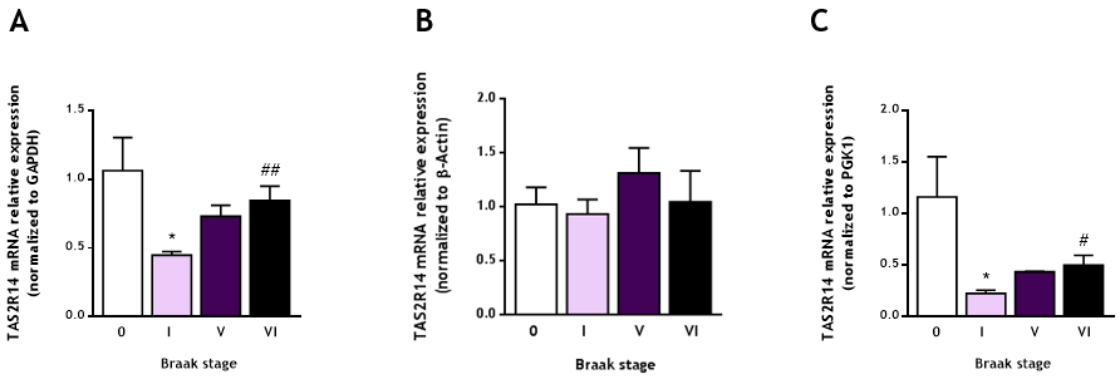

*Figure 30 - TAS2R14 mRNA relative expression in female samples of orbitofrontal cortex. Values are mean ± SEM, relative to age-matched controls (Braak stage 0) and normalized to GAPDH (A), B-Actin (B) and PGK1 (C). * p< 0.05, significantly different from Braak stage 0. # p<0.05, ## p<0.01, significantly different from Braak stage I.*

5. Olfactory and taste receptors expression in choroid plexus

Although *GAPDH* appeared to be a highly expressed gene in the other tissues employed in this study (salivary gland and orbitofrontal cortex) and to be characterized by expression stability in orbitofrontal cortex samples as shown previously in section 3, a different pattern was observed in male choroid plexus samples. As shown in Figure 31, *GAPDH* showed a particularly variable behaviour characterized by a large Ct amplifications range that went from 30 to 36. Consequently, *GAPDH* didn't meet the required characteristics to be a suitable reference gene for choroid plexus samples.

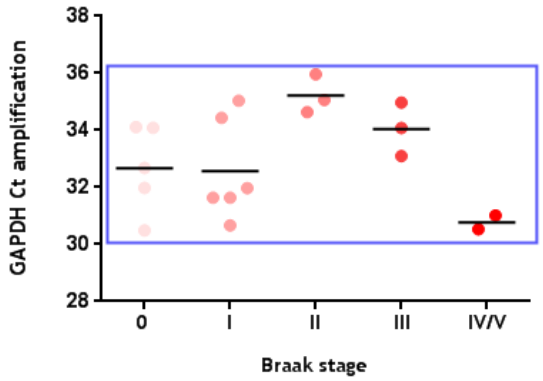

Figure 31 - GAPDH Ct values of amplification of male choroid plexus samples by Braak stage of AD. Braak stage 0 corresponds to age-matched controls.

Despite these results, one more housekeeping gene was verified – *PGK1* (Figure 32). In this case though, no differences were observed under the different Braak stages of AD and age-matched

controls (Braak stage 0) except for the stage II whose behaviour stepped out of the norm. Apart from AD Braak stage II irregularity, in the overall *PGK1* was characterized by expression stability and Ct amplification values around 30.5, and for these reasons was considered a suitable reference gene candidate.

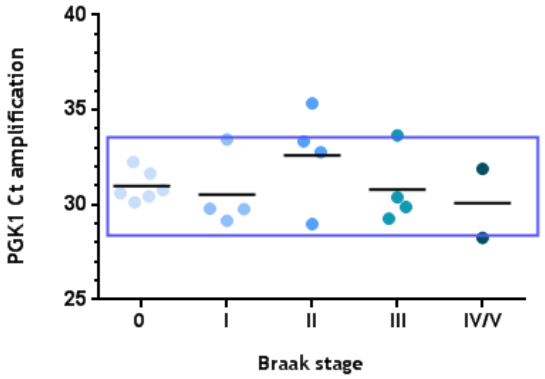

Figure 32 - PGK1 Ct values of amplification of male choroid plexus samples by Braak stage of AD. Braak stage 0 corresponds to age-matched controls.

In light of these results, it was then performed the RT-qPCR with one of the taste and olfactory receptor genes that showed the highest level of expression by PCR testing – *TAS2R14* and *OR2K2*.

Not surprisingly, even though it was employed a substantial amount of cDNA per reaction, *TAS2R14* in male choroid plexus samples amplified in a range that went from 34 to 37 Cts and *OR2K2* amplified in a range even lower that went from 35 to 43 Cts. Evidently, these results could not be taken into consideration since they exceed the reliable detection limit for quantification of this technique.

Given the fact that the samples were particularly scarce, we found unnecessary to waste it in attempting to perform the RT-qPCRs with the rest of the taste and olfactory receptors genes in study.

V. Discussion and Conclusions

The finding that taste receptors are expressed in the central nervous system is somewhat expected since *Tas2rs* are responsible for the detection of bitter compounds, such as the natural alkaloids, quinine, caffeine, nicotine and morphine (Singh et al., 2011). Therefore, bitter sensing serves as a central warning signal against the ingestion of potentially harmful substances (Jung et al., 2014). So, it is not surprising that previous studies have found ectopic *Tas2rs* expression in gastrointestinal neuroendocrine cells of the large intestine (Wu et al., 2002; Wu et al., 2005), chemosensory cells of nasal epithelium (Finger et al., 2003) and human airway cells (Shah et al., 2009; Deshpande et al., 2010). In the brain, the first evidence of *Tas2rs* expression was found in 2011 by Singh and colleagues. Using RT-PCR analysis, they found expression of *Tas2r107*, *Tas2r108* and *Tas2r138* in the brainstem, cerebellum, cortex, and nucleus accumbens of rat brain (Singh et al., 2011). The corresponding orthologues in human are *TAS2R10*, *TAS2R4* and *TAS2R38*. Transcripts of *Tas2r109* and *Tas2r144* (corresponding human orthologue is *TAS2R40*) were also found in rat choroid plexus alongside with their corresponding proteins in CP explants and CP epithelial cells by Tomás and colleagues. The functionality of these bitter receptors was also assessed by calcium imaging, revealing that a bitter compound elicits calcium responses in CP epithelial cells in a dose-dependent manner and that this response could be suppressed by a bitter receptor blocker (Tomás et al., 2016).

Tas1rs were also described to be expressed in the mouse brain, including the cortex and intra-ventricular epithelial cells of the CP (Ren et al., 2009). However, these authors have described that expression of these receptors (*Tas1r1*, *Tas1r2*, and *Tas1r3*) is lower in cortex. Transcripts of these receptors were also found in rat choroid plexus along with some of the downstream signalling molecules (Tomás et al., 2016). Despite these findings in mouse and rat, one cannot extrapolate to human. In fact, in the present study we could not detect *TAS1Rs* in orbitofrontal cortex by means of RT-qPCR. However, this could be due to low expression and therefore standing bellow the detection limit of the technique. To our knowledge, no studies have shown to date expression of *TAS1Rs* in human brain.

The existence of olfactory receptors outside the olfactory sensory system was first documented in mammalian germ cells, and it was suggested that these ectopic *ORs* could have a role in chemotaxis during fertilization (Parmentier et al., 1992). After this initial discovery, mammalian *ORs* genes were found in various additional non-olfactory tissues including the brain (Feldmesser et al., 2006). Three receptors, *M71*, *C6*, and *OR3* were detected in the mouse cerebral cortex (Otaki et al., 2004). Additionally, the odorant receptor, *MOL2.3*, was shown to be expressed in the mouse ganglia of the autonomic nervous system (Weber et al., 2002). Some ORs and olfactory signalling pathway components were also found to be expressed and to be functional in murine CP, suggesting that they might be involved in the CP chemical surveillance apparatus in detecting alterations in the CSF composition and eliciting responses that modulate and maintain brain homeostasis (Gonçalves et al., 2016).

Nevertheless, the first evidence that several *ORs* are widely expressed in the human CNS was revealed in 2013 by Garcia-Esparcia and colleagues. Using TaqMan PCR analysis, they found

expression of several *ORs* in cerebral cortex, thalamus, selected nuclei of the brainstem, and Purkinje cells of the cerebellum (Garcia-Esparcia et al., 2013). Interestingly, certain nuclei of the brainstem together with Purkinje cells showed strong *OR* expression (at least for the *ORs* examined *OR2H2*, *OR2A4*, and *OR6K3*) and within the cerebral cortex, the major expression occurred not only in the CA1 area and hilus of the hippocampus but also in the entorhinal cortex and neocortical areas examined. Central *OR* neuronal expression was accompanied by the obliged functional molecules of the *OR* pathway in sensory olfactory neurons, *AC3*, and Ga_{olf}, indicating that the *OR* machinery is also able to operate, at least, in selected regions of the CNS and, particularly, in the cerebral cortex.

In fact, some recent studies have reported the regulation of olfactory and taste receptors in diverse physiological and pathological settings. Previous gene array studies identified two clusters of dysregulated *ORs* and *TASRs* in the cerebral cortex in Parkinson's disease, which were validated by RT-qPCR, demonstrating for the first time dysregulation of *ORs* and *TASRs* in the cerebral cortex (and substantia nigra) in this disease (Garcia-Esparcia et al., 2013). The same genes were analysed in AD, Progressive Supranuclear Palsy and Creutzfeldt-Jakob disease, and although with disease-specific patterns, *ORs* and *TASRs* were found to be dysregulated in the frontal cortex in these diseases (Ansoleaga et al., 2013). More precisely in AD, two out of eight *ORs* analysed in entorhinal cortex (*OR4F4* and *OR11H1*) were dysregulated at Braak stages III–IV and V–VI, but one additional *OR* (*OR10G8*) and two *TASRs* (*TAS2R5* and *TAS2R10*) were only dysregulated at advanced stages of the disease. In frontal cortex, only one *OR* (*OR52L1*) mRNA analysed was significantly altered at stages III–IV and V–VI and no *TASR* mRNA levels were found altered (Ansoleaga et al., 2013). Thus, this data suggest increased gene dysregulation (manifested either as down- or upregulation depending on the receptor) with AD progression. These previous observations also indicate disease-specific dysregulation of *ORs* and *TASRs* in several neurodegenerative diseases with abnormal protein aggregates. Nevertheless, down-regulation of *ORs* and *TASRs* in the prefrontal cortex was also found in schizophrenia, a disease not linked to abnormal protein aggregates (Ansoleaga et al., 2015).

Our transcriptomic analysis revealed that olfactory receptors (*ORs*) and taste receptors (*TASRs*) are expressed in human orbitofrontal cortex and that their mRNA levels are differentially regulated in female and male AD patients.

Indeed, olfactory receptors *OR2K2*, *OR2H2* and *OR1L8* and taste receptor *TAS2R14* were downregulated at some AD Braak stages when compared to age-matched controls in the orbitofrontal cortex of female AD patients. More precisely, *OR2H2*, *OR1L8* and *TAS2R14* were downregulated at AD Braak stage I, and *OR2K2* besides stage I was also downregulated at AD Braak stages V and VI. Although not reaching statistical significance, it was also noticeable in *OR2H2*, *OR1L8* and *TAS2R14* the tendency to be downregulated in stages V and VI. On the other hand, even though no regulation was observed in *TAS2R5* when normalized to two out of three housekeeping genes, when normalized to *PGK1*, *TAS2R5* was also downregulated in AD Braak stage I and presented the same tendency to be downregulated in stages V and VI.

These findings present us the urge to increase the number of subjects in order to strengthen these results and some of the perceptible differences.

Additionally, in female, it was evident the same sort of ascendant ladder pattern between AD Braak stages I to VI in most of the chemoreceptors studied, i.e. stage V seemed to be upregulated compared to stage I, and stage VI seemed to be upregulated compared to stages I and V. In fact, olfactory receptors *OR2K2*, *OR2H2*, *OR1L8* and taste receptor *TAS2R14* shared this tendency except for *TAS2R5*. Furthermore, *OR2K2*, *OR2H2* and *TAS2R14* were indeed upregulated at stage VI compared to stage I as revealed by statistical analysis.

These findings lead us to believe that, downregulation of *ORs* and *TASRs* at a very early stage (AD Braak stage I), is an early event in the pathogenesis of the disease and despite their tendency to increase in later stages, probably as a response to the progression of the disease (at the biochemical and structural level) the orbitofrontal cortex is not capable of restoring the levels observed in control patients.

In contrast, in the orbitofrontal cortex of male AD patients no regulation was observed in these same chemoreceptors compared to age-matched controls. Despite not reaching statistical significance, it was noticeable in *OR2K2* and *OR1L8* the tendency to be upregulated in AD Braak stage V and in *OR1L8* and *TAS2R5* the tendency to be downregulated in AD Braak stage IV compared to age-matched controls.

These variations reveal the need to enlarge the number of subjects of each AD Braak stage so that the results could be more homogenous and also could possibly reach statistical significance. At the moment, we can only conclude that, in male, these chemoreceptors are not dysregulated.

On the other hand, other chemoreceptors in study, namely the olfactory receptors *OR13A1*, *OR7A17* and the taste receptors type I *TAS1R1*, *TAS1R2* and *TAS1R3*, failed to be detected or quantifiable by RT-qPCR, i.e. either their amplification was in the edge or exceeded the reliable detection limit of this technique or even they did not amplify at all.

The present findings indicate sex-specific vulnerability of certain *ORs* and *TASRs* in AD, thus suggesting that at least a subpopulation of these chemoreceptors in orbitofrontal cortex could be modulated by steroid hormones or their derivatives.

Interestingly, recent studies have provided insight into the neuroprotective effects of sex hormones and their beneficial effects in neurodegenerative diseases (Bourque et al., 2009; Carroll et al., 2012), particularly in AD, a pathology often associated with sexual hormone levels decline. Also, steroid hormones such as androstenone and androstadienone had been identified as *ORs* ligands (Keller et al., 2007).

Additionally, a recent study from CICS (Centro de Investigação em Ciências da Saúde, UBI) showed for the first time the response of the transcriptome of female and male rat CP to a decline in sex hormone levels induced by gonadectomy (Quintela et al., 2013). Compared to

sham animals, gonadectomy generated more transcriptional changes in females than in males. The decline of hormone levels clearly induced in choroid plexus of female rats, among others, an upregulation of 7 genes in the taste transduction pathway, and upregulation of 102 genes and downregulation of 282 genes in the olfactory transduction pathway. On the contrary, in choroid plexus of male rats it only induced an upregulation of 42 genes in the olfactory transduction pathway. This study provided the first evidence that the expression of taste and olfactory-related genes in rat CP are under the control of sex steroid hormones (Quintela et al., 2013).

Nevertheless, when we tried to detect the olfactory and taste receptors in study in human male CP samples, the same struggle arose as mentioned before in the detection of *OR13A1*, *OR7A17* and the *TAS1Rs* in orbitofrontal cortex. In fact, extrapolate their expression from rat to human is no small task as it is known that exists a great variability between species in the number and distribution of taste and olfactory receptors. Additionally, using human post-mortem tissues for gene expression studies is particularly challenging. Besides the problem of impaired RNA one has to face a very high degree of biological variance within a sample set. Variations of individual parameters like age, body mass, health, but also the cause and circumstances of death and the post-mortem interval can lead to a rather inhomogeneous collection of samples (Vennemann & Koppelkamm, 2010). And, indeed despite the efforts made, it was impossible to detect or quantify any of the chemoreceptors in study in this tissue by the RT-qPCR technique. Which can possibly mean that some of them are not even expressed in choroid plexus, or that it is needed a more sensitive and precise technique in order to potentiate their detection and amplification.

Therefore, a suitable technique to perform these low-level gene expression analyses would be the Digital PCR. This is supported by the fact that where RT-qPCR shows limitations, Digital PCR shows a significantly higher sensitivity due to the improvement in accuracy and precision of the assay by counting larger numbers of molecules individually. Digital PCR is based on the concept of limiting dilutions. Practically a reaction is split into a large number of sub-reactions so that individual target copies are separated by the process of partitioning. After thermal cycling and read-out this leads to the classification of each partition as either positive (containing target) or negative (no target present). As a consequence, Digital PCR is an absolute quantification strategy by default. This is quite different from RT-qPCR, which is based on the proportionality between fluorescence and DNA mass and where quantification is always relative (Lievens et al, 2016).

Furthermore, we cannot speculate whether the olfactory and taste receptors transcripts that we have found to be expressed in both CP and cortex are functional or not. Then, in order to identify additional function profiles of these receptors, we will check whether the transcripts are being translated into protein, by means of western blot or immunohistochemistry. However, there are limitations posed by the small number of antibodies available. The main issue to struggle with is that these *GPCRs* have a restricted extracellular surface where epitopes can be

ligand sensitive, and also they are characterized by high conformation variability (Salon et al., 2011; Jo & Jung, 2016). Currently, the only antibody commercially available and suitable for these applications is *OR2H2*, so we cannot validate the protein expression for the other *ORs* described in this study.

Additionally, functional studies will be performed in rat primary cultures of cortical cells and CP (where we will previously check the expression of the corresponding orthologues) by adding synthetic compounds and checking activation of the corresponding signaling pathways and downstream effectors.

VII. References

ACOSTA-BAENA N, SEPULVEDA-FALLA D, LOPERA-GÓMEZ CM, et al. (2011) Pre-dementia clinical stages in presenilin 1 E280A familial early-onset Alzheimer's disease: a retrospective cohort study. *Lancet Neurol*, 10(3):213-20.

ADIPIETRO KA, MAINLAND JD, MATSUNAMI H (2012) Functional evolution of mammalian odorant receptors. *PLoS Genet*, 8(7):e1002821.

ALBERT MS, DEKOSKY ST, DICKSON D, DUBOIS B, FELDMAN HH, FOX N, et al.(2011) The diagnosis of mild cognitive impairment due to Alzheimer's disease: recommendations from the National Institute on Aging–Alzheimer's Association workgroups on diagnostic guidelines for Alzheimer's disease. *Alzheimers Dement,* 7:270–9.

ALIYEV A, SEYIDOVA D, RZAYEV N, OBRENOVICH ME, LAMB BT, CHEN SG, SMITH MA, PERRY G, DE LA TORRE JC, ALIEV G (2004) Is nitric oxide a key target in the pathogenesis of brain lesions during the development of Alzheimer's disease? *Neurol Res,* 26(5):547–53.

ALONI R, OLENDER T, LANCET D (2006) Ancient genomic architecture for mammalian olfactory receptor clusters. *Genome Biol*, 7(10):R88.

ALVIRA-BOTERO X, CARRO EM (2010) Clearance of amyloid-beta peptide across the choroid plexus in Alzheimer's disease. *Curr Aging Sci,* 3(30):219–29.

ANSOLEAGA B, GARCIA-ESPARCIA P, LLORENS F, MORENO J, ASO E, FERRER I (2013) Dysregulation of brain olfactory and taste receptors in AD, PSP and CJD, and AD-related model. *Neuroscience*, 248:369-82.

ANSOLEAGA B, GARCIA-ESPARCIA P, PINACHO R, HARO JM, RAMOS B, FERRER I (2015) Decrease in olfactory and taste receptor expression in the dorsolateral prefrontal cortex in chronic schizophrenia. *J Psychiatric Res*, 60:109-16.

ANSTEY KJ, CHERBUIN N, BUDGE M, YOUNG J (2011) Body mass index in midlife and late-life as a risk factor for dementia: A meta analysis of prospective studies. *Obes Rev*, 12(5):e426–37.

ANSTEY KJ, VON SANDEN C, SALIM A, O'KEARNEY R (2007) Smoking as a risk factor for dementia and cognitive decline: A meta-analysis of prospective studies. *Am J Epidemiol*, 166(4):367–78.

ANTEQUERA D, VARGAS T, UGALDE C, et al (2009) Cytoplasmic gelsolin increases mitochondrial activity and reduces Abeta burden in a mouse model of Alzheimer's disease. *Neurobiol Dis*, 36:42–50

ANTHONY SG, SCHIPPER HM, TAVARES R, HOVANESIAN V et al. (2003) Stress protein expression in the Alzheimer-diseased choroid plexus. *J Alzheimers Dis*, 5(3)171-7.

APTER JT, SHASTRI K, PIZANO K (2015) Update on Disease-Modifying/Preventive Therapies in Alzheimer's Disease. *Curr Geriatr Rep*, 4(4):312-317.

BARRET LF, SIMMONS WK (2015) Interoceptive predicitions in the brain. *Nat Rev Neurosci*, 16(7):419-29.

BEHRENS M, MEYERHOF W (2006) Bitter taste receptors and human bitter taste perception. *Cell Mol Life Sci*, 63(13):1501–9.

BEHRENS M, MEYERHOF W (2010) Oral and extraoral bitter taste receptors. *Results Probl Cell Differ*, 52:87-99.

BEKRIS LM, YU CE, BIRD TD, TSUANG DW (2010) Genetics of Alzheimer disease. *J Geriatr Psychiatry Neurol,* 23(4):213–27.

BEZENÇON C, LE COUTRE J, DAMAK S (2007) Taste-signaling proteins are coexpressed in solitary intestinal epithelial cells. *Chem Senses*, 32:41–9.

BLASS JP (2002) Alzheimer's disease and Alzheimer's dementia: distinct but overlapping entities. *Neurobiol Aging*, 23:1077-84.

BOURQUE M, DLUZEN DE, DI PAOLO T (2009) Neuroprotective actions of sex steroids in Parkinson's disease. *Front Neuroendocrinol*, 30:142–57.

BRAAK H, ALAFUZOFF I, ARZBERGER T, KRETZSCHMAR H, DEL TREDICI K (2006) Staging of Alzheimer disease-associated neurofibrillary pathology using paraffin sections and immunocytochemistry. *Acta Neuropathol*, 112(4):389-404.

BRAUN T, VOLAND P, KUNZ L, PRINZ C, GRATZL M (2007) Enterochromaffin cells of the human gut: sensors for spices and odorants. *Gastroenterology*, 132:1890-901.

BUTTERFIELD DA, POON HF, ST CLAIR D, KELLER JN, PIERCE WM, KLEIN JB, MARKESBERY WR (2006) Redox proteomics identification of oxidatively modified hippocampal proteins in mild cognitive impairment: insights into the development of Alzheimer's disease. *Neurobiol Dis,* 22(2):223-32.

CALKINS MJ, MANCZAK M, MAO P, SHIRENDEB U, REDDY PH (2011) Impaired mitochondrial biogenesis, defective axonal transport of mitochondria, abnormal mitochondrial dynamics and synaptic degeneration in a mouse model of Alzheimer's disease. *Hum Mol Genet*, 20(23):4515-29.

CALVO SS & EGAN JM (2015) The endocrinology of taste receptors. *Nat Rev Endocrinol*, 11(4):213-27.

CARRO E, TREJO JL, SPUCH C, BOHL D, HEARD JM, TORRES-ALEMAN I (2006) Blockade of the insulin-like growth factor I receptor in the choroid plexus originates Alzheimer's-like neuropathology in rodents: new cues into the human disease? *Neurobiol Aging*, 27:1618–1631.

CARROLL JC, ROSARIO ER (2012) The potential use of hormone-based therapeutics for the treatment of Alzheimer's disease. *Curr Alzheimer Res*, 9(1):18-34.

CASTELLANI RJ, ROLSTON RK, SMITH MA (2010) Alzheimer Disease. *Dis Mon*, 56(9):484-546.

CHAUDHARI N (2014) Synaptic communication and signal processing among sensory cells in taste buds. *J Physiol*, 592(16):3387-92.

CHAUDHARI N, ROPER SD (2010) The cell biology of taste. *J Cell Biol*, 190(3):285-96.

CHEN X, GUO C, KONG J (2012) Oxidative stress in neurodegenerative diseases. *Neural Regen Res*, 7(5):376-85.

CHIAVARAS MM, PETRIDES M (2000) Orbitofrontal sulci of the human and macaque monkey brain. *J Comp Neurol*, 422(1):35-54.

CHODOBSKI A, SZMYDYNGER-CHODOBSKA J (2001) Choroid plexus: target for polypeptides and site of their synthesis. *Microsc Res Tech*, 52:65–82

CLARK AA, LIGGETT SB, MUNGER SD (2012) Extraoral bitter taste receptors as mediators of off-target drug effects. *FASEB J*, 26(12):4827-31.

COHEN SP, BUCKLEY BK, KOSLOFF M, GARLAND AL, BOSCH DE, CHENG G, Jr et al. (2012) Regulator of G-protein signaling-21 (RGS21) is an inhibitor of bitter gustatory signaling found in lingual and airway epithelia. *J Biol Chem*, 287:41706–19.

CORNUTIU G (2015) The Epidemiological Scale of Alzheimer's Disease. *J Clin Med Res.*, 7(9):657-666

COTTRELL DA, BLAKELY EL, JOHNSON MA, INCE PG, TURNBULL DM (2001) Mitochondrial enzyme-deficient hippocampal neurons and choroidal cells in AD. *Neurology* 57(2):260–4.

CROSSGROVE JS, LI GJ, ZHENG W (2005) The choroid plexus removes beta-amyloid from brain cerebrospinal fluid. *Exp Biol Med (Maywood),* 230:771–776

CROSSGROVE JS, SMITH EL, ZHENG W (2007) Macromolecules involved in production and metabolism of beta-amyloid at the brain barriers. *Brain Res,* 1138:187–95.

DAMKIER HH, BROWN PD, PRAETORIUS J (2013) Cerebrospinal fluid secretion by the choroid plexus. *Physiol Rev*, 93(4):1847-92.

DAMOISEAUX JS, SEELEY WW, ZHOU J, et al. (2012) Alzheimer's Disease Neuroimaging Initiative Gender modulates the APOE ε4 effect in healthy older adults: convergent evidence from functional brain connectivity and spinal fluid tau levels. *J Neurosci*, 32(24):8254–62.

DE LA CRUZ O, BLECHMAN R, ZHANG X, NICOLAE D, FIRESTEIN S, GILAD Y (2009) A signature of evolutionary constraint on a subset of ectopically expressed olfactory receptor genes. *Mol Biol Evol*, 26:491-4.

DEHKORDI O, ROSE JE, FATEMI M, ALLARD JS, BALAN KV et. (2012) Neuronal expression of bitter taste receptors and downstream signaling molecules in the rat brainstem. *Brain Res*, 1475:1-10.

DE-PAULA VJ, RADANOVIC M, DINIZ BS, FORLENZA OV (2012) Alzheimer's disease. *Subcell Biochem*, 65:329-52.

DESHPANDE DA, WANG WCH, MCILMOYLE EL, ROBINETT KS, SCHILLINGER RM, AN SS et al. (2010) Bitter taste receptors on airway smooth muscle bronchodilate by localized calcium signaling and reverse obstruction. *Nat Med*, 16:1299–304.

DIETRICH MO, SPUCH C, ANTEQUERA D, et al. (2008) Megalin mediates the transport of leptin across the blood-CSF barrier. *Neurobiology of Aging,* 29(6):902–912.

DOTSON CD, ZHANG L, XU H, SHIN YK, VIGUES S, OTT SH et al. (2008) Bitter taste receptors influence glucose homeostasis. *PLoS One*, 3:e3974.

DURZYNSKI L, GAUDIN JC, MYGA M, SZYDLOWSKI J, GOZDZICKA-JOZEFIAK A, HAERTLE T (2005) Olfactory-like receptor cDNAs are present in human lingual cDNA libraries. *Biochem Biophys Res Commun*, 333:264-72.

FEINGOLD EA, PENNY LA, NIENHUIS AW, FORGET BG (1999) An olfactory receptor gene is located in the extended human beta-globin gene cluster and is expressed in erythroid cells. *Genomics*, 61:15-23.

FELDMESSER E, OLENDER T, KHEN M, YANAI I, OPHIR R, LANCET D (2006) Widespread ectopic expression of olfactory receptors genes. *BMC Genomics*, 7:121.

FINGER TE, BÖTTGER B, HANSEN A, ANDERSON KT, ALIMOHAMMADI H, SILVER WL (2003) Solitary chemoreceptor cells in the nasal cavity serve as sentinels of respiration. *Proc Natl Acad Sci USA*, 100(15):8981-6.

FORLENZA OV, DINIZ BS, GATTAZ WF (2010) Diagnosis and biomarkers of predementia in Alzheimer's disease. *BMC Med*, 8:89.

FOSTER SR, PORRELLO ER, PURDUE B, CHAN HW, VOIGT A, FRENZEL S et al. (2013a) Expression, regulation and putative nutrient-sensing function of taste GPCRs in the heart. *PLoS One*, 8:e64579.

FOSTER SR, ROURA E, THOMAS WG (2013b) Extrasensory perception: odorant and taste receptors beyond the nose and mouth. *Pharmacol Ther*, 142(1):41-61.

FOSTER SR, ROURA E, THOMAS WG (2014) Extrasensory perception: Odorant and taste receptors beyond the nose and mouth. *Pharmacol Ther,* 142(1):41–61.

FUKUDA N, YOMOGIDA K, OKABE M, TOUHARA K (2004) Functional characterization of a mouse testicular olfactory receptor and its role in chemosensing and in regulation of sperm motility. *J Cell Sci*, 117:5835-45.

FUKUMOTO N, FUJII T, COMBARROS O et al. (2010) Sexually dimorphic effect of the Val66Met polymorphism of BDNF on susceptibility to Alzheimer's disease: New data and meta-analysis. *Am J Med Genet B Neuropsychiatr Genet, 153B(1):235-42*.

GAILLARD I, ROUQUIER S, GIORGI D (2004) Olfactory receptors. *Cell Mol Life Sci*, 61(4):456-69.

GARCÍA-ESCUDERO V, MARTÍN-MAESTRO P, PERRY G, AVILA J (2013) Deconstructing mitochondrial dysfunction in Alzheimer disease. *Oxid Med Cell Longev*, 2013:162152.

GARCIA-ESPARCIA P, SCHLÜTER A, CARMONA M, MORENO J, ANSOLEAGA B, TORREJÓN-ESCRIBANO B, GUSTINCICH S, PUJOL A, FERRER I (2013) Functional genomics reveals dysregulation of cortical olfactory receptors in Parkinson disease: novel putative chemoreceptors in the human brain. *J Neuropathol Exp Neurol*, 72(6):524-39.

GASPARD N, VANDERHAEGHEN P (2011) Laminar fate specification in the cerebral cortex. *F1000 Biol Rep*, 3:6.

GAUDIN JC, BREUILS L, HAERTLE T (2001) New GPCRs from a human lingual cDNA library. *Chem Senses*, 26:1157-66.

GENECARDS HUMAN GENE DATABASE (2016) *Weizmann Institute of Science*. [Accessed February 11th 2016]. Available from: http://www.genecards.org/

GERSPACH AC, STEINERT RE, SCHÖNENBERGER L, GRABER-MAIER A, BEGLINGER C (2011) The role of the gut sweet taste receptor in regulating GLP-1, PYY and CCK release in humans. *Am J Physiol Endocrinol Metab*, 301:E317–25.

GOLDMAN JS, HAHN SE, BIRD T (2011) Genetic counseling and testing for Alzheimer disease: Joint practice guidelines of the American College of Medical Genetics and the National Society of Genetic Counselors. *Genet Med*, 13:597–605.

GOLDMAN JS, HAHN SE, CATANIA JW et al. (2012) Genetic counseling and testing for Alzheimer disease: Joint practice guidelines of the American College of Medical Genetics and the National Society of Genetic Counselors. *Genet Med*, 13(6):597-605.

GONÇALVES I, HUBBARD PC, TOMÁS J, QUINTELA T, TAVARES G, CARIA S, BARREIROS D, SANTOS CR (2016) "Smelling" the cerebrospinal fluid: olfactory signaling molecules are expressed in and mediate chemosensory signaling from the choroid plexus. *FEBS J*, 283(9):1748-66.

GOTO T, SALPEKAR A, MONK M (2001) Expression of a testis-specific member of the olfactory receptor gene family in human primordial germ cells. *Mol Hum Reprod*, 7:553-8.

GOTZ J, CHEN F, VAN DORPE J, NITSCH RM (2001) Formation of neurofibrillary tangles in P301l tau transgenic mice induced by Abeta 42 fibrils. *Science*, 293:1491-5.

GOURAS GK, WILLÉN K, TAMPELLINI D (2012) Critical role of intraneuronal Aß in Alzheimer's disease: technical challenges in studying intracellular Aß. *Life Sci*, 91(23-24):1153-8.

GREEN RC, CUPPLES LA, GO R, BENKE KS, EDEKI T, GRIFFITH PA, et al.(2002) Risk of dementia among white and African American relatives of patients with Alzheimer disease. *JAMA*, 287:329–36.

GREENBERG SM, GUROL ME, ROSAND J, SMITH EE (2004) Amyloid angiopathy-related vascular cognitive impairment. *Stroke*, 35(11 Suppl 1):2616-9.

GRIFFIN CA, KAFADAR KA, PAVLATH GK (2009) MOR23 promotes muscle regeneration and regulates cell adhesion and migration. *Dev Cell*, 17:649-61.

GU Y, NIEVES JW, STERN Y, LUCHSINGER JA, SCARMEAS N (2010) Food combination and Alzheimer disease risk: A protective diet. *Arch Neurol*, 67(6):699–706.

GUSKIEWICZ KM (2005) Association between recurrent concussion and latelife cognitive impairment in retired professional football players. *Neurosurgery*, 57:719–26.

HAKAK Y, SHRESTHA D, GOEGEL MC, BEHAN DP, CHALMERS DT (2003) Global analysis of G-protein-coupled receptor signaling in human tissues. *FEBS Lett*, 550:11-7.

HENION TR, SCHWARTING GA (2007) Patterning the developing and regenerating olfactory system. *J Cell Physiol*, 210(2):290–7.

HOLLAND D, DESIKAN RS, DALE AM, MCEVOY LK (2013) Higher rates of decline for women and APOE ε4 carriers. *AJNR Am J Neuroradiol*, 34(12):2287-93.

HOLTZMAN DM, HERZ J, BU G (2012) Apolipoprotein E and apolipoprotein E receptors: Normal biology and roles in Alzheimer disease. *Cold Spring Harb Perspect Med*, 2(3):a006312.

HOOZEMANS JJ, VEERHUIS R, VAN HAASTERT ES, et al. (2005) The unfolded protein response is activated in Alzheimer's disease. *Acta Neuropathol*, 110:165-72.

HORNAK J, BRAMHAM J, ROLLS ET, MORRIS RG, O'DOHERTY J, BULLOCK PR, POLKEY CE (2003) Changes in emotion after circumscribed surgical lesions of the orbitofrontal and cingulate cortices. *Brain*, 126:1671–1712.

HUANG W, QIU C, VON STRAUSS E, WINBLAD B, FRATIGLIONI L (2004) APOE genotype, family history of dementia, and Alzheimer's disease risk: a 6-year follow-up study. *Arch Neurol*, 61(12):1930-4.

HUANG YA, ROPER SD (2010) Intracellular Ca (2+) and TRPM5-mediated membrane depolarization produce ATP secretion from taste receptor cells. *J Physiol*, 588(Pt 13):2343-50.

ICHIMURA A, HIRASAWA A, POULAIN-GODEFROY O, BONNEFOND A, HARA T, YENGO L et al. (2012) Dysfunction of lipid sensor GPR120 leads to obesity in both mouse and human. *Nature*, 483:350–4.

INSEL PA, SNEAD A, MURRAY F, ZHANG L, YOKOUCHI H, KATAKIA T et al. (2012) GPCR expression in tissues and cells: Are the optimal receptors being used as drug targets? *Br J Pharmacol*, 165(6):1613-1616.

IQBAL K, LIU F, GONG CX, GRUNDKE-IQBAL I (2010) Tau in Alzheimer Disease and related tauopathies. *Curr Alzheimer Res*, 7(8):656-64.

ITAKURA S, OHNO K, UEKI T, SATO K, KANAYAMA N (2006) Expression of Golf in the rat placenta: Possible implication in olfactory receptor transduction. *Placenta*, 27:103-8.

JACK CR, KNOPMAN DS, JAGUST WJ, SHAW LM, AISEN PS, WEINER MW, PETERSEN RC, TROJANOWSKI JQ (2010) Hypothetical model of dynamic biomarkers of the Alzheimer's pathological cascade. *Lancet Neurol*, 9:119-28.

JANG HJ, KOKRASHVILI Z, THEODORAKIS MJ, CARLSON OD, KIM BJ, ZHOU J et al. (2007) Gut-expressed gustducin and taste receptors regulate secretion of glucagon-like peptide-1. *Proc Natl Acad Sci USA*, 104:15069–74.

JEON TI, SEO YK, OSBORNE TF (2011) Gut bitter taste receptor signaling induces ABCB1 through a mechanism involving CCK. *Biochem J*, 438:33–7.

JO M, JUNG ST (2016) Engineering therapeutic antibodies targeting G-protein-coipled receptors. *Exp Mol Med*, 48:e207.

JOHANSON C, MCMILLAN P, TAVARES R, SPANGENBERGER A, DUNCAN J, SILVERBERG G, STOPA E (2004) Homeostatic capabilities of the choroid plexus epithelium in Alzheimer's disease. *Cerebrospinal Fluid Res*, 10(1):3

JOHNSTON M, ZAKHAROV A, KOH L, ARMSTRONG D (2005) Subarachnoid injection of Microfil reveals connections between cerebrospinal fluid and nasal lymphatics in the non-human primate. *Neuropathol Appl Neurobiol*, 31(6)632-40.

JUNG BH, JEON MJ, BAI SW (2008) Hormone-dependent aging problems in women. *Yonsei Med*, 49(3):345-51.

JUNG HY, KIM W, YOO DY, NAM SM, KIM JW, CHOI JH, YOON YS, KIM HY, HWANG IK (2014) Intragastric gavage with denatonium benzoate acutely induces neuronal activation in the solitary tract nucleus via the vagal afferent pathway. *J Vet Sci*, 15(4):459-64.

KAJI I, KARAKI S, FUKAMI Y, TERASAKI M, KUWAHARA A (2009) Secretory effects of a luminal bitter tastant and expressions of bitter taste receptors, T2Rs, in the human and rat large intestine. *Am J Physiol Gastrointest Liver Physiol*. 296:G971–81.

KANAGESWARAN N, DEMOND M, NAGEL M, SCHREINER BSP, BAUMGART S, SCHOLZ P, et al. (2015) Deep Sequencing of the Murine Olfactory Receptor Neuron Transcriptome. *PLoS One*, 10(1): e0113170.

KANG N, KOO J (2012) Olfactory receptors in non-chemosensory tissues. *BMP Rep*, 45(11):612-22.

KATRITCH V, CHEREZOV V, STEVENS RC (2013) Structure-function of the G protein-coupled receptor superfamily. *Annu Rev Pharmacol Toxicol*, 53:531-56.

KEIL U, BONERT A, MARQUES CA, et al. (2004) Amyloid beta-induced changes in nitric oxide production and mitochondrial activity lead to apoptosis. *J Biol Chem*, 279(48):50310–20.

KELLER A, ZHUANG H, CHI Q, VOSSHALL LB, MATSUNAMI H (2007) Genetic variation in a human odorant receptor alters odour perception. *Nature*, 449: 468–472.

KHLISTUNOVA I, BIERNAT J, WANG Y, et al. (2006) Inducible expression of Tau repeat domain in cell models of tauopathy: aggregation is toxic to cells but can be reversed by inhibitor drugs. *J Biol Chem*, 281:1205-14.

KIM SH, YOON YC, LEE AS, KANG N, KOO J, RHYU MR, PARK JH (2015) Expression of human olfactory receptor 10J5 in heart aorta, coronary artery, and endothelial cells and its role in angiogenesis. *Biochem Biophys Res Commun,* 460:404-8.

KIROVA AM, BAYS RB, LAGALWAR S (2015) Working memory and executive function decline across normal aging, mild cognitive impairment, and Alzheimer's disease. *Biomed Res Int*, 2015:748212.

KNOPMAN DS, PARISI JE, SALVIATI *A et al*. (2003) Neuropathology of cognitively normal elderly. *J Neuropathol Exp Neurol, 62:1087-95.*

KOH L, ZAKHAROV A, NAGRA G, ARMSTRONG D, FRIENDSHIP R, JOHNSTON M (2006) Development of cerebrospinal fluid absorption sites in the pig and rat: connections between the subarachnoid space and lymphatic vessels in the olfactory turbinates. *Anat Embryol*, 211(4):335-44.

KRINGELBACH ML (2005) The orbitofrontal cortex: linking reward to hedonic experience. *Nat Rev Neurosci,* 6:691–702.

KRZYZANOWSKA A, CARRO E (2012) Pathological alterations in the choroid plexus of Alzheimer's disease: implications for new therapy approaches. *Front Pharmacol*, 3;3:75.

LAGERSTROM MC, SCHIOTH HB (2008) Structural diversity of G protein-coupled receptors and significance for drug discovery. Nat Rev Drug Discov, 7(4):339-57.

LEE RJ, XIONG G, KOFONOW JM, CHEN B, LYSENKO A, JIANG P et al. (2012) T2R38 taste receptor polymorphisms underlie susceptibility to upper respiratory infection. *J Clin Invest*, 122:4145–59.

LEHTINEN MK, ZAPPATERRA MW, CHEN X, YANG YJ et al. (2011) The cerebrospinal fluid provides a proliferative niche for neural progenitor cells. *Neuron*, 69(5):893-905.

LEWIS J, DICKSON DW, LIN WL, et al. (2001) Enhanced neurofibrillary degeneration in transgenic mice expressing mutant tau and APP. *Science*, 293:1487-91.

LI X, STASZEWSKI L, XU H, DURICK K, ZOLLER M, ADLER E (2002) Human receptors for sweet and umami taste. *Proc Natl Acad Sci USA*, 99(7):4692-6.

LIEVENS A, JACCHIA S, KAGKLI D, SAVINI C, QUERCI M (2016) Measuring Digital PCR quality: performance parameters and their optimization. *PLoS One*, 11(5):e0153317.

LIU CC, KANEKIYO T, XU H, BU G (2013) Apolipoprotein E and Alzheimer's disease: risk, mechanisms, and therapy. *Nat Rev Neurol*, 9(2):106-18.

LIU Y, PAAJANEN T, WESTMAN E, et al. (2010) AddNeuroMed Consortium Effect of APOE ε4 allele on cortical thicknesses and volumes: the AddNeuroMed study. *J Alzheimers Dis*, 21(3):947–66.

LIU Y, YU JT, WANG HF, HAN PR, TAN CC, WANG C, MENQ XF, RISACHER SL, SAYKIN AJ, TAN L (2015) APOE genotype and neuroimaging markers of Alzheimer's disease: systematic review and meta-analysis. *J Neurol Neurosurg Psychiatry*, 86(2):127-34.

LIVAK KJ, SCHIMITTGEN TD (2001) Analysis of relative gene expression data using realt-time quantitative PCR and the 2(-Delta Delta C(T)) Method. *Methods*, 25(4):402-8.

LOBUE C, DENNEY D, HYNAN L et al. (2016) Self-reported traumatic brain injury and mild cognitive impairment: increased risk and earlier age of diagnosis. *J Alzheimers Dis*, 51(3):727-36.

LOEF M, WALACH H (2013). Midlife obesity and dementia: Meta-analysis and adjusted forecast of dementia prevalence in the United States and China. *Obesity (Silver Spring)*, 21(1):E51–5.

LOPEZ SALON M, MORELLI L, CASTANO EM, SOTO EF, PASQUINI JM (2000) Defective ubiquitination of cerebral proteins in Alzheimer's disease. *J Neurosci Res*, 62:302-10.

LOURIDA I, SONI M, THOMPSON-COON J, PURANDARE N, LANG IA, UKOUMUNNE OC, et al. (2013) Mediterranean diet, cognitive function, and dementia: A systematic review. *Epidemiol*, 24:479–89.

LOUVEAU A, HARRIS TH, KIPNIS J (2015) Revisiting the mechanisms of CNS immune priviledge. Trends Immunol, 36(10):569-77.

LOY CT, SCHOFIELD PR, TURNER AM, KWOK JBJ (2014) Genetics of dementia. *Lancet*, 383:828–40.

LUN MP, MONUKI ES, LEHTINEN MK (2015) Development and functions of the choroid plexus-cerebrospinal fluid system. *Nat Rev Neurosci*, 16(8):445-57.

LUND TC, KOBS AJ, KRAMER A, NYQUIST M, KUROKI MT, OSBORN J et al. (2013) Bone marrow stromal and vascular smooth muscle cells have chemosensory capacity via bitter taste receptor expression. *PLoS One*, 8:e58945.

MAKI PM, HENDERSON VW (2012) Hormone therapy, dementia, and cognition: the Women's Health Initiative ten years on. *Climateric*, 15(3):256-62.

MALNIC B, GODFREY PA, BUCK LB (2004) The human olfactory receptor gene family. *Proc Natl Acad Sci USA*, 101(8):2584-9.

MAYEUX R, STERN Y (2012) Epidemiology of Alzheimer disease. *Cold Spring Harb Perspect Med,* 2(8).

MCGINNIS SM, BRICKHOUSE M, PASCUAL B, DICKERSON BC (2011) Age-related changes in the thickness of cortical zones in humans. *Brain Topogr*, 24(3-4):279-91.

MCKHANN GM, KNOPMAN DS, CHERTKOW H, HYMAN BT, JACK CR, KAWAS CH, et al.(2011) The diagnosis of dementia due to Alzheimer's disease: recommendations from the National Institute on Aging–Alzheimer's Association workgroups on diagnostic guidelines for Alzheimer's disease. *Alzheimers Dement*; 7:263–9.

MENG XF, YU JT, WANG HF, TAN MS, WANG C, TAN CC, TAN L (2014) Midlife vascular risk factors and the risk of Alzheimer's disease: A systematic review and meta-analysis. *J Alzheimers Dis*, 42(4):1295–310.

MEYER D, VOIGT A, WIDMAYER P, BORTH H, HUEBNER S, BREIT A et al. (2012) Expression of Tas1 taste receptors in mammalian spermatozoa: functional role of Tas1r1 in regulating basal Ca2+ and cAMP concentrations in spermatozoa. *PLoS One*, 7:e32354.

MEYERHOF W, BATRAM C, KUHN C, BROCKHOFF A, CHUDOBA E, BUFE B, APPENDINO G, BEHRENS M (2010) The molecular receptive ranges of human TAS2R bitter taste receptors. *Chem Senses*, 35(2):157-70.

MIELKE MM, VEMURI P, ROCCA WA (2014) Clinical epidemiology of Alzhiemer's disease: assessing sex and gender differences. *Clin Epidemiol*, 6:37-48.

MISAWA T, ARIMA K, MIZUSAWA H, SATOH J (2008) Close association of water channel AQP1 with amyloid-beta deposition in Alzheimer disease brains. *Acta Neuropathol*, 116:247–260.

MORTAZAVI MM, GRIESSENAUER CJ, ADEEB N, DEEP A et al. (2014) The choroid plexus: a comprehensive review of its history, anatomy, function, histology, embryology, and surgical considerations. *Childs Nerv Syst*, 30(2):205-14.

MUFSON EJ, MALEK-AHMADI M, PEREZ SE, CHEN K (2016) Braak staging, plaque pathology, and APOE status in elderly persons without cognitive impairment. *Neurobiol Aging*, 37:147-53.

NAKAMURA M, NESTOR PG, MCCARLEY RW, LEVITT JJ, HSU L, KAWASHIMA T, et al. (2007) Altered orbitofrontal sulcogyral pattern in schizophrenia. *Brain*, 130:693–707.

NCBI NUCLEOTIDE DATABASE, Bethesda (2016): National Library of Medicine (US), *National Center for Biotechnology Information*. [Acessed February 11th 2016] Available from: http://www.ncbi.nlm.nih.gov/nuccore

NELSON G, CHANDRASHEKAR J, HOON MA, FENG L, ZHAO G, RYBA NJ, ZUKER CS (2002) An amino-acid taste receptor. *Nature*, 416(6877):199-202.

NELSON G, HOON MA, CHANDRASHEKAR J, ZHANG Y, RYBA NJ, ZUKER CS (2001) Mammalian sweet taste receptors. *Cell*, 106(3):381-90.

NELSON PT, BRAAK H, MARKESBERY WR (2009) Neuropathology and cognitive impairment in Alzheimer disease: a complex but coherent relationship. *J Neuropathol Exp Neurol*, 68:1-14.

NESTOR PG, NAKAMURA M, NIZNIKIEWICZ M et al., (2013) In search of the functional neuroanatomy of sociality: MRI subdivisions of orbital frontal cortex and social cognition. *Soc Cogn Affect Neurosci*, **8**(4): 460-7.

NEUHAUS EM, ZHANG W, GELIS L, DENG Y, NOLDUS J, HATT H (2009) Activation of an olfactory receptor inhibits proliferation of prostate cancer cells. *J Biol Chem*, 284:16218-25.

NIIMURA Y (2012) Olfactory receptor multigene family in vertebrates: from the viewpoint of evolutionary genomics. *Curr Genomics*, 13(2):103-14.

NIIMURA Y, NEI M (2007) Extensive gains and losses of olfactory receptor genes in mammalian evolution. *PLoS ONE*, 2(8):e708.

NIKI M, YOSHIDA R, TAKAI S, NINOMIYA Y (2010) Gustatory signaling in the periphery: Detection, transmission and modulation of taste information. *Biol Pharm Bull*, 33(11):1772-7.

NUNOMURA A, PERRY G, ALIEV G, et al. (2001) Oxidative damage is the earliest event in Alzheimer disease. *J Neuropathol Exp Neurol*, 60:759-67.

ODDO S, CACCAMO A, SHEPHERD JD, et al. (2003) Triple-transgenic model of Alzheimer's disease with plaques and tangles: intracellular Abeta and synaptic dysfunction. *Neuron*, 39:409-21.

OLENDER T, LANCET D, NEBERT DW (2008) Update on the olfactory receptor (OR) gene superfamily. *Hum Genomics*, 3(1):87-97.

OLGIATI P, POLITIS AM, PAPADIMITRIOU GN, RONCHI DD, SERRETTI A (2011) Genetics of Late-Onset Alzheimer's disease: update from the Alzgene Database and analysis of shared pathways. *Int J Alzheimers Dis*, 2011:832379.

ORSMARK-PIETRAS C, JAMES A, KONRADSEN JR, NORDLUND B, SÖDERHÄLL C, PULKKINEN V et al. (2013) Transcriptome analysis reveals upregulation of bitter taste receptors in severe asthmatics. *Eur Respir J*, 42:65–78.

OTAKI JM, YAMAMOTO H, FIRESTEIN S (2004) Odorant receptor expression in the mouse cerebral cortex. *J Neurobiol*, 58(3):315-27.

OVERINGTON JP, AL-LAZIKANI B, HOPKINS AL (2006) How many drug targets are there? *Nat Rev Drug Discov*, 5(12):993-6.

PARMENTIER M, LIBERT F, SCHURMANS S, SCHIFFMANN S, LEFORT A, et al. (1992) Expression of members of the putative olfactory receptor gene family in mammalian germ cells. *Nature*, 355: 453-455.

PENDLEBURY ST, ROTHWELL PM (2009) Prevalence, incidence, and factors associated with pre-stroke and post-stroke dementia: a systematic review and meta-analysis. *Lancet Neurol*, 8(11):1006–18.

PEREZ-GRACIA E, BLANCO R, CARMONA M, CARRO E, FERRER I (2009) Oxidative stress damage and oxidative stress responses in the choroid plexus in Alzheimer's disease. *Acta Neuropathol*, 118(4):497-504.

PLASSMAN BL, LANGA KM, FISHER GG, et al. (2007) Prevalence of dementia in the United States: the aging, demographics, and memory study. *Neuroepidemiology*, 29(1-2):125-32

PLUZNICK JL, CAPLAN MJ (2012) Novel sensory signaling systems in the kidney. *Curr Opin Nephrol Hypertens*, 21:404-9.

QUERFURTH HW & LAFERLA FM (2010) Alzheimer's disease. *N Engl J Med*, 362(4):329-44.

QUINTELA T, GONÇALVES I, CARRETO LC, SANTOS MAS, MARCELINO H, et al. (2013) Analysis of the Effects of Sex Hormone Background on the Rat Choroid Plexus Transcriptome by cDNA Microarrays. *PLoS One*, 8(4):e60199.

RANSOHOFF RM, ENGELHARDT B (2012) The anatomical and cellular basis of immune surveillance in the central nervous system. *Nat Rev Immunol*, 12(9):623-35.

READNOWER RD, SAUERBECK AD, SULLIVAN PG (2011) Mitochondria, Amyloid *β*, and Alzheimer's Disease. *Int J Alzheimers Dis*, 2011:104545.

REED T, PERLUIGI M, SULTANA R, PIERCE WM, KLEIN JB, TURNER DM, COCCIA R, MARKESBERY WR, BUTTERFIELD DA (2008). Redox proteomic identification of 4-hydroxy-2-nonenal-modified brain proteins in amnestic mild cognitive impairment: insight into the role of lipid peroxidation in the progression and pathogenesis of Alzheimer's disease. *Neurobiol Dis*, 30(1): 107–20.

REITZ C, BRAYNE C, MAYEUX R (2011) Epidemiology of Alzheimer disease. *Nat Rev Neurol*, 7(3):137–52.

REN X, ZHOU L, TERWILLIGER R, NEWTON SS, DE ARAUJO IE (2009) Sweet taste signaling functions as a hypothalamic glucose sensor. *Front Integr Neurosci*, 3:12.

ROBINETT KS, DESHPANDE DA, MALONE MM, LIGGETT SB (2011) Agonist-promoted homologous desensitization of human airway smooth muscle bitter taste receptors. *Am J Respir Cell Mol Biol*, 45:1069–74.

ROHER AE, ESH C, RAHMAN A, KOKJOHN TA, BEACH TG (2004) Atherosclerosis of cerebral arteries in Alzheimer disease. *Stroke*, 35(11 Suppl 1):2623-7.

RÖNNEMA E, ZETHELIUS B, LANNFELT L, KILANDER L (2011) Vascular risk factors and dementia: 40-year follow-up of a population-based cohort. *Dement Geriatr Cogn Disord*, 31(6):460–6.

ROPER SD (2013) Taste buds as peripherial chemosensory processors. *Semin Cell Dev Biol*, 24(1):71-9.

ROZENGURT N, WU SV, CHEN MC, HUANG C, STERNINI C, ROZENGURT E (2006) Colocalization of the alpha-subunit of gustducin with PYY and GLP-1 in L cells of human colon. *Am J Physiol Gastrointest Liver Physiol*, 291:G792–G802.

RUSANEN M, KIVIPELTO M, QUESENBERRY CP, ZHOU J, WHITMER RA (2011) Heavy smoking in midlife and long-term risk of Alzheimer disease and vascular dementia. *Arch Intern Med*, 171(4):333–9.

SALON JA, LODOWSKI DT, PALCZEWSKI K (2011) The significance of G protein-coupled Receptor Crystallography for drug discovery. *Pharmacol Rev*, 63(4):901-37.

SCHELTENS P, BLENNOW K, BRETELER MM, DE STROOPER B et al. (2016) Alzheimer's disease. *Lancet*, pii:S0140-6736(15)01124-1.

SEELEY WW (2008) Selective functional, regional, and neuronal vulnerability in frontotemporal dementia. *Curr Opin Neurol*, 21:701–7.

SEKITA A, NINOMIYA T, TANIZAKI Y, DOI Y, HATA J, YONEMOTO K, ARIMA H, et al. (2010) Trends in prevalence of Alzheimer's disease and vascular dementia in a Japanese community: the Hisayama Study. *Acta Psychiatr Scand*, 122(4):319-325.

SEROT JM, BENE MC, FOLIGUET B, FAURE GC (2000) Morphological alterations of the choroid plexus in late-onset Alzheimer's disease. *Acta Neuropathol*, 99(2):105–8.

SHAH AS, BEN-SHAHAR Y, MONINGER TO, KLINE JN, WELSH MJ (2009) Motile cilia of human airway epithelia are chemosensory. *Science*, 325:1131–4.

SHEPARD BD, PLUZNICK JL (2016) How does your kidney smell? Emerging roles for olfactory receptors in renal function. *Pediatr Nephrol*, 31:715-23.

SHERWOOD L (2013) Human physiology: from cells to systems, 8th Ed. *Cengage Learning*, USA.

SILVERBERG GD, MAYO M, SAUL T, RUBENSTEIN E, MCGUIRE D (2003) Alzheimer's disease, normal-pressure hydrocephalus, and senescent changes in CSF circulatory physiology: a hypothesis. *Lancet Neurol*, 2:506–511.

SINGH N, VRONTAKIS M, PARKINSON F, CHELIKANI P (2011) Functional bitter taste receptors are expressed in brain cells. *Biochem Biophys Res Commum*, 406(1):146-51.

SKUP M, ZHU H, WANG Y, GIOVANELLO KS, LIN JA, SHEN D, SHI F, GAO W, LIN W, FAN Y, ZHANG H (2011) Sex differences in grey matter atrophy patterns among AD and aMCI patients: results from ADNI. *Alzheimer's Disease Neuroimaging Initiative Neuroimage, 56(3):890-906.*

SOLOMON A, KIVIPELTO M, WOLOZIN B, ZHOU, J, WHITMER, RA (2009) Midlife serum cholesterol and increased risk of Alzheimer's and vascular dementia three decades later. *Dement and Geriatr Disord*, 28:75–80.

SPEHR M, GISSELMANN G, POPLAWSKI A, RIFFELL JA, WETZEL CH, ZIMMER RK, HATT H (2003) Identification of a testicular odorant receptor mediating human sperm chemotaxis. *Science* 299:2054-8.

SPERLING RA, AISEN PS, BECKETT LA, BENNETT DA, CRAFT S, FAGAN AM, et al.(2011) Toward defining the preclinical stages of Alzheimer's disease: recommendations from the National Institute on Aging–Alzheimer's Association workgroups on diagnostic guidelines for Alzheimer's disease. *Alzheimers Dementia,* 7:280–92.

SPINNEY L (2014) Alzheimer's disease: The forgetting gene. *Nature*, 510(7503):26–8.

SPITZER M, FISCHBACHER U, HERMBERGER B, GROEN G, FEHR E (2007) The neural signature of social norm compliance. *Neuron*, 56:185–96.

SPUCH C, ORTOLANO S, NAVARRO C (2012) New insights in the amyloid-beta interaction with mithochondria. *J Aging Res*, 2012:324968.

SUMMERS MJ, SAUNDERS NL (2012) Neuropsychological measures predict decline to Alzheimer's dementia from mild cognitive impairment. *Neuropsychology*, 26(4):498-508.

TAKAHASHI RH, CAPETILLO-ZARATE E, LIN MT, MILNER TA, GOURAS GK (2013) Accumulation of intraneuronal ß-amyloid 42 peptides is associated with early changes in microtubule-associated protein 2 in neurites and synapses. *PLoS One*, 8(1):e51965.

TANDON PN (2013) Not so "silent": the human prefrontal cortex. *Neurol India*, 61(6):578-80.

TANIGUCHI K (2004) Expression of the sweet receptor protein, T1R3, in the human liver and pancreas. *J VetMed Sci*, 66:1311–4.

TARAWNEH R, HOLTZMAN DM (2012) The clinical problem of symptomatic Alzheimer disease and mild cognitive impairment. *Cold Spring Harb Perspect Med*, 2(5):a006148.

TEKIN S, CUMMINGS JL (2002) Frontal-subcortical neuronal circuits and clinical neuropsychiatry: an update. *J Psychosom Res*, 53(2):647-54.

TER LAAN M, VAN DIJK JM, ELTING JW, STAAL MJ, ABSALON AR (2013) Sympathetic regulation of cerebral blood flow in humans: a review. *Br J Anaesth*, 111(3):361-7.

THAL DR, RÜB U, ORANTES M, BRAAK H (2002) Phases of A ß-deposition in the human brain and its relevance for the development of AD. *Neurology, 58:1791-800.*

THAL DR, RÜB U, SCHULTZ C, SASSIN I, GHEBREMEDHIN E, DEL TREDICI K, BRAAK E, BRAAK H (2000) Sequence of Aß-protein deposition in the human medial temporal lobe. *J Neuropathol Exp Neurol, 59:733-48.*

TOMÁS J, SANTOS CR, QUINTELA T, GONÇALVES I (2016) "Tasting" the cerebrospinal fluid: Another function of the choroid plexus? *Neuroscience*, 320:160-71.

TOYONO T, SETA Y, KATAOKA S, TOYOSHIMA K (2007) CCAAT/enhancer-binding protein beta regulates expression of human T1R3 taste receptor gene in the bile duct carcinoma cell line, HuCCT1. *Biochim Biophys Acta*, 1769:641–8.

TRZEPACZ PT, YU P, BHAMIDIPATI PK, WILLIS B et al., (2013) Frontolimbic atrophy is associated with agitation and aggression in mild cognitive impairment and Alzheimer's disease. *Alzheimers Dement*, 9(5 Suppl):S95-S104.e1.

UNGAR L, ALTMANN A, GREICIUS MD (2013) Apolipoprotein E, gender, and Alzhiemer's disease: an overlooked, but potent and promising interaction. *Brain Imaging Behav*, 8(2)262-73.

VANDERHAEGHEN P, SCHURMANS S, VASSART G, PARMENTIER M (1997) Specific repertoire of olfactory receptor genes in the male germ cells of several mammalian species. *Genomics*, 39:239-46.

VARGAS T, UGALDE C, SPUCH C, ANTEQUERA D, MORAN MJ, et al (2010) Abeta accumulation in choroid plexus is associated with mitochondrial-induced apoptosis. *Neurobiol Aging,* 31:1569–1581

VEGEZZI G, ANSELMI L, HUYNH J, BAROCELLI E, ROZENGURT E, RAYBOULD H, STERNIN C (2014) Diet-induced regulation of bitter taste receptor subtypes in the mouse gastrointestinal tract. *PLoS One*, 19;9(9):e107732.

VEITINGER T, RIFFELL JR, VEITINGER S, NASCIMENTO JM et al (2011) Chemosensory Ca^{2+} dynamics correlate with diverse behavioral phenotypes in human sperm. *J Biol Chem*, 286:17311-25.

VENNEMANN M, KOPPELKAMM A (2010) Postmortem mRNA profiling II: Practical considerations. *Forensic Sci Int*, 203(1-3):76-82.

VINCENT AS, ROEBUCK-SPENCER TM, CERNICH A (2014) Cognitive changes and dementia risk after traumatic brain injury: implications for aging military personnel. *Alzheimers Dement*, 10(3 Suppl):S174-87.

WALLIS JD (2006) Evaluating apples and oranges. *Nat Neurosci*, 9(5):596-8.

WANG X, WANG W, LI L, PERRY G, LEE HG, ZHU X (2014) Oxidative stress and mitochondrial dysfunction in Alzheimer's disease. *Biochim Biophys Acta*, 1842(8):1240-7.

WAUSON EM, ZAGANJOR E, LEE AY, GUERRA ML, GHOSH AB, BOOKOUT AL et al. (2012) The G protein-coupled taste receptor T1R1/T1R3 regulates mTORC1 and autophagy. *Mol Cell*, 47:851–62.

WEBER M, PEHL U, BREER H, STROTMANN J (2002) Olfactory receptor expressed in ganglia of the autonomic nervous system. *J Neurosci Res*, 68(2):176-84.

WIENER A, SHUDLER M, LEVIT A, NIV MY (2012) BitterDB: a database of bitter compounds. *Nucleic Acids Res, 40(Database issue):D413-419.* [Accessed February 17th 2016] Available from: http://bitterdb.agri.huji.ac.il/dbbitter.php.

WILLIS BL, GAO A, LEONARD D, DEFINA LF, BERRY JD (2012) Midlife fitness and the development of chronic conditions in later life. *Arch Intern Med*, 172(17):1333–40.

WILSON RS, SEGAWA E, BOYLE, PA, ANAGNOS SE, HIZEL LP, BENNETT DA (2012) The natural history of cognitive decline in Alzheimer's disease. *Psychol Aging*, 27(4):1008–17. 2.

WOLBURG H, PAULUS W (2010) Choroid plexus: biology and pathology. *Acta Neuropathol*, 119(1):75–88.

WU C, JIA Y, LEE JH, KIM Y, SEKHARAN S, BATISTA VS, LEE SJ (2015) Activation of OR1A1 suppresses PPAR-gamma expression by inducing HES-1 in cultured hepatocytes. *Int Biochem Cell Biol* 64:75-80.

WU SV, CHEN MC, ROZENGURT E (2005) Genomic organization, expression, and function of bitter taste receptors (T2R) in mouse and rat. *Physiol Genomics*, 22(2):139-49.

WU SV, ROZENGURT N, YANG M, YOUNG SH et al. (2002) Expression of bitter taste receptors of the T2R family in the gastrointestinal tract and enteroendocrine STC-1cells. *Proc Natl Acad Sci USA*, 99(4):2392-7.

XU J, CAO J, IQUCHI N, RIETHMACHER D, HUANG L (2013) Functional characterization of bitter-taste receptors expressed in mammalian testis. *Mol Hum Reprod*, 19(1):17-28.

XU LL, STACKHOUSE BG, FLORENCE K, ZHANG W, SHANMUGAN N, SESTERHENN IA et al (2000) PSGR, a novel prostate-specific gene with homology to a G protein-coupled receptor, is overexpressed in prostate cancer. *Cancer Res*, 60:6568-72.

YAMAMOTO K, ISHIMARU Y (2013) Oral and extra-oral taste perception. *Semin Cell Dev Biol*, 24(3):240-6.

YASUO T, KUSUHARA Y, YASUMATSU K, NINOMIYA Y (2008) Multiple receptor systems for glutamate detection in the taste organ. *Biol Pharm Bull*, 31(10):1833-7.

YOUNG RL, SUTHERLAND K, PEZOS N, BRIERLEY SM, HOROWITZ M, RAYNER CK et al. (2009) Expression of taste molecules in the upper gastrointestinal tract in humans with and without type 2 diabetes. *Gut*, 58:337–46.

YUAN TT, TOY P, MCCLARY JA, LIN RJ, MIYAMOTO NG, KRETSCHMER PJ (2001) Cloning and genetic characterization of an evolutionarily conserved human olfactory receptor that is differentially expressed across species. *Gene*, 278:41-51.

ZHANG X, BEDIGIAN AV, WANG W, EGGERT US (2012) G protein-coupled receptors participate in cytokinesis. *Cytoskeleton (Hoboken)*, 69:810-8.

ZHANG X, DE LA CRUZ O, PINTO JM, NICOLAE D, FIRESTEIN S, GILAD Y (2007) Characterizing the expression of the human olfactory receptor gene family using a novel DNA microarray. *Genome Biol*, 8:R86.

ZHANG Y, HOON MA, CHANDRASHEKAR J, MUELLER KL, COOK B, WU D, ET al. (2003) Coding of sweet, bitter, and umami tastes: Different receptor cells sharing similar signalling pathways. *Cell*, 112(3):293–301.

ZHENG J, ZAGOTTA WN (2004) Stoichiometry and assembly of olfactory cyclic nucleotide-gated channels. *Neuron*, 42(3):411–21.

VIII. Supplementary tables

Supplementary Table 1 - Overview of identified human ORs and their associated signalling components expressed in non-chemosensory tissues. Modified from Kang & Koo, 2012 and Foster et al., 2014.

Tissue or cell used	*OR* identified	Putative function	Analysis method used	References
Testis	*OR7A5, OR4D1, OR1D2*	Chemotaxis, Chemokinesis	RT-PCR, CI	Veitinger et al., 2011
	OR1D2, OR1E1	Chemotaxis	RT-PCR, CI	Spehr et al., 2003
	HT2, HTPCR92, -16, -25, -86	-	RT_PCR, RPA	Vanderhaeghen et al., 1997
Tongue	*OR1E1, OR8B8, OR5P3, OR8D1, OR8D2, OR10A5*	-	RT-PCR	Gaudin et al., 2001
	OR6Q1, OR10A4, OR7A5, OR2K2, OR5P2, OR10A5	-	RT-PCR	Durzynski et al., 2005
Heart	*OR10G4*	-	RT-PCR	Zhang et al., 2007
Spleen	*PSGR*	-	NB	Yuan et al., 2001
Prostate	*OR51E2*	-	NB	Yuan et al., 2001
	OR51E2	Inhibition of prostate cancer cells	RT-PCR, WB, CI	Neuhaus et al., 2009
	OR51E2	-	RT-PCR, NB, ISH	Xu et al., 2000
Germ cells	*OR7E24*	-	RT-PCR	Goto et al., 2001
Liver	*OR51E2*	-	NB	Yuan et al., 2001
	OR10G4	-	RT-PCR	Zhang et al., 2007
Kidney	*OR6N2, OR2T1*	-	RT-PCR	Zhang et al., 2007

GI tract	*OR1A1, OR1G1, OR1E3, OR5D18*	Odorant-mediated serotonin release	RT-PCR, CI, serotonin ELISA	Braun et al., 2007
Placenta	*MOR125-1, MOR126-1, MOR140-1, MOR145-5, MOR216-1, MOR263-9*	-	RT-PCR	Itakura et al., 2006
HeLa cell	*OR1A2, OR2A4*	Cytokinesis	RT-PCR, WB/IHC (OR2A4), siRNA screen	Zhang et al., 2012
Erythroid cells	*OR52A1*	-	RT-PCR, RPA	Feingold et al., 1999
Frontal cortex	*OR2L13, OR1E1, OR2J3, OR52L1, OR11H, Gaolf, AC3*	-	Microarray, RT-qPCR, IHC	Garcia-Esparcia et al., 2013
Various	Many	-	Microarray	Hakak et al., 2003
	Many	-	Microarray, EST	Feldmesser et al., 2006
Various (testis, lung, kidney, heart, liver)	32 *ORs* expressed exclusively in non-olfactory tissues	-	Microarray, RT-PCR	Zhang et al., 2007
Various (liver, lung, heart, testis)	Many	-	Microarray	De la Cruz et al., 2009

GI tract: gastrointestinal tract, CI: Ca2+ imaging, RPA: Rnase protection assay, NB: Northern blot, ISH: *in situ* hybridization, WB: western blot, IHC: immunohistochemistry.

Supplementary Table 2 - Approved gene symbols and previous symbols and aliases for human and mouse taste GPCR. Data from the Human Gene Database GeneCards (GeneCards, 2016) and from the NCBI Nucleotide database (NCBI, 2016).

Human		Mouse	
Approved symbols	**Previous symbols and aliases**	**Approved symbols**	**Previous symbols and aliases**
Taste receptor, type 1			
TAS1R1	*T1R1, TR1, GPR70*	*Tas1r1*	*GPR70*
TAS1R2	*T1R2, TR2, GPR71*	*Tas1r2*	*T1R2, GPR71*
TAS1R3	*T1R3*	*Tas1r3*	*T1R3*
T*aste receptor, type 2*			
TAS2R1	*T2R1, TRB7*	*Tas2r102*	*T2R102, mT2R51, STC9-7*
TAS2R3	*T2R3*	*Tas2r103*	*T2R103, T2R10, TRB2*
TAS2R4	*T2R4*	*Tas2r104*	*T2R104, mT2R45*
TAS2R5	*T2R5*	*Tas2r105*	*T2R105, T2R5, T2R9*
TAS2R7	*T2R7, TRB4*	*Tas2r106*	*T2R106, mT2R44*
TAS2R8	*T2R8, TRB5*	*Tas2r107*	*T2R107, mT2R43, T2R4, STC5-1*
TAS2R9	*T2R9, TRB6*	*Tas2r108*	*T2R4, T2R8*
TAS2R10	*T2R10, TRB2*	*Tas2r109*	*T2R109, mT2R62*
TAS2R13	*T2R13, TRB3*	*Tas2r110*	*T2R110, mT2r57, STC 9-1*
TAS2R14	*T2R14, TRB1*	*Tas2r113*	*T2R113, mT2R58*
TAS2R16	*T2R16*	*Tas2r114*	*T2R114, mT2R46*
TAS2R19	*TAS2R48, TAS2R23, T2R19, T2R23*	*Tas2r115*	
TAS2R20	*TAS2R49, T2R20, T2R56*	*Tas2r116*	*T2R116, mT2R56, TRB1, TRB4*
TAS2R22	*T2R22*		
TAS2R30	*TAS2R47, T2R30*	*Tas2r117*	*T2R117, mT2R54*
TAS2R31	*TAS2R44, T2R31, T2R53*	*Tas2r118*	*T2R16, T2R18, mt2r40*
TAS2R33	*T2R33*		
TAS2R36	*T2R36*		
TAS2R37	*T2R37*		
TAS2R38	*PTC, T2R61*	*Tas2r119*	*T2R119, T2R19*
TAS2R39	*T2R39, T2R57*	*Tas2r120*	*T2R120, mT2R47*
TAS2R40	*T2R40, T2R58, GPR60*	*Tas2r121*	*T2R13, T2R121, mT2R48*
TAS2R41	*T2R41, T2R59*	*Tas2r122*	
TAS2R42	*T2R24, T2R42, T2R55, TAS2R55, T2R55*	*Tas2r123*	*T2R123, T2R23, mT2R55, STC9-2*
TAS2R43	*T2R43, T2R52*	*Tas2r124*	*T2R124, mT2R50*
TAS2R45	*T2R45, GPR59, ZG24P*	*Tas2r125*	*T2R125, mT2R59*
TAS2R46	*T2R46, T2R54*	*Tas2r126*	*T2R41, T2R12, T2R26*
TAS2R50	*T2R50, T2R51*	*Tas2r129*	*T2R129, mT2R60*
TAS2R60	*T2R56; T2R60*	*Tas2r130*	*T2R7, T2R6, T2R30, STC7-4,*

Tas2r131	*mT2R42*
Tas2r134	*T2R134, T2R34*
Tas2r135	*T2R135, T2R35, mT2r38*
Tas2r136	*T2R136, T2R36, mT2r52*
Tas2r137	*T2R3, T2R137, T2R37, mT2r41*
Tas2r138	*T2R38, T2R138, mT2R31*
Tas2r139	*T2R39, mT2R34*
Tas2r140	*T2R140, T2R40, T2R8, T2R13, mT2r64, mTRB3, mTRB5*
Tas2r143	*T2R143, T2R43, mT2R36*
Tas2r144	*T2R40, mT2R33*

TAS2R22 is an uncategorized gene. No data available on orthologs for *TAS2R22*, *TAS2R33*, *TAS2R36* and *TAS2R37* genes.

Supplementary Table 3 - List of human bitter receptors and number of their known ligands. Data from the BitterDB, database of bitter compounds (Wiener et al., 2012).

Human bitter receptors	
Approved symbols	**Number of known ligands**
TAS2R1	35
TAS2R3	1
TAS2R4	21
TAS2R5	1
TAS2R7	9
TAS2R8	3
TAS2R9	3
TAS2R10	32
TAS2R13	2
TAS2R14	125
TAS2R16	10
TAS2R19	0
TAS2R20	2
TAS2R30	10
TAS2R31	8
TAS2R38	21
TAS2R39	78
TAS2R40	11
TAS2R41	1
TAS2R42	0
TAS2R43	16
TAS2R45	0
TAS2R46	28
TAS2R50	2
TAS2R60	0

Supplementary Table 4 - Overview of identified human TASRs and their associated signalling components expressed in non-chemosensory tissues. Modified from Foster et al., 2014.

System	Tissue or cell used	OR identified	Putative function	Analysis method used	References
Gastrointestinal	Pancreas, liver	*T1R3*	-	IHC	Taniguchi, 2004
	Colon, Gut Hu-Tu 80 cells, NCI-H716 cells	*T1R3, T2Rs (T2R3, 4, 5, 10, 13, 38, 39, 40, 42, 43, 44, 45, 46, 47, 49, 50 and 60), Gat3*	-	RT-PCR, IHC (*Gat3*), CI	Rozengurt et al., 2006
	Stomach, small instestine, colon	*T1Rs (T1R1, 2, 3), Gat3, Gγ13, PLCβ2*	-	RT-PCR, IHC (*T1R1, T1R3, Gat3, Gγ13, PLCβ2*)	Bezençon et al., 2007
	Duodenum, NCI-H716 cells	*T1R2, T1R3, Gat3, Gβ3, Gγ13, PLCβ2, TRPM5*	Regulation of *GLP-1* secretion in gut	RT-PCR,WB/IHC (*T1R2, T1R3, Gat3, Gβ3, Gγ13, PLCβ2, TRPM5*), siRNA (*Gat3*), CI, glucose gavage, hormone measurements	Jang et al., 2007
	Liver, HuCCT1 cells	*T1R1, T1R2, T1R3*	-	RT-PCR, IHC (*T1R2, T1R3*)	Toyono et al., 2007
	Cecum, NCI-H716 cells	*T1R3, T2R7*	-	RT-PCR, GLP-1 measurements, CI, siRNA (*Gat3*)	Dotson et al., 2008
	Colon	*T2Rs (T2R1, 4 and 38)*	Anion secretion	RT-PCR, Ussing chamber experiments	Kaji et al., 2009
	Duodenum, jejunum	*T1R2, T1R3, T1R2, T1R3, Gat3, TRPM5*	Regulated by blood glucose in diabetes patients	RT-PCR, IHC (*Gat3*), glucose perfusion	Young et al., 2009
	Caco-2 cells, intestine	*Gat3, PLCβ2, TRPM5*	*ABCB1*-induced efflux via *CCK* release	RT-PCR, siRNA (*T2R38*), oral gavage	Jeon et al., 2011
	Stomach	No evidence of *TR*	-	Infusion of *T1R3* antagonist, hormone measurements	Gerspach et al., 2011
	Adipose tissue, stomach, small intestine, colon, (and lung)	*FFA4*	Dietary fat sensing and control of energy balance	RT-qPCR, WB (*FFA4*), *GLP-1* secretion assay	Ichimura et al., 2012

	Pancreatic MIN6 cells; H9C2 cells, HeLa cells	*T1R1, T1R3*	Direct sensing of amino acids and regulation of mTORC1 and autophagy	RT-qPCR, CI, WB (*T1R3*) siRNA (*T1R1, T1R3*), amino acid analysis, autophagy assays	Wauson et al., 2012
	HeLa cells; DU145 cells	*T1R2; T2R13*	Cytokinesis	siRNA screen, RT-qPCR	Zhang et al., 2012
	Heart	*T1R3, T2Rs (T2R3, 4, 5, 9, 10, 13, 14, 19, 20, 30, 31, 43, 45, 46, 50)*	Nutrient-sensing	RT-qPCR, ISH	Foster et al., 2013a
	Airways	*T2Rs (T2R1, 3, 4, 7, 8, 9, 10, 13, 14)*	Motile cilia mediate cell-autonomous clearance of inhaled pathogens	Microarray, RT-PCR, IHC (*T2R4, T2R43, T2R46, Gat3, PLCB2*), CI, ciliary beat frequency assay	Shah et al., 2009
	Airway smooth muscle, trachea	*T2Rs (T2R1, 3, 4, 5, 8, 9, 10, 13, 14, 19, 20, 30, 31, 42, 45, 46, 50), Gat3*	Relaxation of isolated ASM and dilation of airways	RT-qPCR, CI, isolated trachea, single cell mechanics/membrane potentials	Deshpande et al., 2010
Cardiovascular/ pulmonary/ muscle	Airway smooth muscle cells	No evidence of TR	Agonist-promoted homologous desensitization of TR	Ca^{2+} assays, agonist-promoted desensitization assays, intact airway desensitization	Robinett et al., 2011
	16HBE cells	*T2R38, T2R46*	-	RT-PCR, Ca^{2+} mobilization, cAMP accumulation	Cohen et al., 2012
	Upper respiratory epithelium	*T2R38*	NO-mediated increase in ciliary beat frequency/mucous clearance and antibacterial effects in respiratory infection	IHC (*T2R38*), CI, NO production, ciliary beat frequency assay, mucous clearance assay, bactericidal assay	Lee et al., 2012
	BMSCs, VSMCs	*T2R46*	-	Flow cytometry, IHC (*T2R46*), RT-PCR, CI	Lund et al., 2013
CNS	Frontal cortex	*T2R5, T2R50, T2R10 and T2R13*	-	Microarray, RT-qPCR	Garcia-Esparcia et al., 2013
Reproductive	Testis	*T1R1*	Regulation of basal Ca2+ and cAMP levels in spermatozoa	RT-PCR, IHC, TUNEL assay, sperm motility, CI, cAMP accumulation	Meyer et al., 2012

Immune	Leukocytes	*T2Rs (T2R4, 5, 10, 13, 14, 19, 20, 31, 45, 46* and *50*)	Anti-inflammatory role in asthma	Microarray, RT-qPCR, cytokine ELISA	Orsmark-Pietras et al., 2013

CI: Ca^{2+} imaging, IHC: immunohistochemistry, WB: western blot.